

AN ABSTRACT OF THE THESIS OF

Joanna L. Lipske for the degree of Master of Science in Geology presented on June 3, 2002.

Title: Advanced Argillic and Sericitic Alteration in the Buckskin Range, Nevada: A Product of Ascending Magmatic Fluids from the Deeper Yerington Porphyry Copper Environment

Abstract approved: _____


John H. Dilles

Jurassic rocks exposed in the Buckskin Range of the Yerington district, represent the upper 1 to 2 km of a large magmatic-hydrothermal system with porphyry copper deposits at 1-4 km depth. These rocks include, from deep to shallow, the Yerington batholith, the Artesia Lake Volcanics (intruded by the batholith), and the Fulstone Spring Volcanics. Hydrothermal minerals characteristic of advanced argillic, sericitic, and chlorite-bearing alteration assemblages have been detected in the Buckskin Range via PIMA infrared spectroscopy and hand-lens, together with selected X-ray diffraction, petrography, and microprobe analysis. A map of hydrothermal alteration assemblages covering a 2 km² area was constructed mainly by PIMA identification of minerals on over 700 geographically located samples by comparison with mineral standards. Field relations suggest the high-level advanced argillic and sericitic alteration in the Buckskin Range is broadly contemporaneous and transitional downward into sericitic alteration and pyrite deposition in the porphyry copper environment.

The spatial and temporal relationships of hydrothermal assemblages and veins in the Buckskin Range suggest a temporal evolution from very acidic, sulfide- and sulfate- rich fluids to weakly acidic, sulfur-poor hydrothermal fluids. Early acidic fluids produced feldspar-destructive, pyrite-rich assemblages containing quartz + alunite + pyrophyllite ± kaolinite ± dickite, or quartz + muscovite, and are restricted to the Artesia Lake Volcanics. These assemblages are cross-cut and overlain by porphyry dikes and the basal dacite flow of the Fulstone Spring Volcanics that are affected by sericite + hematite + chlorite alteration. A second fluid, possibly derived from circulating sedimentary brines responsible for Na-Ca alteration in the deeper porphyry copper environment, is responsible for feldspar-stable (albite and orthoclase) assemblages with calcite + chlorite + hematite in the overlying Fulstone Spring lavas. It is currently thought that these fluids exited the system along steeply-dipping, east-west-striking Jurassic faults that cut across advanced argillic and sericitic alteration and the lowest lavas of the Fulstone Spring Volcanics to produce hematite-magnetite-Au-Cu vein mineralization.

Hydrogen and oxygen isotope compositions of muscovite ($\delta D = -56 \text{ ‰}$, $\delta^{18}O = 11.8 \text{ ‰}$) and pyrophyllite ($\delta D = -59 \text{ ‰}$, $\delta^{18}O = 9.7 \text{ ‰}$) are calculated to be in equilibrium at 350°C and 300°C with waters of $\delta D = -24$ and -25 ‰ , and $\delta^{18}O = 10.4$ and 4.3 ‰ , respectively. Sulfur isotope data give $\delta^{34}S$ values of 8.7-8.8 per mil for alunite (n=2) and -4.7 per mil (n=1) for pyrite. In thin section, alunite typically occurs with pyrophyllite as 20 to 150- μm -long tabular grains in 10 to 50-

μm -diameter quartz. These isotopic and petrographic data suggest that pyrophyllite and coarse-grained alunite has likely formed at 250°-300°C by the condensation of acidic hydrothermal fluids derived from magmatic vapors.

Advanced Argillic and Sericitic Alteration in the Buckskin Range, Nevada:
A Product of Ascending Magmatic Fluids from the Deeper
Yerington Porphyry Copper Environment

by
Joanna L. Lipske

A THESIS

submitted to

Oregon State University

in partial fulfillment of
the requirements for the
degree of

Master of Science

Presented June 3, 2002
Commencement June 2003

Master of Science thesis of Joanna L. Lipske presented on June 3, 2002.

APPROVED:



Major Professor, representing Geology



Head of the Department of Geosciences

Dean of the Graduate School

I understand that my thesis will become part of the permanent collection of Oregon State University libraries. My signature below authorizes release of my thesis to any reader upon request.



Joanna L. Lipske, Author

ACKNOWLEDGMENTS

I would like to thank my thesis committee, with special regards to my advisor and co-author, John Dilles for introducing me to this project. John has made an incredible impact on my career, academically and professionally, and especially in the field. He has always been readily available for questions or discussions. As an advisee, I have had the opportunity to make valuable contacts with academia and industry, many with whom I have shared discussions and ideas that greatly benefit this research.

This project has been funded by several research grants from the Society of Economic Geologists. Portions of the field work were funded by the OSU Ore Geology Fund and the University of Arizona. Ron Lyon and Marco Einaudi from Stanford as well as the Kennecott Corporation in Reno, NV have graciously furnished the PIMA spectrometers used during this study. Abel Vanegas and George Brimhall from the Earth Resources Center at UC Berkeley provided unlimited computer support during my trials and tribulations with pen computers. Sulfur isotope analysis was conducted by Cy Field from OSU. Hydrogen and oxygen isotope data was collected by Lihua Zhang from OSU and Dave Johnson from the University of Arizona.

Special thanks go out to the family of Bruce and Cindy Frechette of Wellington, NV (and the chickens!) for extending their hospitality and comfort during my second field season. Hats off to my fabulous friends (especially those I have met in Corvallis) and to my wonderful parents, Ron and Susie, for their love,

support, and unlimited patience, Patience, and PATIENCE! Last but not least, I would like to thank Joel for his encouragement, emotional support, and happiness throughout the “salad days”.

TABLE OF CONTENTS

	<u>Page</u>
1 Introduction.....	1
2 Advanced Argillic and Sericitic Alteration in the Buckskin Range, Nevada: A Product of Ascending Magmatic Fluids from the Deeper Yerington Porphyry Copper Environment.....	7
3 Conclusion.....	75
 Bibliography.....	 78
 Appendices.....	 84
Appendix A Infrared Spectra.....	85
Appendix B Electron Microprobe Data.....	86
Appendix C X-ray Diffraction Data.....	107

LIST OF FIGURES

<u>Figure</u>	<u>Page</u>
1. Schematic cross-section of typical volcanic-hydrothermal system	2
2. Simplified geology and location of field area	4
3. Generalized alteration zones in the Yerington district	10
4. Characteristic infrared patterns of alunite	17
5. Characteristic infrared patterns of illite and muscovite	19
6. Examples of deconvoluted infrared spectra for each alteration type	20
7. Common lithologic textures of the Artesia Lake Volcanic sequence	24
8. Paragenetic sequence of hypogene alteration and mineralization	34
9. Common texture of alunite in hand sample	36
10. Photomicrographs of quartz-rich alteration assemblages	38
11. Electron backscatter image of muscovite replacing pyrophyllite	40
12. Photomicrographs of silexite	44
13. Photomicrograph of sericite-hematite-chlorite alteration	46
14. Outcrop with specular hematite veins	47
15. Photomicrograph of calcite-chlorite-hematite alteration	51
16. Calculated isotopic composition of Yerington magmatic-hydrothermal fluids	52
17. Plot of sulfide and sulfate isotopic compositions	57
18. Mineral stability diagram in the $K_2O-Al_2O_3-SiO_2$ system	60

LIST OF FIGURES (CONTINUED)

<u>Figure</u>	<u>Page</u>
19. Evolution of Jurassic volcanism and hydrothermal alteration in the central Buckskin Range	66

LIST OF TABLES

<u>Table</u>	<u>Page</u>
1. Oxygen and Hydrogen Isotopic Compositions of Minerals	53
2. Isotopic Compositions and Sample Descriptions of Sulfates Measured for Sulfur Isotopes	56

**ADVANCED ARGILLIC AND SERICITIC ALTERATION IN THE
BUCKSKIN RANGE, NEVADA: A PRODUCT OF ASCENDING
MAGMATIC FLUIDS FROM THE DEEPER YERINGTON
PORPHYRY COPPER ENVIRONMENT**

CHAPTER 1: INTRODUCTION

Much literature has been published on the alteration and mineralization zones and their causative processes involved within and adjacent to porphyry copper centers (Lowell and Guilbert, 1970; Sillitoe, 1973; Gustafson and Hunt, 1975; Dilles and Einaudi, 1992). An excellent model of porphyry copper genesis has been developed as a result of extensive work at El Salvador, Chile, combined with general comparison with other well-documented porphyry copper deposits and genetic models (Gustafson and Hunt, 1975). Current models of porphyry copper deposits propose that a shallow, epithermal ore environment may lie above a porphyry copper system (Henley and Ellis, 1983; Hedenquist and Lowenstern, 1994, Hedenquist et al., 1998). This environment also serves as the discharge area for deep-seated ore-bearing hydrothermal fluids.

Advanced argillic alteration is typically found in high-sulfidation epithermal systems at shallow depths where K^+/H^+ and Na^+/H^+ activity ratios and temperatures of aqueous hydrothermal fluids are very low, resulting in the formation of minerals such as alunite with pyrophyllite at high temperatures, and kaolinite, dickite, etc at lower temperatures. The formation of acidic hydrothermal fluids responsible for advanced argillic alteration assemblages can occur through several processes (Figure 1). At depth, a degassing magma releases aqueous fluids

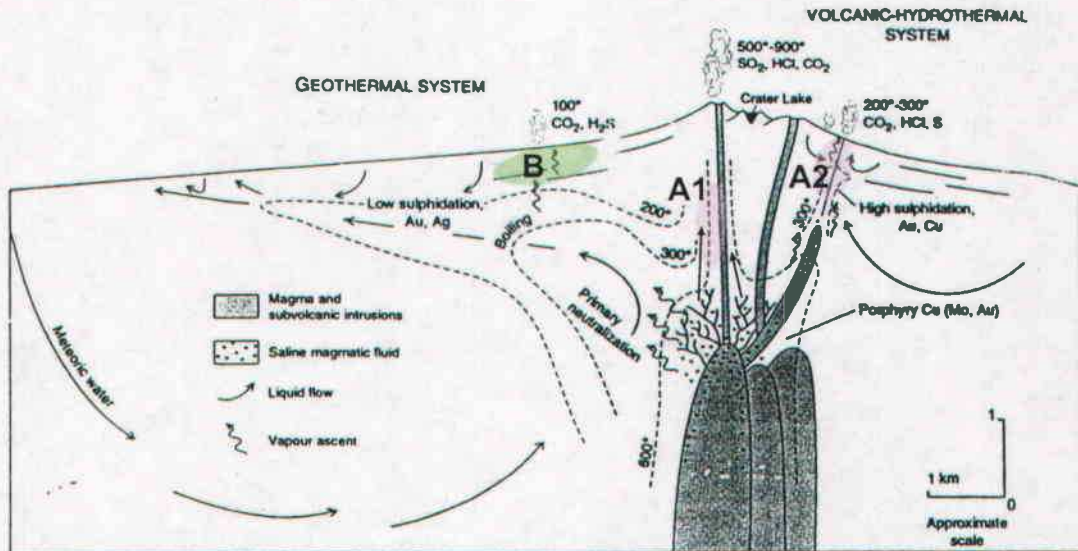


Figure 1. Schematic cross-section showing the relationship between a deep porphyry copper system to a shallow-epithermal, high and low sulfidation system. The hydrothermal system spans from the degassing magma to fumaroles and springs. High sulfidation systems are characterized by acidic waters that form by the ascension of a magmatic vapor plume at 500-900°C (A1) or ascending magmatic vapor derived from deep magmatic liquid-vapor immiscibility at 300-400°C (A2). Low sulfidation systems represent more neutral waters that boil to produce overlying steam-heated zones at ~100°C. (modified from Hedenquist and Lowenstern, 1994)

rich in SO_2 , H_2S , or HCl that can remain as a single fluid phase (A1) or may undergo exsolution to produce a liquid brine and low-salinity vapor phase (A2) if the pressure decreases (Henley and McNabb, 1978). Ascending magmatic vapor may condense where it encounters cooler, shallow meteoric water to form low-pH, moderate-temperature fluids that produce acid-sulfate high-sulfidation alteration characterized by alunite, quartz, pyrophyllite, and dickite (A1). Ascending dilute, nearly-neutral, low-temperature (200-300°C) fluids typical of low-sulfidation environments can boil upon ascension. Vapors produced by such boiling condensation at $\leq 100^\circ\text{C}$ to produce steam-heated acid-sulfate alteration typified by alunite, kaolinite, and chalcedonic or opaline silica (B).

Exposures of the Artesia Lake and Fulstone Spring Volcanics in the Buckskin Range represent the uppermost part of the Jurassic Yerington porphyry copper system and contain advanced argillic and sericitic alteration assemblages (Figure 2). The Yerington district is located approximately 80 km southeast of Reno, Nevada, within the Great Basin portion of the Basin and Range Province. The Yerington batholith hosts four porphyry copper deposits and is associated with nearby copper skarn and iron deposits as well as gold-copper veins. The main economic producer in the area is the Yerington Mine, which has produced 162 million tons at 0.55% Cu (Dilles and Proffett, 1995). The present surface of the district is exposed in cross-section due to 60° - 90° W-tilting produced by Miocene Basin-and-Range extension (Proffett, 1977), representing a paleo-cross section that

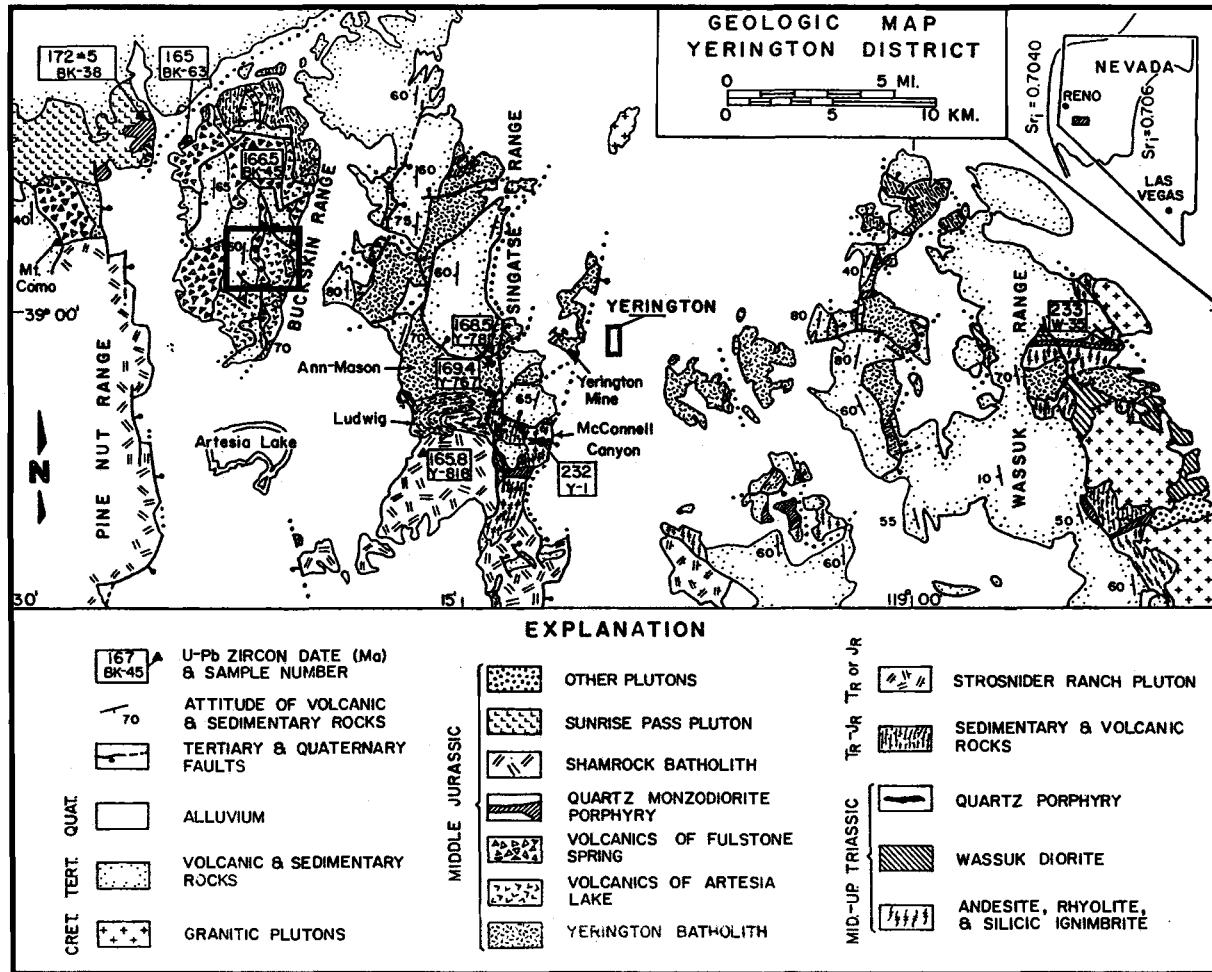


Figure 2. Simplified geologic map and geographical location of the Yerington district (upper right). Field area in the central Buckskin Range is shown in box. Numbers correspond to sample locations used for U-Pb chronology in a previous study. (from Dilles and Wright, 1988)

extends from approximately 0 to 1 km depth in the Buckskin Range and 1 to 7 km in the Singatse Range. The field area is denoted by box in Figure 2.

The exposure of a large vertical range of igneous bodies and alteration assemblages has made the Yerington district a well-studied area for surficial alteration mapping and remote sensing research (Hudson, 1983; Rubin, 1991; Dilles and Einaudi, 1992). The magmatic and hydrothermal features related to porphyry copper mineralization in the Yerington district from 1 to 6 km of paleodepth have been well-documented in previous studies (Proffett and Dilles, 1984; Dilles, 1987; Dilles and Einaudi, 1992). Previous work in the Buckskin Range has shown the presence of characteristic advanced argillic alteration minerals such as andalusite, pyrophyllite, and alunite (Hudson, 1983).

This purpose of this study is to characterize the distribution and mineralogy of advanced argillic and sericitic alteration in the Buckskin Range, deduce physio-chemical conditions of hydrothermal alteration, and attempt to link the timing and origins of the causative fluids and their relationship with the well-studied, deeper porphyry copper environment. The distribution and mineralogy of hydrothermal alteration zones in the Buckskin Range was delineated by short-wave infrared spectroscopy (SWIR) and hand lens-based mapping, confirmed by X-ray diffraction, electron microprobe analysis, and supplemented by stable isotopes and petrography. Data presented below suggest such alteration is due to ascending magmatic-hydrothermal fluids at 0-1 km depths resulting in zones of advanced

argillic alteration characterized by feldspar destructive, pyrite-rich assemblages containing quartz + alunite + pyrophyllite \pm kaolinite \pm dickite, within widespread zones of quartz + muscovite alteration. Feldspar-stable (albite and orthoclase) assemblages with added sericite + hematite + chlorite or calcite + chlorite + hematite cross-cut advanced argillic zones and overlie these zones in younger volcanic rocks. Data presented below suggests these later fluids reflect a decrease in magmatic acids and sulfur input.

The sulfide-rich advanced argillic and sericitic alteration zones sampled in this study were affected by weathering and intense supergene alteration in which sulfides were oxidized to produce acids. A key question addressed in this study concerns the origin of alunite in such rocks. Application of sulfur isotopes, alunite compositions via microprobe analysis, and the petrographic criteria of Thompson (1990), Thompson and Thompson (1996), and Ebert (1997) have been used to determine whether alunite formed via moderate-temperature magmatic-hydrothermal fluids, a Jurassic steam-heated environment, or via supergene weathering of sulfide-rich assemblages.

CHAPTER 2

ADVANCED ARGILLIC AND SERICITIC ALTERATION IN THE BUCKSKIN RANGE, NEVADA: A PRODUCT OF ASCENDING MAGMATIC FLUIDS FROM THE DEEPER YERINGTON PORPHYRY COPPER ENVIRONMENT

Joanna L. Lipske and John H. Dilles

Department of Geosciences, Oregon State University, Corvallis, OR 97331-5506

Abstract

Jurassic rocks exposed in the Buckskin Range of the Yerington district represent the upper 1 to 2 km of a large magmatic-hydrothermal system with porphyry copper deposits at 1-4 km depth. These rocks include, from deep to shallow, the Yerington batholith, the Artesia Lake Volcanics (intruded by the batholith), and the Fulstone Spring Volcanics. Hydrothermal minerals characteristic of advanced argillic, sericitic, and chlorite-bearing alteration assemblages have been detected in the Buckskin Range via PIMA infrared spectroscopy and hand-lens, together with selected X-ray diffraction, petrography, and microprobe analysis. A map of hydrothermal alteration assemblages covering a 2 km² area was constructed mainly by PIMA identification of minerals on over 700 geographically located samples by comparison with mineral standards. Field relations suggest the high-level advanced argillic and sericitic alteration in the Buckskin Range is broadly contemporaneous and transitional downward into sericitic alteration and pyrite deposition in the porphyry copper environment.

The spatial and temporal relationships of hydrothermal assemblages and veins in the Buckskin Range suggest a temporal evolution from very acidic, sulfide- and sulfate- rich fluids to weakly acidic, sulfur-poor hydrothermal fluids. Early acidic fluids produced feldspar-destructive, pyrite-rich assemblages containing quartz + alunite + pyrophyllite \pm kaolinite \pm dickite, or quartz + muscovite, and are restricted to the Artesia Lake Volcanics. These assemblages are cross-cut and overlain by porphyry dikes and the basal dacite flow of the Fulstone Spring Volcanics that are affected by sericite + hematite + chlorite alteration. A second fluid, possibly derived from circulating sedimentary brines responsible for Na-Ca alteration in the deeper porphyry copper environment, is responsible for feldspar-stable (albite and orthoclase) assemblages with calcite + chlorite + hematite in the overlying Fulstone Spring lavas. It is currently thought that these fluids exited the system along steeply-dipping, east-west-striking Jurassic faults that cut across advanced argillic and sericitic alteration and the lowest lavas of the Fulstone Spring Volcanics to produce hematite-magnetite-Au-Cu vein mineralization.

Hydrogen and oxygen isotope compositions of muscovite ($\delta D = -56$ ‰, $\delta^{18}O = 11.8$ ‰) and pyrophyllite ($\delta D = -59$ ‰, $\delta^{18}O = 9.7$ ‰) are calculated to be in equilibrium at 350°C and 300°C with waters of $\delta D = -24$ and -25 ‰, and $\delta^{18}O = 10.4$ and 4.3 ‰, respectively. Sulfur isotope data give $\delta^{34}S$ values of 8.7-8.8 per mil for alunite (n=2) and -4.7 per mil (n=1) for pyrite. In thin section, alunite typically occurs with pyrophyllite as 20- to 150- μm -long tabular grains in 10- to

50- μm -diameter quartz. These isotopic and petrographic data suggest that pyrophyllite and coarse-grained alunite has likely formed at 250°-300°C by the condensation of acidic hydrothermal fluids derived from magmatic vapors.

Introduction

The Yerington district, located approximately 80 km southeast of Reno, Nevada, hosts four Jurassic porphyry Cu \pm Mo deposits, several Cu-skarn and Fe-Cu deposits in calc-silicate host rocks, and local Cu-Au-Fe vein lodes that have an approximate total resource of 6 Mt Cu and over 100 Mt Fe. The main economic producer in the area is the Yerington Mine, which has produced 162 million tons at 0.55 wt.% Cu (Dilles and Proffett, 1995). Exposures of the Artesia Lake Volcanics in the Buckskin Range that contain advanced argillic and sericitic alteration minerals such as alunite, sericite, pyrophyllite, and pyrite, represent the uppermost part of the Jurassic Yerington magmatic-hydrothermal system at estimated depths of 1 km, in contrast to the 1-7 km exposed in the Ann Mason area of in the Singatse Range (Dilles and Einaudi, 1992).

Hydrothermal alteration in the Yerington district is characterized by a central core of K-silicate alteration and main-stage sulfide-ore deposition at 3-4 km of depth produced by a magmatic-dominated fluid (Figure 3). K-silicate alteration is transitional upward through sericite-pyrite alteration at 1-3 km of depth into quartz-rich sericitic and advanced argillic alteration assemblages in the Buckskin

Hydrothermal Alteration Zones of the Yerington District

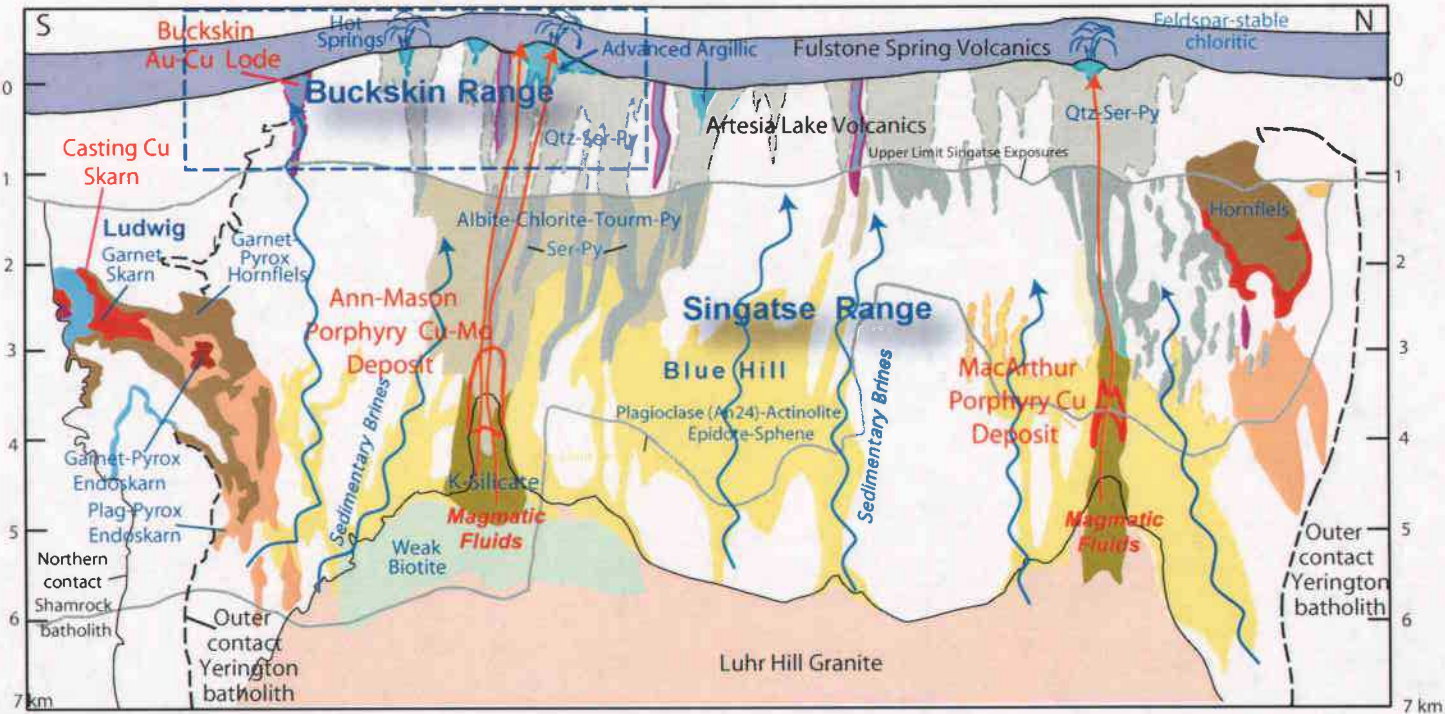


Figure 3. Generalized north-south cross section of alteration zones in and around the Yerington batholith based on data from Ludwig, Ann-Mason, Blue Hill, MacArthur, and the Buckskin Range (J. H. Dilles, unpublished; Einaudi, 1982, 2000; Dilles and Einaudi, 1992; Harris and Einaudi, 1982; and Lipske and Dilles, 2000). Red arrows represent the path of magmatic fluids; Blue wavy arrows represent the paths of sedimentary brines. Modified from Dilles et al., 2000.

Range. Sodic-calcic alteration, a product of circulating sedimentary brines from the Triassic-Jurassic sedimentary section characterized by the presence of plagioclase (An₂₄), actinolite, epidote, and sphene, is widespread throughout the Yerington batholith at 2-6 km of depth (Dilles and Einaudi, 1992; Dilles et al., 2000). Contact metasomatism at the northern and southern parts of the contact aureole with the Yerington batholith has resulted in large volumes of hornfels and endoskarn alteration assemblages associated with Cu-sulfide bearing skarns and Fe-oxide replacement bodies. Intermediate-depth (2-4 km) "propylitic"-actinolite alteration occurs between the deep-level sodic-calcic alteration and shallow-level feldspar-stable chlorite-bearing alteration assemblages in the Buckskin Range (Dilles and Einaudi, 1992; Dilles et al., 2000).

The geology of the Buckskin Range was previously evaluated by the Anaconda Minerals Company during Cu-Au exploration in the 1970s. Parts of the central Buckskin Range have been mapped extensively for structure, lithology, and hand lens-based alteration mineralogy by J. Proffett in 1970-71 and 1987-88, G. Salas in 1971, W. Sumner in 1983, K. Meeker in 1987, and J. Dilles in 1983 (Proffett and Dilles, 1991). Advanced argillic and sericitic altered rocks are widely distributed in the Artesia Lake Volcanics and locally in the Yerington Batholith in the Buckskin Range, and the younger and overlying Fulstone Spring Volcanics are typically less altered to chlorite-bearing assemblages (Hudson, 1983; Hudson and Oriel, 1979; Proffett and Dilles, 1991; and Dilles and Proffett, 1991; Lyon and Honey, 1990; Rubin, 1991).

Hudson (1983) conducted extensive X-ray diffraction, petrography, and geologic mapping of the southern Buckskin Range in surface exposures and drillcore and documented advanced argillic minerals such as andalusite, corundum, diaspore, pyrophyllite, and alunite. Hudson concluded that these minerals formed by the reaction of wall rocks with acidic fluids formed by the ascension of magmatic SO₂ from the deeper porphyry copper environment that mixed with meteoric water at shallow depths. It is alternatively possible that the reported andalusite and corundum in the southern Buckskin Range may be the result of metamorphism of earlier-formed kaolinite, pyrophyllite, and diaspore by the younger intrusions such as Miocene dacite plugs and the Jurassic Shamrock Batholith (Proffett and Dilles, 1984).

A technique for producing alteration maps using GEOSCAN airborne short-wave infrared imaging spectroscopy has been tested in the central Buckskin Range (Lyon and Honey, 1990; Rubin, 1991). The resulting aerial images identified minerals such as alunite, pyrophyllite, and muscovite and delineated zones in which advanced argillic assemblages are enveloped by areas of sericitic alteration.

The purpose of this study is to (1) document the spatial distribution of alteration minerals in the Buckskin Range via short-wave infrared spectroscopy and hand lens-based mapping, supplemented by local X-ray diffraction, electron microprobe analysis, stable isotopes, and petrography; (2) determine the relative age and genetic relationships of advanced argillic and sericitic alteration with chlorite-bearing assemblages and (3) estimate pressure and temperature

conditions and geochemistry of hydrothermal alteration fluids that produced advanced argillic and sericitic alteration so as to compare these physio-chemical conditions with deeper porphyry copper alteration. Efforts have been made to differentiate between hypogene and supergene alteration effects as field work was conducted exclusively on weathered exposures. This particular study is the first detailed study of advanced argillic alteration on the surface of the Yerington district in which the geology has already been well constrained.

Methods

Mapping

Surface exposures and road cuts were mapped in detail at 1:6000 scale over an approximate area of 2 km² in the central Buckskin Range. Features mapped directly in the field were geology, structure, sample locations, and any major alteration boundaries. A major portion of mapping was completed by hand on orthorectified aerial photographs. A pen computer with PenMap® and GeoMapper software was also used for field mapping in GIS format (Condor Earth Technologies, 1998; Brimhall, 1999). Orthorectified aerial photographs and a vectorized topographic map, loaded onto the computer, were used as a base maps. The geographically located hand samples were analyzed with the use of PIMA-II infrared field spectrometers, provided by Kennecott Corporation and Stanford

University to identify the characteristic alteration minerals. Each sample location was assigned to an alteration type based on mineralogy and plotted in ArcView3.2 to construct a detailed hydrothermal alteration map.

Analytical Techniques

Petrographic analysis was completed on 14 standard thin sections and 39 polished thin sections. Major element geochemical data was collected from selected micas and alunites in 6 samples using a CAMECA SX-50 electron microprobe at Oregon State University in order to test the accuracy of identification via the PIMA-II spectrometer. Refer to Appendix B for detailed methods and standards used.

X-ray diffraction (XRD) analysis was performed on 16 samples at Oregon State University. Samples were prepared according to the procedures for clay mineral separation of Glasmann (1999) and scanned using a Phillips 3100 XRG automated X-ray diffractometer with Cu radiation ($\lambda=1.54178 \text{ \AA}$) at 40 kV and 30 mA at a scan rate of ca. $1^\circ 2\theta/\text{minute}$. X-ray diffraction patterns were analyzed with the Jade 3.1® computer program, which allows mineral identification via 2θ -peak fitting.

Sulfur isotopic data were collected from 3 samples containing jarosite and alunite from the Buckskin Range. These sulfates were converted with Thode solution to acanthite, which was then burnt to produce sulfur dioxide. SO_2 was

extracted by Cyrus W. Field at Oregon State University and analyzed by Edward M. Ripley at Indiana University. Hydrogen and oxygen isotopes were measured on 2 handpicked samples of muscovite and pyrophyllite. Hydrogen was extracted by Lihua Zhang at Oregon State University using the U-reduction method as described in Bigeleison et al. (1951), and was analyzed with a mass spectrometer at Washington State University. Oxygen was extracted and analyzed at the University of Arizona using ClF_3 extraction in nickel bombs at 550°C . Replicate hydrogen analyses of NBS-30 biotite at OSU yields δD of $-59 \pm 7 \text{‰}$ (2σ , $n=12$) relative to V-SMOW. Blue gas standard was measured at $47.6 \pm 0.8 \text{‰}$ (V-SMOW) at the University of Arizona.

Infrared Spectroscopy

Short-wave infrared spectroscopy (SWIR) detects absorption in the 1300-2500 nm range from chemical bonds that include OH^- , H_2O , SO_4^{-2} , and CO_3^{-2} , so it is very sensitive to clays, sulfates, and hydrous silicates. A PIMA-II (Portable Infrared Mineral Analyzer) spectrometer was employed in the field in this study, and it can identify alunite and various hydrous silicates, notably micas, to as little as 3 volume percent of the rock sample by comparison with X-ray diffraction and petrographic data (Thompson et al., 1999). When mixtures are present, the PIMA can detect up to three minerals accurately.

The PIMA-II spectrometer is a compact, shoe box-sized field instrument that weighs approximately 2.5 kg. It measures the percentage of radiation reflected

from the surface of a sample for 30 seconds with a 0.2-cm-diameter circular aperture by using an internal light source, which requires minimal calibration.

The PIMA-II is not very sensitive to variations in temperature and humidity, so calibration in this study was only performed every ~15 measurements as recommended in the study of Thompson et al.(1999).

Minerals such as feldspars, carbonates, and chlorite have low reflectance and may require an abundance of greater than 20 volume percent to be detected with SWIR spectroscopy (Thompson et al., 1999). X-ray diffraction and petrographic analysis were used to identify low reflectance minerals not detected by infrared spectrometry.

Spectral data were collected on over 700 representative hand samples from outcrops by taking two measurements on a broken rock surface without obvious supergene mineral coating and locally other measurements on veins and fracture fillings. Several spectra were also collected on anomalous hand samples. The digital spectral data was imported into PimaView 3.1 (Integrated Spectronics Ltd., 1999) and SpecWin 1.6 (Spectral International, Inc., 2000) and comparison of distinctive features such as wavelength position, and the shape and intensity of absorption features with reference spectral libraries were used to identify individual minerals or mineral assemblages in the central Buckskin Range.

For example, alunite from the Buckskin Range has $K/K+Na$ molar ratios (0.08-0.66) that range in composition between natroalunite and K-rich alunite endmembers as denoted by the shift in ~1480 nm and ~1490 nm peaks (Figure 4a).

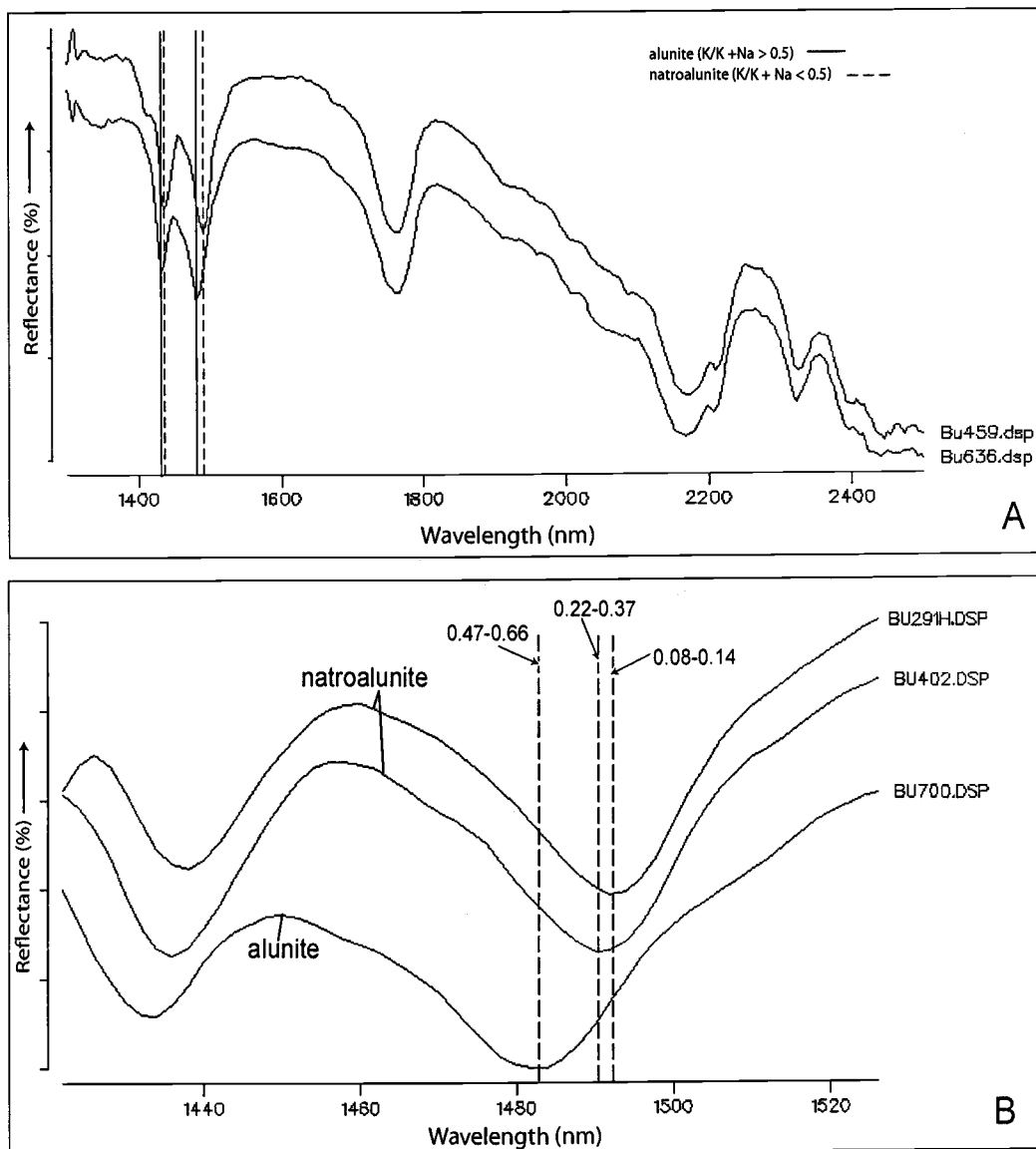


Figure 4. A) Examples of typical alunite and natroalunite spectra from the central Buckskin Range. Vertical lines demonstrate the position of major absorption features for Na- and K-bearing alunite. B) Detailed spectra (1430-1520 nm range) of alunite and natroalunite detected with the PIMA demonstrating the positive shift in wavelength as Na-content increases. K/K+Na values are based on microprobe analyses. Reflectance values are not shown on stacked plots.

The wavelengths of alunite absorption features between 1400 and 1500 nm shift to greater wavelengths as Na-content in alunite increases (Figure 4b). For mica and clay minerals, muscovite and illite have similar spectral characteristics and cannot be identified solely on the 'OH' and water' and 'Al-OH' absorption features (1400 and 2200 nm peaks, respectively) as the two micas have similar chemical compositions in the central Buckskin Range. Using SWIR criteria, illite spectra, similar to most clays, have a distinctive molecular water absorption at 1900 nm and the muscovite spectra have a positive slope near ~2450 nm (Figure 5).

With these concepts in mind, spectra from altered rocks with the presence of two or more individual minerals have been deconvoluted according to the methods stated above (Figure 6). Note that most accessory minerals in each of the assemblages are not detectable via SWIR due to low relative abundance or obscuring absorption features of abundant minerals such as clays, micas, or alunite in spectra. Mineral standards used for the deconvolution of spectra shown here are derived from the SPECMIN™ Spectral Library (Hauff, 1993), with the exception of Bu278.dsp, a muscovite standard from the Buckskin Range verified via XRD. XRD and electron microprobe analyses have been employed to confirm the presence of clays and micas and to determine more specifically, the chemistry and lattice structure, where applicable, and will be reported in the hydrothermal alteration section of the text.

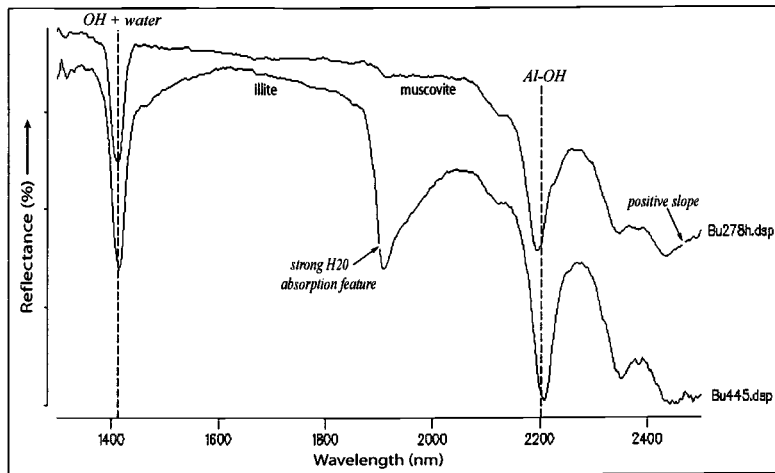


Figure 5. Examples of muscovite and illite from the central Buckskin Range plotted to show differences in spectral characteristics. Reflectance values are not shown on stacked plots.

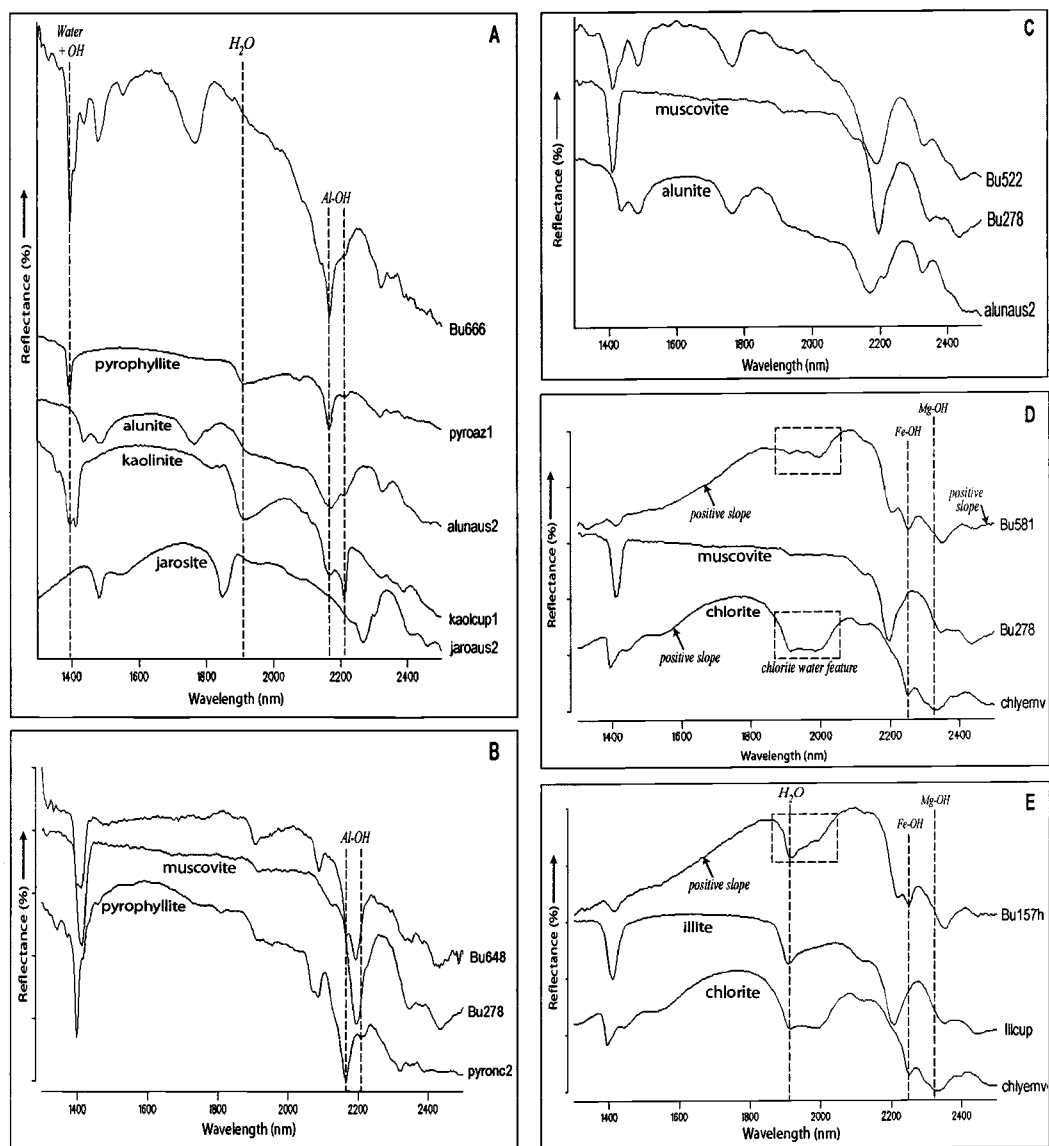


Figure 6. Stack plots of deconvoluted spectra representing mappable alteration assemblages in the central Buckskin Range with characteristic absorption features. Top spectrum of each plot represents actual data from the central Buckskin Range. Individual spectra shown below actual data are reference spectra from the SPECMIN database except for Bu278, a muscovite reference from the central Buckskin Range. Each frame represents a separate alteration assemblage and are shown as follows: A) AA1, B) AA2, C) AA3, D) SC, E) P. Reflectance values are not shown on stack plots. Absorption features are derived from Pontual et al. (1995).

Many hydrous aluminosilicate minerals share common absorption features, however the positions of these features may shift slightly according to molar proportions of elements (Figure 6a-b). Note the distinctive H₂O-absorption feature of chlorite and positive slope between 1400-1800 nm that is prominent in mixtures with chlorite and white mica (Figure 6e-f). Identification of muscovite in mixtures with chlorite is based on the positive slope at ca. 2450 nm (Figure 6d). Illite in samples mixed with chlorite results in a stronger H₂O-absorption feature at ca. 1900 nm and a flat slope at ca. 2450 nm (Figure 6e). The chlorite identified in sample Bu157H closely resembles a SPECMINTM mineral database Fe-Mg- chlorite standard from the Yerington district, however the chlorite in these mixtures display more absorption at the Fe-OH feature than at the Mg-OH feature, suggesting an Fe-rich composition. Appendix A contains all PIMA data collected in this study in addition to viewing software, a table of geographic sample locations, and designated alteration type. Sample locations are plotted on a map on Plate C.

Geology and Structure

The oldest rocks in the central Buckskin Range consist of a sequence of upper Triassic through lower Jurassic volcanic and sedimentary rocks. These units are not exposed in the central Buckskin Range, however the uppermost units have been observed in drill core (Dilles and Wendell, 1982). Mid-Jurassic magmatism followed lower Jurassic sedimentation and produced intermediate to silicic calc-

alkaline volcanic and plutonic rocks between 170 and 165 Ma (Dilles and Wright, 1988). These include the Artesia Lake and Fulstone Springs Volcanics and the Yerington batholith.

The Yerington Batholith

The Yerington batholith comprises three phases, each successively smaller in volume with deeper emplacement, from oldest to youngest; McLeod Hill quartz monzodiorite, Bear quartz monzonite, and Luhr Hill granite. The granite locally grades into porphyry dikes above granite cupolas (Dilles, 1987). The only exposures of the batholith in the Buckskin Range are the McLeod Hill quartz monzodiorite that intrudes the base of the Artesia Lake Volcanics and late-stage granite porphyry dikes, further discussed in this section, that intrude the Artesia Lake Volcanics and possibly the base of the Fulstone Spring Volcanics. The detailed geology of the central Buckskin Range is shown on Plate A.

Artesia Lake Volcanics

The Artesia Lake Volcanics is an approximately 1-km-thick sequence of dacite and andesite that is thought to be the extrusive equivalent of the Yerington batholith due to chemical, isotopic and hydrothermal alteration evidence (Dilles, 1987; Dilles and Wright, 1988). The Artesia Lake Volcanics section is overlain by the Fulstone Spring Volcanics, which include a lava high in the section dated at 166.5 Ma. The base of the Artesia Lake Volcanics is intruded by and is therefore

older than the quartz monzodiorite of the Yerington Batholith dated at 169.4 Ma (Dilles and Wright, 1988).

The Artesia Lake Volcanics consist of subareal andesitic lava flows, breccias, sandstones, and ignimbrites. These rocks are commonly hydrothermally altered to sericite- and quartz-rich assemblages that once contained abundant pyrite, suggested by copious limonite minerals and boxwork structures on weathered surfaces. Primary textures in these rocks have generally been obliterated in central Buckskin Range exposures.

Artesia andesite (Jaa) lava flows and flow-breccias locally occur in subplanar map units that are roughly parallel to Artesia sedimentary bedding. Where primary texture is visible, Artesia andesite contains 1-30 vol. % 0.2 to 2-mm-long plagioclase, 5-12 vol. % 0.2-mm-long mafic minerals, and trace local hematite with lesser magnetite. The shapes of mafic mineral sites, now altered, suggest hornblende and locally pyroxene.

Rhyolitic ignimbrite (Jai) is exposed as planar units parallel to andesite lavas and volcanoclastic sedimentary rocks. Ignimbrite is identified by distinctive, up to 5-cm-long fiamme with a 5:1 to 10:1 compaction ratio (Figure 7a). Artesia ignimbrite, now strongly altered, have 5-10 vol. % 0.5-1-mm-diameter embayed quartz and originally contained 10-15 vol. % 0.5-2-mm-diameter feldspar phenocrysts.

Clastic rocks (Jas) have poor to prominent clastic textures and local and poorly developed bedding. Protoliths include fine-grained volcanoclastic sandstone

Figure 7. Common lithologic textures found in the Artesia Lake Volcanics, as described in text. Scale bar = 1 cm. A) Artesia ignimbrite with outlines of fiammé on weathered surfaces. Located at 4322004N, 296030E. B) Silexite breccia with matrix-supported subangular to angular clasts of hydrothermal quartz and silicified Artesia Lake Volcanics in a matrix of hydrothermal quartz. Located at 4321932N, 295848E. C) Sample # Bu036. Breccia with silica-rich clasts in goethite-healed matrix where brecciation is likely of Cenozoic tectonic origin.

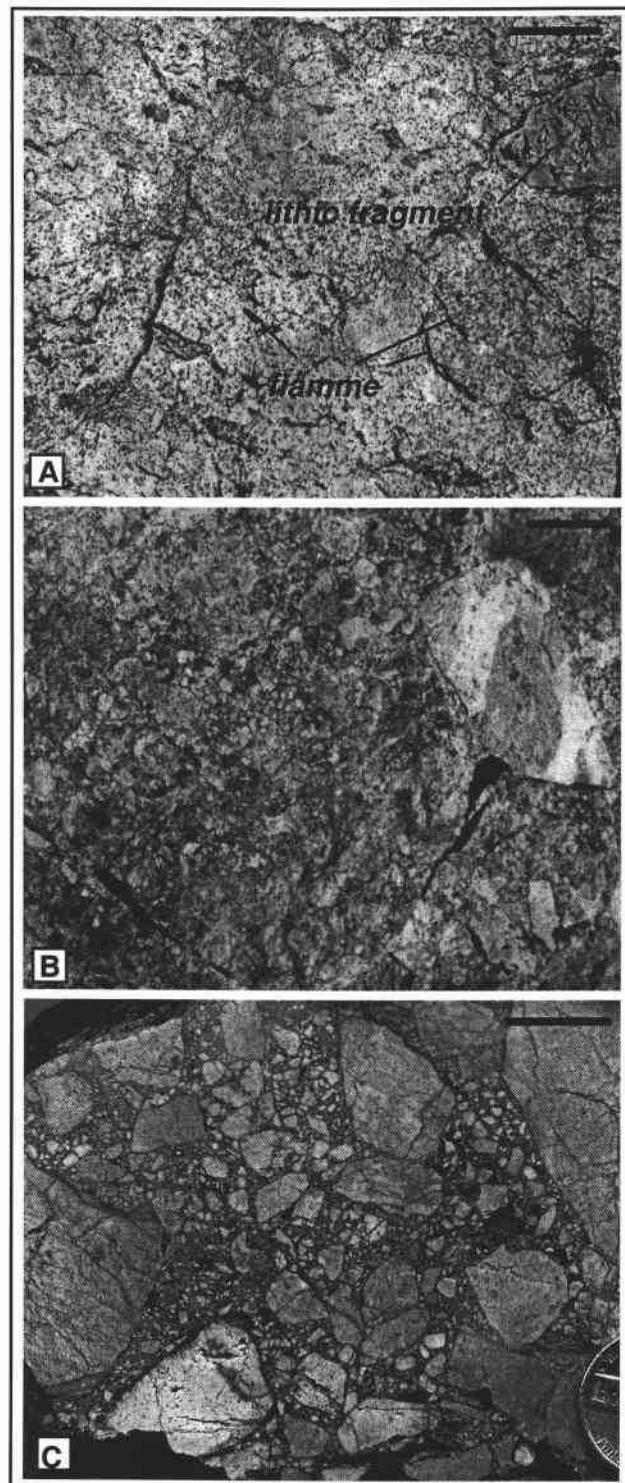


Figure 7

with <1 cm bedding, thick-bedded conglomerate, and massive breccia. Massive to poorly bedded sedimentary breccia and conglomerate have beds 0.3-1-m-thick and 1 to 30 cm subrounded to subangular clasts. Bedded rocks typically have a north-northwest strike and a steep dip to the west.

Silexite or hydrothermal quartz forms ledges that are both concordant and discordant to sedimentary bedding in the Artesia Lake Volcanics, and protoliths are difficult to determine. The concordant bodies commonly appear to be silicified versions of the bedded volcanoclastic units (Figure 7b). In some exposures, silexites are discordant to bedding and resemble massive hydrothermal breccias with matrix-supported angular 1-10 cm clasts in a hydrothermal quartz matrix. Silexite outcrops are shown on Plate B and will be considered as an alteration type in the remainder of this text.

“Goethite-breccias” that commonly surround but are not restricted to silexite bodies contain silexite clasts and have a characteristic fine-grained transported-goethite matrix of supergene origin (Figure 7c). The origin of these breccias is unknown, however the supergene goethite matrix must have formed during the weathering of sulfides. Consequently, many of these bodies likely originated as a product of brecciation related to Quaternary brittle normal faulting where transported goethite healed permeable spaces in the breccia. Hudson (1983) interpreted a hydrothermal origin.

Fulstone Spring Volcanics

The Fulstone Spring Volcanics lie disconformably atop the Artesia Lake Volcanics and can be divided into several units of latitic to dacitic lava flows, domes, and flow-breccias, silicic ignimbrites and ignimbrite-breccias, and dacitic ignimbrites. In the central Buckskin Range, bedded Artesia units locally appear to be truncated in up to 20° angular discordance by the overlying Fulstone Spring Volcanics. The Fulstone units are weakly to moderately hydrothermally altered to chlorite-hematite-rich assemblages with a low sulfide content, which suggests they postdate much or all of porphyry copper mineralization (Proffett and Dilles, 1991).

The dominant Fulstone lithology is massive quartz latite or dacite porphyry (Jfl) that contains abundant phenocrysts of 10-30 vol. % 1- to 7-mm-long plagioclase, 4-10 vol. % 1- to 5-mm-long hornblende, 0.25-3 vol. % 2- to 5-mm-diameter quartz, 0.25-1 vol. % 1- to 2-cm-diameter alkali feldspar, 0.5-1 vol. % magnetite, and trace biotite (Proffett and Dilles, 1991). This lithology can be further divided into three distinctive flows in the central Buckskin Range based on differences in phenocryst abundance and mineralogy (Proffett and Dilles, 1991, Figure 1 therein); the base and tops of these lavas are locally marked by auto-brecciated horizons. Individual flows were not differentiated during the field work for this project.

Sandstone, conglomerate, and sedimentary breccias (Jfs), characterized by a distinctive red-purple hematite staining, occur within several different horizons of the Fulstone sequence and are locally silicified (Jfss). The Fulstone Spring

conglomerates and breccias commonly contain clasts of several Artesia and Fulstone lithologies, including silexites. Clasts of Fulstone dacite porphyry (Jfd) and granite porphyry (Jgp) are absent (Proffett and Dilles, 1991).

Fulstone dacite porphyry (Jfd) is the basal lava of the Fulstone and overlies the Artesia Lake Volcanics along a contact locally marked by the presence of sedimentary breccia (Jfs) or silicified sedimentary breccia (Jfss), discussed below. The dacite porphyry unit contains 20-30 vol. % weakly aligned 0.5- to 2-mm-long plagioclase, 4-5 vol. % 0.5- to 1-mm-long hornblende and clinopyroxene, 1-2 vol. % 0.5-mm-long biotite, and 2-3 vol. % magnetite in a plagioclase-rich groundmass and is locally flow banded (Proffett and Dilles, 1992). Fulstone dacite porphyry can be differentiated in the field from other Fulstone lavas by its distinctive lower abundance of phenocrysts and lower silica content. Petrographically and chemically similar to the Artesia Lake Volcanics andesite flows, the dacite porphyry has been grouped with the Fulstone Spring volcanics due to a lack of silica-rich alteration.

Porphyry Dikes and Other Intrusions

The McLeod Hill quartz monzodiorite (Jqmd) phase of the Yerington batholith is an equigranular intrusion with 40-45 vol. % 0.5- to 1-mm-long plagioclase, 30-35 vol. % alkali feldspar, 5-10 vol. % quartz, 6-12 vol. % hornblende and biotite, and 1-2 vol. % pyroxene. The quartz monzodiorite intrudes

the base of the Artesia Lake Volcanics and is cut by a quartz latite porphyry dike along a range front fault.

Granite porphyry (Jgp) dikes and plugs in the Buckskin Range intrude the McLeod Hill quartz monzodiorite phase of the Yerington batholith and all units of the Artesia Lake Volcanics but cannot be traced past the lowermost units of the Fulstone Spring Volcanics. These dikes are petrographically similar to a 168.5 ± 0.4 Ma porphyry dike of the Luhr Hill granite phase of the Yerington batholith from Ann-Mason (Dilles and Wright, 1988). A granite porphyry dike from the central Buckskin Range (Plate A; 4321800N, 295900E) has been dated by U-Th-Pb on zircon at 166.9 ± 0.60 Ma using laser-ablation ICP-MS at Australian National University (C. Allen, pers. commun., 2002). This age is analytically distinct from and younger than the age of granite porphyry dikes determined by Dilles and Wright (1988), but is analytically indistinguishable from the U/Pb zircon age of 166.5 ± 0.4 Ma obtained by Dilles and Wright (1988) on a lava flow from the upper part of the Fulstone Volcanics. At face value, the porphyry dike in the central Buckskin Range is therefore related to Fulstone magmatism as opposed to the Yerington Batholith. However, the various lab techniques may show that the ages are all within error.

These porphyries contain phenocrysts of 2-3 vol. % 0.25- to 1-mm-diameter quartz with 25-30 vol. % 1 to 4-mm-long plagioclase, 5-7 vol. % 0.2- to 0.5-mm-long hornblende, 3-5 vol. % 0.2- to 0.5-mm-long biotite, and 1-3 vol. % 1-cm-

diameter alkali feldspar in an aplitic groundmass of quartz, feldspar, and hematite.

Narrow 1- to 2-m-wide zones of igneous hydrothermal breccia occur locally along the margins of porphyry dikes.

Granite porphyry dikes are commonly associated with and may intrude or be intruded by dacite dikes (Jad) that contain 20-30 vol. % phenocrysts of 10-15 vol. % 1- to 2-mm-long plagioclase, <1 vol. % embayed quartz, and 5-10 vol. % 1-mm-long hornblende and pyroxene, in an aplitic groundmass of quartz and feldspar.

Quartz latite porphyry (Jlp) dikes may be age equivalent to the basal quartz-latite flows of the Fulstone Spring Volcanics due to petrographic similarities and cross-cutting relationships as they have not been traced past the base of the Fulstone sequence. These dikes are locally flow banded with 20-30 vol. % weakly-aligned 0.5- to 2-mm-long plagioclase phenocrysts, 4-5 vol. % 0.5- to 1-mm-diameter hornblende and pyroxene, 1-2 vol. % 0.5-mm-diameter biotite, 2-3 vol. % magnetite, and <1 vol. % embayed quartz in a plagioclase-rich groundmass.

Mesozoic Structure

Jurassic volcanics in the central Buckskin Range older than the basal Fulstone Spring quartz latite lavas are cut and offset by several east-west-striking, nearly vertical faults, one of which has Fe-oxide-Au-Cu mineralization deposited along (Plate A, hydrothermal veins). The Buckskin Vein has been deposited along a similar Jurassic structure in the southern Buckskin Range. Vein mineralization

will be discussed further in the section following. These nearly-vertical, Jurassic structures are cut and offset to the east by several sets of Cenozoic east-dipping normal faults, discussed below.

Cenozoic Geology and Structure

Mesozoic rocks in the Buckskin Range, as in the Singatse Range, are unconformably overlain by Oligocene ignimbrites and Miocene lavas (Proffett and Proffett, 1977; Hudson and Oriel, 1979). A series of Miocene to recent, down-to-the-east normal faults have cut and tilted all Oligocene and older rocks 80-90°W so that they now are exposed in cross-section (Proffett, 1977; Hudson and Oriel, 1979; Dilles and Gans, 1995). The oldest normal faults, due to rotation of fault blocks, are now gently dipping to the east and are cut and offset by late Miocene to recent range-front faults dip that approximately 60° to the east (cross-section, Plate A, Dilles and Proffett, 1991). The Cenozoic faults are readily identified in the Fulstone Spring and Cenozoic volcanic section, but are difficult to trace within the older Jurassic rocks. The geologic map represents the current best mapping of these faults and shows that the Artesia Lake Volcanics are cut by several gently east- to southeast-dipping faults, which repeat the section between the range front and Alunite Hill.

Hydrothermal Alteration And Mineralization

The spatial distribution of minerals has been compiled into a map of hypogene alteration mineral associations and veins (Plate B). Alteration generally increases in intensity upward in the Artesia Lake Volcanic section towards the Fulstone Spring contact, and is characterized by an increase in feldspar-destructive advanced argillic and quartz-sericite alteration. Advanced argillic alteration zones are both concordant and discordant to the bedded breccias in the upper part of the Artesia Lake Volcanics, and are enveloped by quartz-sericite assemblages, which in turn may be enveloped by sericite-hematite-chlorite alteration.

Some Artesia andesite lavas, e.g. those located near the northern contact with the overlying Fulstone Spring Volcanics (Plate A; 4322250N, 295750E), and the Fulstone dacite porphyry both possess feldspar-stable sericite-hematite-chlorite alteration, described below. Granite porphyry and andesite dikes, which contain feldspar-stable alteration with chloritized mafics and vein-controlled sericite-hematite-chlorite alteration, cross-cut the advanced argillic and sericitic alteration in the Artesia Lake section.

Fulstone Spring rocks that overlie the Fulstone dacite porphyry possess feldspar-stable assemblages of weak to moderate chlorite-calcite-hematite accompanied by the addition of alkali feldspar. Cenozoic rocks are typically unaltered with the exception of minor clay, chlorite, and hematite, and are not considered further below. It is deduced that nearly all silicate alteration of the Mesozoic rocks formed in the middle Jurassic. Hypogene hydrothermal mineral

paragenesis with respect to Jurassic magmatism in the central Buckskin Range is displayed in Figure 8.

Advanced Argillic and Quartz-Sericite Alteration

The abundance of sulfides in the advanced argillic and quartz-sericite altered rocks suggest that these alteration types may be contemporaneous with the main event of sericitic alteration and pyrite deposition in the deeper porphyry copper environment. Temporal relationships between quartz-sericite and hypogene advanced argillic alteration remains ambiguous due to the lack of clear cross-cutting relationships and overprinting relationships that may be obscured by supergene weathering. The age of advanced argillic and quartz-sericite alteration is constrained, however, to be older than the overlying 166.5 Ma sulfide-poor Fulstone latite-dacite lavas. Advanced argillic alteration is also cross-cut and therefore older than a 166.9 ± 0.4 Ma granite porphyry dike altered to feldspar-stable sericite-hematite-chlorite alteration, discussed below.

Advanced Argillic Alteration

In the Buckskin Range, advanced argillic assemblages are defined by the presence of alunite or natroalunite, or of $2M_1$ -pyrophyllite. Other common minerals include dickite, kaolinite, pyrite, and diaspore. In hand sample, pyrophyllite is typically coarse-grained (1- to 2-mm-long) with common radiating

	Artesia Lake Volcanics	Porphyry Dikes Fulstone Dacite Porphyry	Fulstone Lavas
Alunite			
Pyrophyllite			
Dickite	---		
Diaspore		
Pyrite	—	---	
Chalcopyrite	
Kaolinite	---		
Rutile	
Muscovite	—	---	---
Hematite	—		
Magnetite		—	---
Chlorite	—		
Epidote		
Calcite			---
Montmorillonite	
Illite		—	—

MAJOR ——— MINOR - - - - - TRACE

Figure 8. Paragenetic sequence of hydrothermal alteration and hypogene mineralization with respect to Jurassic magmatism in the central Buckskin Range.

sheaves and has a whitish color with pearly luster. Kaolinite and halloysite commonly occur in fault zones and as late fracture-fillings.

Alunite is rarely visible with the hand lens, but when visible, gives a light buff-to-pink colored appearance to the rock (Figure 9). Infrared spectroscopy and petrography indicate this material is commonly a mixture of alunite with quartz, dickite, kaolinite, or pyrophyllite. Alunite has more than one nature of occurrence: most alunite forms as euhedral 30- to 150- μm -diameter tabular crystals disseminated within massive 10- to 50- μm -diameter quartz, some occurs as 30- to 150- μm -diameter grains in clots or aggregates reminiscent of feldspar phenocrysts; and some occurs as subhedral 80- to 200- μm -diameter crystals intergrown with 80- to 200- μm -diameter quartz in massive replacement zones.

It is difficult to assess the abundance of sulfide in hypogene mineralization, as complete oxidation has occurred to depths of approximately 60 to 100 ft. below the surface (Raney, 1977, unpublished Anaconda progress report). Careful distinction between hypogene and supergene mineralization has been made in the field, however, as exposures in the Buckskin Range have been heavily blanketed by supergene transported Fe-oxides.

Hypogene mineralization in these rocks, inferred on the basis of Fe-oxide pseudomorphous of sulfides, include up to 10 vol. % disseminated pyrite with local chalcopyrite (>50:1 py:cp). Subsequent weathering of pyrite-bearing rocks has resulted in abundant goethite and jarosite in the linings of cubic cavities pseudomorphous of pyrite. Supergene goethite, jarosite, and hematite occur up to

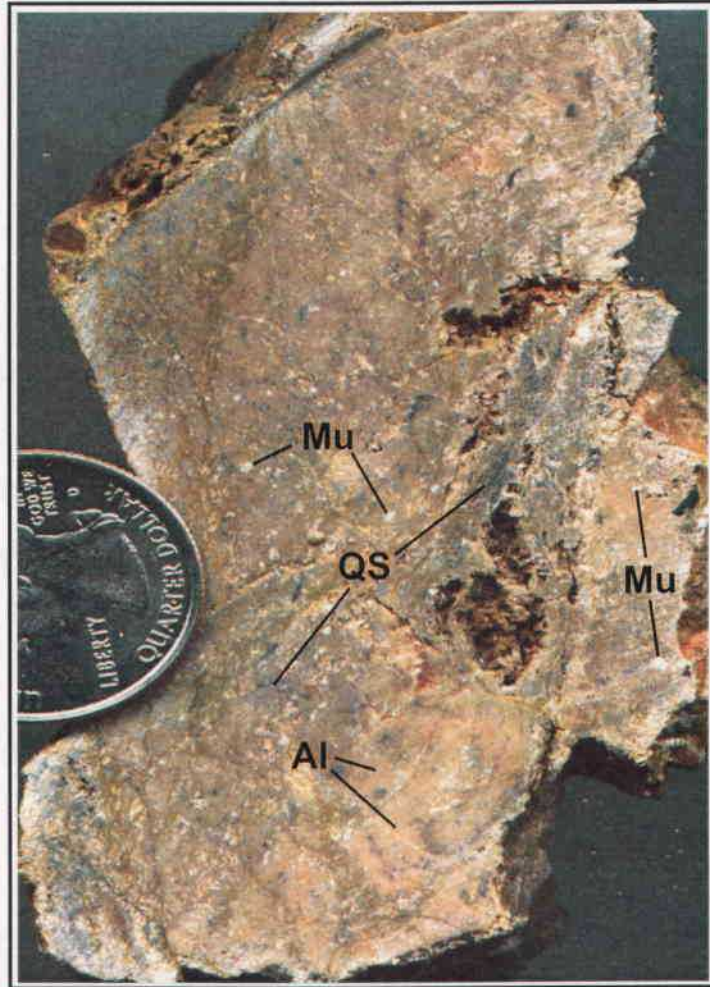


Figure 9. Common texture of alunite in hand sample (Bu409) from the central Buckskin Range. Fine-grained mixture of alunite, quartz, muscovite, and kaolinite in an altered and brecciated Artesia Lake andesitic lava. Primary textures completely obliterated. Alunite (Al) occurs as pinkish mineral intermixed with fine-grained (<0.1-mm-diameter) quartz-sericite alteration (QS) and disseminated coarse-grained (~1-mm-diameter) muscovite (Mu). Note vugs with boxwork texture which are often lined with fine-grained jarosite and goethite which suggests rock originally contained 5-10 vol. % pyrite.

10 vol. % on weathered surfaces and fractures, and up to 35 vol. % in breccias with the goethite matrix, described above.

Three advanced argillic mineral associations mapped via infrared spectroscopy are defined as follows.

Quartz-Alunite-Pyrophyllite (AA1)

This alteration commonly occurs all units of the Artesia Lake Volcanics and is the most abundant advanced argillic assemblage (Figure 10a). Associated minerals are commonly dickite, diaspore, pyrite, and rare corundum. Dickite is rarely visible in thin section or hand sample, but has been indicated frequently via infrared spectroscopy and XRD. Locally, it is present rimming pyrophyllite and as <0.1-mm-featherlike-sheaves. In one thin section, diaspore (AlO-OH) occurs as rare 0.1-mm needles. Corundum has been detected only via X-ray diffraction in one sample collected near a quartz latite porphyry dike intrusion in the central Buckskin Range, likely resulting from the breakdown of diaspore with the addition of heat from the intrusion.

Anhedral, 5- to 20- μ m-diameter quartz replaces the wallrock up to 85 vol. %, and is intergrown with disseminated 3-15 vol.% 20- to 50- μ m-diameter euhedral alunite. Approximately 3-5 vol. % 1- to 5-mm-long sheaves and local radiating aggregates of pyrophyllite (K/K+Na \sim 0.2) with dickite rims are enclosed by 10- to 50- μ m-diameter intergranular quartz and alunite with trace to 3 vol. % 0.1- to 0.5-mm-diameter goethite-lined boxwork structures that replace pyrite. In

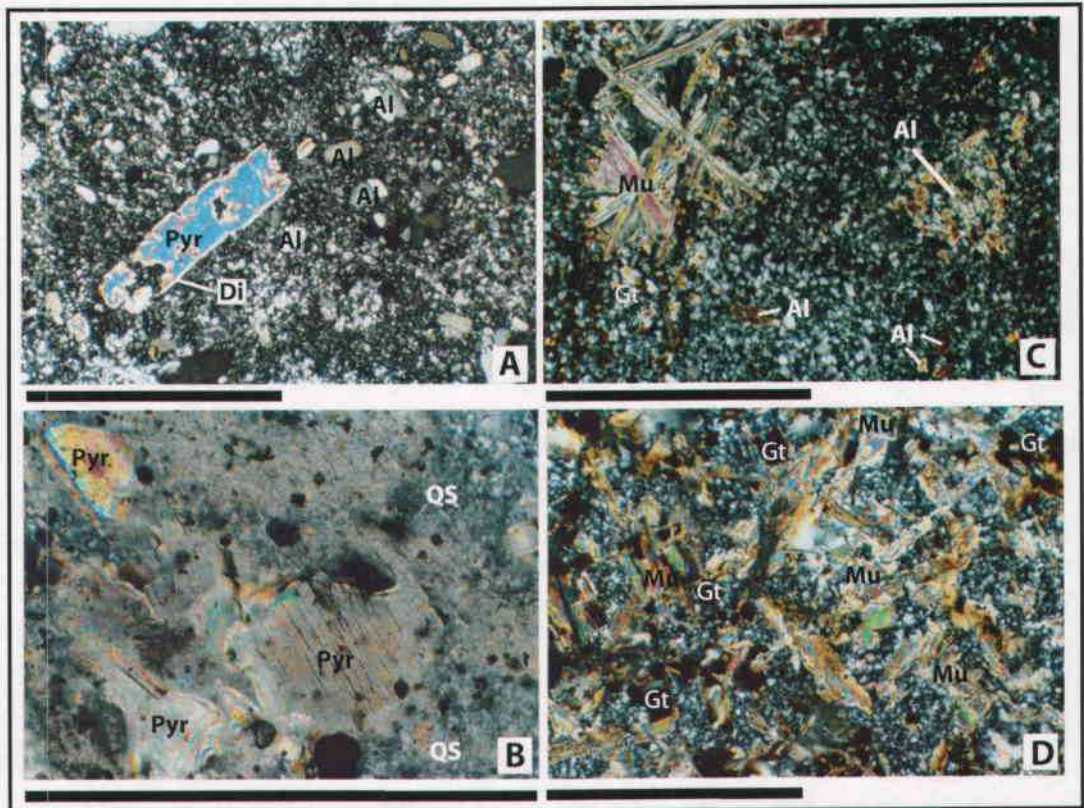


Figure 10. Photomicrographs showing common textures found in advanced argillic and quartz-sericite-altered rocks from the central Buckskin Range. All crossed polars. Scale bar = 0.5mm. A) Bu291. AA1 alteration. Relatively coarse-grained pyrophyllite (Pyr) with dickite rims (Di) in microcrystalline quartz and coarse-grained (<50 μ m) disseminated euhedral alunite (Al). B) Bu329. AA2 alteration. Coarse-grained pyrophyllite (Pyr) aggregates in a fine-grained groundmass of quartz-sericite (QS) and goethite-lined (Gt) cavities replacing primary pyrite. C) Bu036. AA3 alteration. Anhedral to subhedral fine- to coarse-grained alunite (15-80 μ m) in massive fine-grained quartz-muscovite (Mu)-pyrite (goethite) altered rock. D) Bu572. QS alteration. Massive fine-grained microcrystalline quartz intergrown with muscovite (Mu) and goethite-line pyrite cavities (Gt).

sample Bu291, dickite replaces the rims of pyrophyllite grains and also occurs as independent 0.5- to 1-mm-long sheaves (Figure 10a).

Quartz-Pyrophyllite-Muscovite (AA2)

In hand sample, this alteration assemblage is characterized by the appearance of abundant pearly white mica and most commonly occurs in, but is not restricted to, ignimbrite bodies of the Artesia Lake Volcanics. Pyrophyllite (molar $K/K+Na = 0.05-0.72$) typically occurs as 3-6 vol. % single 0.5- to 1-mm-long sheaves and 0.5- to 3-mm-diameter aggregates after feldspars enclosed by 20-50 vol. % anhedral 10- to 40- μ m-diameter quartz intergrown with 40-60 vol. % sericite (muscovite) and 1-3 vol. % 0.3 to 0.5 mm goethite-lined pyrite pseudomorphs (Figure 10b). In sample Bu329, pyrophyllite has been partially replaced by muscovite along edges and cleavage planes as seen in backscatter electron images (Figure 11a). The interesting thing to note here is that fine-grained muscovite (< 0.5 mm) occurs in the groundmass to coarse-grained pyrophyllite (~0.5- to 2-mm-diameter) in the AA2 assemblage. In the quartz-alunite-muscovite (AA3) assemblage, discussed in the following section, muscovite is coarse-grained (~0.5- to 2-mm-diameter) and has a sheave-like crystal habit similar to that of pyrophyllite (Figure 11b).

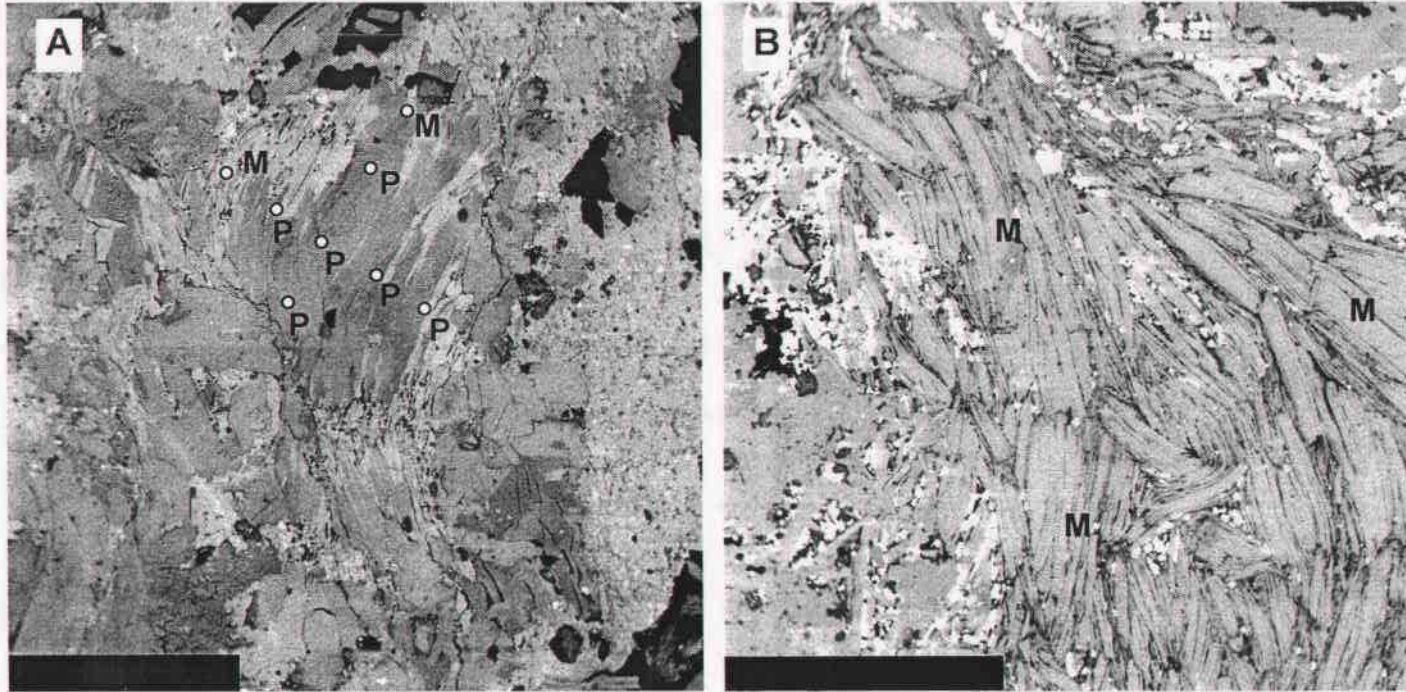


Figure 11. A) Backscattered electron image of pyrophyllite (P-grey) grain from Bu329 that has been partially replaced by muscovite (M-bright) along rims and cleavage planes. Open circles represent mineral phase identified at each measurement. B) Backscattered electron image of muscovite from Bu125 (M). Note similarities in grain size and crystal habit between the muscovite in this sample and pyrophyllite from Bu329. Refer to Plate C for sample locations. Scalebar =150 mm.

Quartz-Alunite-Sericite (AA3)

Quartz and alunite associated with sericite (muscovite or illite) occurs in all units of the Artesia Lake sequence. Approximately 5-10 vol. % 20- to 40- μ m-long muscovite (molar K/K+Na \sim 0.9) or rare illite crystals occur with 5- to 10- μ m-diameter anhedral quartz and 1-3 vol. % 0.1- to 0.5-mm goethite-lined pyrite boxworks. In sedimentary breccias of the Artesia Lake Volcanics, sericite is intergrown with 50-70 vol. % 5- to 10- μ m-diameter anhedral quartz and 3-10 vol. % 15- to 80- μ m-diameter anhedral to subhedral alunite (Figure 10c). It is possible that much of this assemblage was originally quartz + pyrophyllite + alunite \pm sericite in which all of the coarse-grained pyrophyllite has been replaced by sericite during a later hydrothermal event.

Quartz-Sericite Alteration

Texture destructive sericitic alteration with a granular appearance (\sim 0.5- to 2-mm-diameter grains) in the central Buckskin Range, is restricted to the Artesia Lake Volcanics and envelops advanced argillic alteration. This type of alteration has been further subdivided into two mineral associations based on the type of mica identified via infrared spectroscopy or XRD, because it is difficult to make these distinctions in thin section. Quartz + 2M₁-muscovite (QS) and quartz + 2M₁-illite (QSI) were indicated frequently via infrared spectrometry and XRD. Based on the samples analyzed, approximately 70 % muscovite and 30 % illite were identified in this assemblage.

This alteration is quite similar to sericitic (QS) alteration in high structural levels at Ann Mason, where primary textures of the rock have been obliterated by recrystallized quartz and $2M_1$ -muscovite (Dilles and Einaudi, 1992). Sericite is used in the discussion here to discuss the general characteristics of micas detected in these assemblages.

Sericite occurs as 5-20 vol. % 50- to 100- μ m-long radiating sheaves intergrown with quartz. Pyrite and local chalcopyrite (>50:1 pyrite to chalcopyrite) occurs up to 8 vol. % as suggested by the appearance of numerous 0.1- to 0.5-mm-diameter goethite-lined cavities pseudomorphous of pyrite and rare glassy limonite textures (Figure 10d). Slightly deformed crystals of sericite are intergrown with 40- to 80- μ m-diameter euhedral quartz in vugs and fracture fillings, particularly near goethite pseudomorphs of pyrite. Sericite also occurs as 0.1- to 0.3-mm-long sheaves along clast boundaries in breccia bodies within the Artesia Lake Volcanics, as in the quartz-alunite-sericite alteration, described above.

Silexite

Hydrothermal quartz-rich (>95 vol. %) alteration zones, termed "silexites" by Anaconda geologists, occur within in the uppermost exposures of the Artesia Lake Volcanics, as 10- to 50-m-thick massive and brecciated intervals that are both concordant and discordant to sedimentary bedding (Figure 7b). In breccias, silexites contain <1- to 10-cm-diameter angular to subrounded quartz-rich clasts in both clast and matrix support in a fine-grained hydrothermally altered quartz-rich

matrix. Possible protoliths include silicified volcanoclastic breccias or conglomerates and hydrothermal eruption breccias

Silexite quartz is 10- to 50- μm -diameter. Silexite may contain up to 5 vol. % hydrous silicate minerals typical of advanced argillic or sericitic alteration assemblages, and is grouped and mapped on this basis on the alteration map (Plate B). Silexite outcrops in which no hydrous minerals have been detected via infrared spectroscopy, X-ray diffraction or petrography are designated as quartz-only alteration on the map (Plate B).

Typical AA1-altered silexite has a brecciated texture and ~ 20 vol % pore space as noted by the appearance of clasts with 10- to 50- μm -diameter quartz with coarser subhedral quartz and euhedral 30- to 200- μm -long alunite in the matrix (Figure 12a). Quartz-altered silexite contains massive, fine-grained 5- to 50- μm -diameter quartz with local vug-filling quartz and 5-7 vol. % transported goethite along fractures (Figure 12b). QSI-altered silexite consists of 10- to 200- μm -diameter quartz with ~1 vol % sheaves of illite in veinlets or fractures and locally in small vugs (Figure 12c).

Sericite-Hematite-Chlorite Alteration (SC)

Sericite-hematite-chlorite alteration is predominantly restricted to the Fulstone dacite porphyry, granite porphyry dikes, and andesite dikes. However, several exposures of Artesia andesite lavas possess sericite-hematite-chlorite alteration adjacent to advanced argillic- and quartz-sericite-bearing Artesia Lake

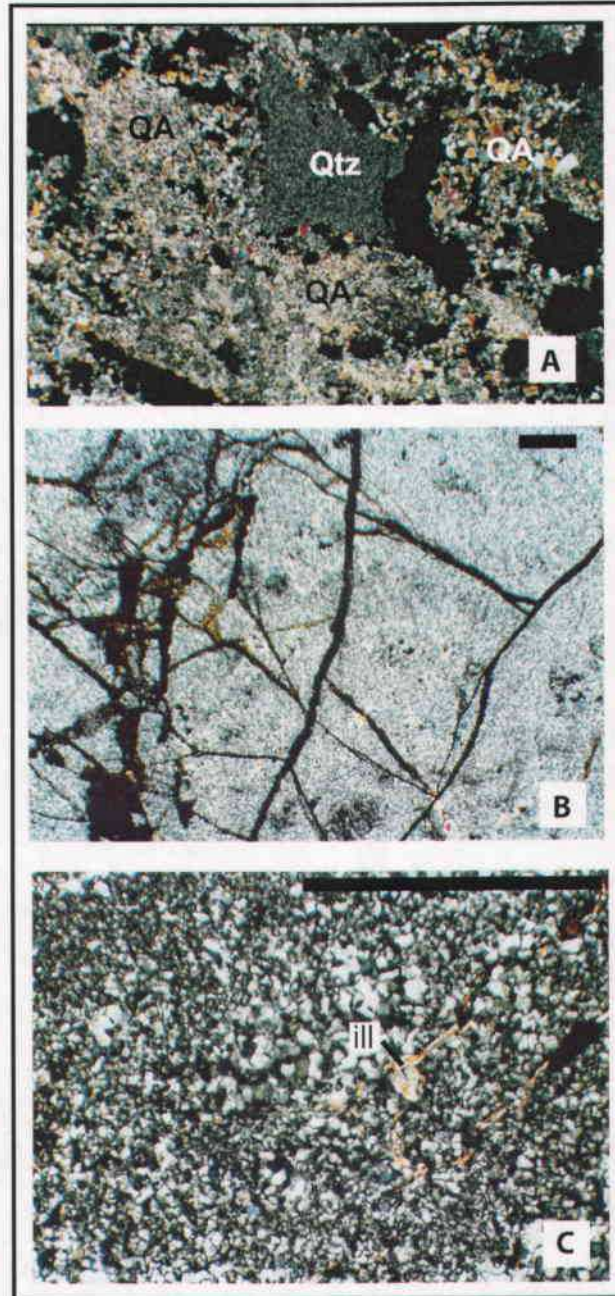


Figure 12. Photomicrographs showing common textures of silexites from the central Buckskin Range. All crossed polars. Scale bar = 0.5mm. A) Bu421. Silexite breccia with angular clasts of microcrystalline quartz (Qtz) in a vuggy matrix of massive 20-200 μm quartz and alunite (QA). B) Bu711. Massive microcrystalline quartz in fractured silexite. C) Bu664. Massive microcrystalline quartz in silexite with local sheaves of illite (ill).

exposures. This relationship suggests that some sericite-hematite-chlorite alteration may have formed contemporaneously with advanced argillic and quartz-sericite alteration, perhaps as an outer halo. Dilles and Einaudi (1992) and Dilles, Proffett, and Einaudi (2000) report a similar style of alteration in the upper levels of Ann Mason in which >50 % mafics have been chloritized and plagioclase is converted to albite and sericite outside of D-veins with quartz-sericite inner selvages and sericite outer selvages. In the central Buckskin Range exposures, primary igneous mafic minerals are altered to $1M_{1b}$ -clinochlore, quartz, sericite, hematite, minor rutile, smectite, and local pyrite. Feldspars are partially altered to quartz, sericite (muscovite or illite), albite, and local pyrite (Figure 13).

Specular hematite, up to 10 vol. %, occurs in these rocks as stockwork veins and veinlets with quartz, in selvages enveloping hematite stockwork veins, and disseminated in the groundmass with local pyrite. Sulfide is far less abundant here than in quartz-sericite-pyrite altered rocks. Where prominent evidence for, hypogene sulfide occurs as goethite-lined pyrite cavities or veinlets typically no more than 3 vol. % and anomalously up to 8 vol. %. Specular hematite, as 1- to 2-cm-wide, NE-striking stockwork veins with minor pyrite have inner selvages that typically contain pervasive microgranular quartz and sericite and 3-7 vol. % disseminated hematite in the groundmass (Figure 14). In the outer selvages, 20-30 vol. % of primary igneous mafic minerals is altered to quartz and chlorite, 25-50 vol. % of plagioclase is altered to quartz and sericite, and alkali feldspar has been

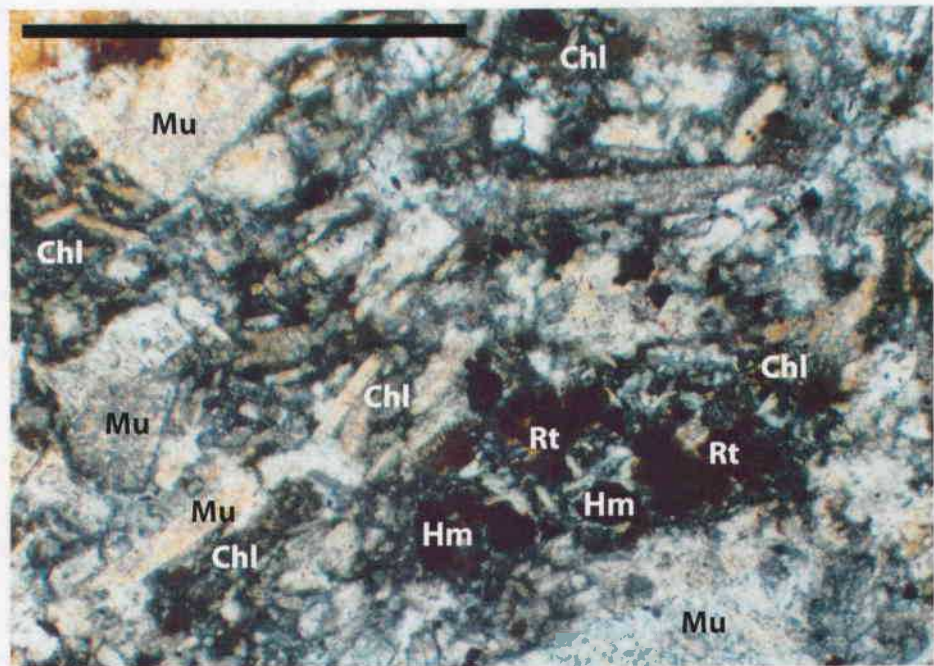


Figure 13. Photomicrograph with crossed polars showing common textures of sericite-hematite-chlorite alteration (SC). Bu538. Fulstone dacite porphyry (Jfd) with feldspars partially altered to muscovite (Mu) and mafics altered to chlorite (Chl), specular hematite (Hem), and rutile (Rt). Approximately half of groundmass is altered to chlorite. Scale bar = 0.5mm.

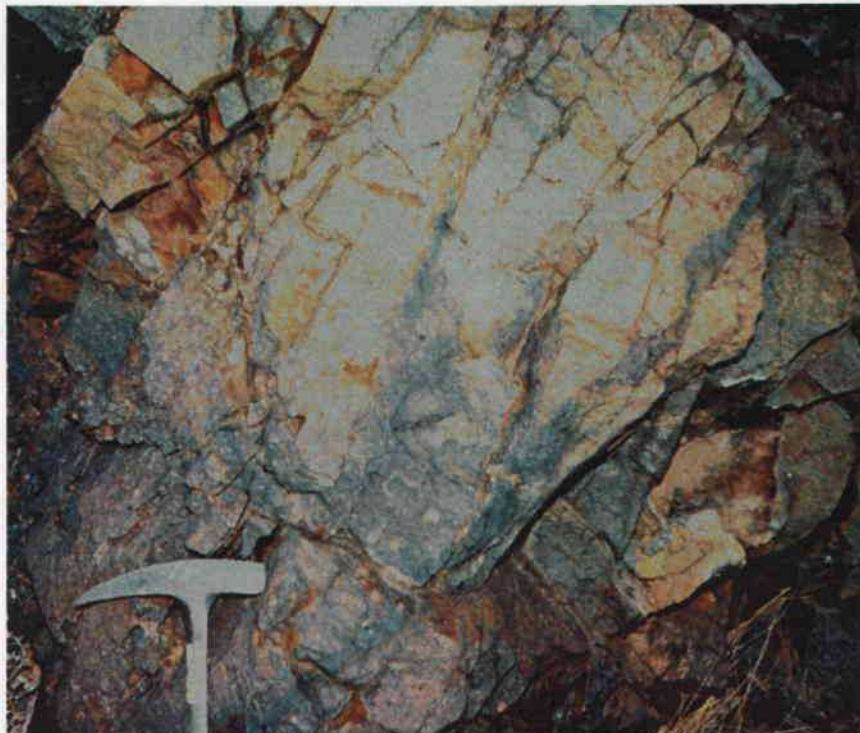


Figure 14. Outcrop with specular hematite veins cutting latite porphyry dike. Hematite veins have specular hematite + sericite selvages that grade outward into sericite-hematite-chlorite altered rock.

converted to albite with sericite. Beyond the stockwork veins, up to 25 vol. % of the stable alkali feldspar in the groundmass of the granite porphyry contains fine-grained sericite with 1-2 vol. % 40- to 100- μm -diameter goethite-lined boxworks. Mafics and feldspars are partially to completely replaced by quartz, sericite, and pyrite.

Hematite-Magnetite-Au-Cu Veins

Most of the ore-grade mineralization in the Buckskin Range is concentrated in Au-Cu-bearing lodes or veins and fractures that are apparently younger than and cut across high-level sericitic and advanced argillic assemblages. Au-mineralization, although highly erratic, has been discovered in 1975 in several 0.3- to 1 m-thick zones of Anaconda drill core with assay values of 0.7-500 gpt Au (Dilles and Wendell, 1982). Au is always associated with chlorite + pyrite \pm magnetite \pm quartz \pm gypsum \pm chalcopyrite veins that cut feldspar-stable altered Jurassic rocks, similar to the WNW-striking, steeply-dipping Buckskin lode gold vein that has been mined in the southern Buckskin Range (Gibson, 1987). Lode-vein-type Au mineralization in the central Buckskin Range has only been observed cutting the Artesia Lake Volcanics and base of the Fulstone Spring Volcanics. These field and drill core observations coupled with a strong correlation between Au and Cu from assay data suggests that Au mineralization is Jurassic in age

(Dilles and Wendell, 1982). District wide porphyry Cu-mineralization is associated with the intrusion of the Yerington batholith (Dilles, 1987; Dilles and Proffett, 1995).

One 0.5- to 1-m-wide vein containing massive specular hematite, quartz, pyrite, magnetite, and minor chalcopyrite occurs along a steeply-dipping brecciated fault zone striking N85°E in the central Buckskin Range (hydrothermal vein, Plate A). This lode is similar to the massive lode/vein mineralization that has been extracted from the Buckskin Mine, except it contains more hematite than magnetite. Massive specular hematite occurs up to 90 vol. % in these veins with local interstitial 1- to 5-mm-long aggregates of radiating muscovite crystals. A bulk sample from a prospect located near an east-west striking Jurassic fault contained 2.38 wt. % Cu and ~0.01 oz/ton Au (Plate A, Dilles and Wendell, 1982). Here, massive specular hematite with minor magnetite contains 1-2 vol. % chalcopyrite pseudomorphs in addition to transported chrysocolla up to 5 vol. % on surfaces and fractures.

Feldspar-Stable Chlorite-Calcite-Hematite Alteration (P)

The Fulstone quartz latite and dacite lava flows and Fulstone sedimentary units possess weak to moderate propylitic alteration minerals in which plagioclase crystals are partially converted to sericite (illite) and albite and alkali feldspar phenocrysts are partially replaced by sericite. Primary igneous mafic minerals are partially to completely altered to quartz, 1M_{1b}- clinocllore, and calcite, with minor

smectite, and locally magnetite (Figure 15). A paucity of sulfides in the Fulstone Spring Volcanics suggests these volcanics post-date the main introduction of sulfur to the porphyry copper system.

The groundmass of typical quartz latite lavas contains 3-5 vol. % 50- to 100- μm -long specular hematite, trace disseminated 10- to 50- μm -diameter weathered pyrite, and microcrystalline alkali feldspar that has been partially replaced by sericite. Magnetite occurs locally in the groundmass and mafic sites and is partially replaced by hematite along grain boundaries and octahedral partings or is entirely replaced by hematite with minor rutile. Calcite occurs as 5-10 vol. % 0.1 to 0.3-mm-diameter euhedral crystals in mafic sites and small vugs locally within the lava flows and pervasively among the matrix of Fulstone sedimentary breccias and conglomerates. Epidote occurs sparsely within the lavas up to 5 vol. % as stringers and in plagioclase sites.

Isotopic Composition of Minerals

Hydrogen and Oxygen Isotopes

Isotopic compositions of waters calculated to be in equilibrium with muscovite and pyrophyllite from the Artesia Lake Volcanics from the Buckskin Range are shown with calculated waters from the Ann-Mason, MacArthur, and Blue Hill areas of the Yerington district (Figure 16, Dilles et al., 1992, J.H. Dilles, unpublished data, 2001). Sericitic, propylitic, and sodic-calcic isotopic

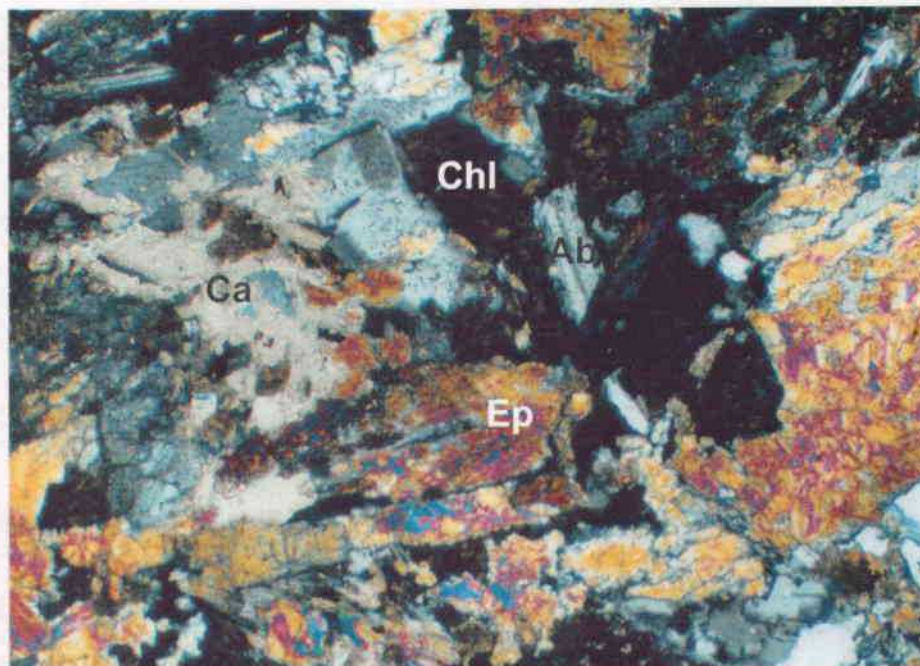


Figure 15. Photomicrograph with crossed polars of feldspar-stable calcite-chlorite hematite (P) altered Fulstone volcaniclastic sandstone (Jfs, #Bu551). Plagioclase is altered to albite (Ab), sericite, epidote (Ep), and calcite (Ca). Calcite partially replaces the groundmass. Mafic grains are completely altered to epidote, chlorite (Chl), and calcite with trace magnetite and rutile. Scale bar = 0.5 mm.

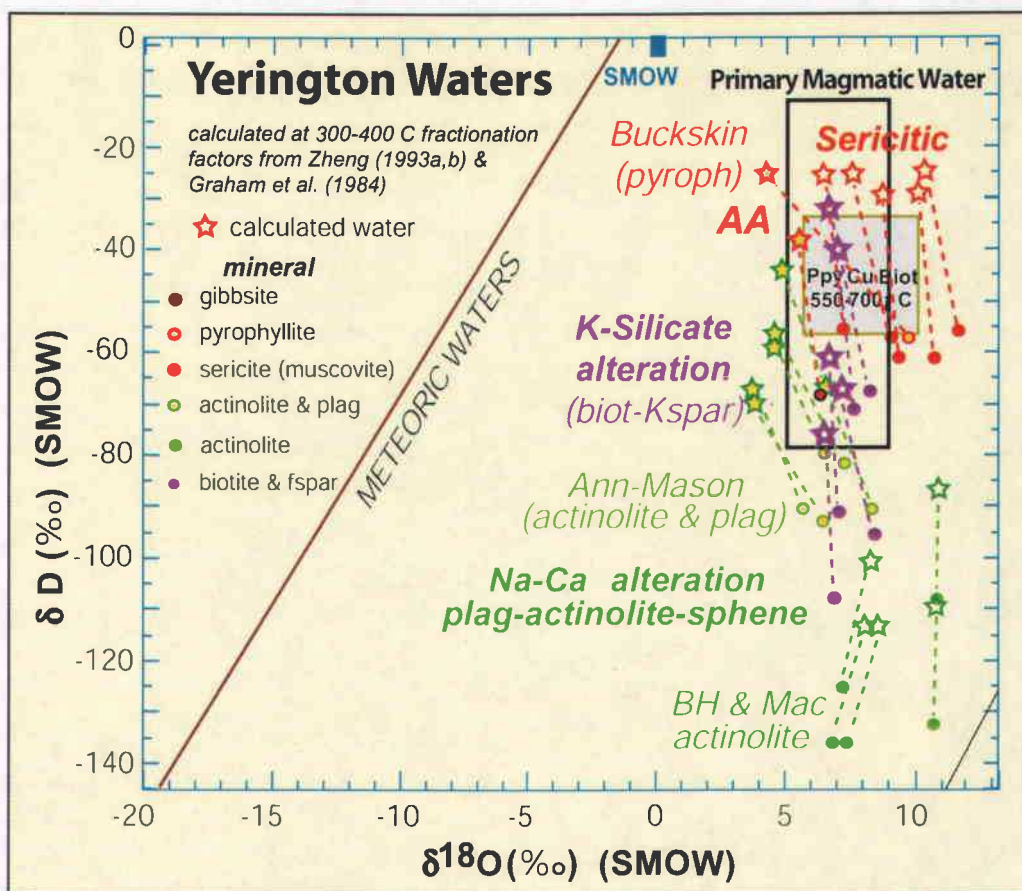


Figure 16. Calculated isotopic compositions of water in equilibrium with alteration minerals. Ann-Mason, MacArthur (Mac), and Blue Hill (BH) data from Dilles et al. (1992) and J. H. Dilles (2001, unpublished data). Sericitic alteration data has been recalculated at 300°C and 350°C. See Table 1 for calculations. AA = advanced argillic.

compositions have been recalculated for temperatures of 350°C, 350°C, and 400°C, respectively (Table 1). Estimated temperatures of alteration minerals stem from mineral phase equilibria (Meyer and Hemley, 1967) and fluid inclusion data (Dilles, 1984; Dilles, 1987; and Dilles and Einaudi, 1992). The $^{18}\text{O}/^{16}\text{O}$ and D/H fractionation factors for calculations have been derived from Zheng (1993a,b) and Graham et al. (1984).

Muscovite for isotopic analysis was handpicked from a sample of quartz-sericite altered Jas from the central Buckskin Range. Pyrophyllite was handpicked from a sample of Jaa containing abundant quartz + alunite + pyrophyllite. The measured $\delta^{18}\text{O}$ isotopic values for muscovite and pyrophyllite are 11.8 and 9.8 per mil, respectively; D/H analyses give values of -56 and -59 per mil. The Yerington data for fresh rock and potassic (K-silicate) alteration have values that fall within the magmatic water range. Sodic-calcic altered samples typically plot outside of the magmatic water box, indicating formation by fluids external to porphyry copper fluids. Sericitic alteration at Ann Mason and QS alteration fluids in the Buckskin Range have near-magmatic values for $\delta^{18}\text{O}$ and δD . Data from pyrophyllite show slight but distinct enrichment in δD and depletion of $\delta^{18}\text{O}$ relative to magmatic water, suggesting a mixed-fluid origin for some advanced argillic alteration assemblages.

Table 1. Oxygen and Hydrogen Isotopic Compositions of Minerals*

Sample no.	Alteration	Mineral	measured isotopic values			calculated waters		
			$\delta^{18}\text{O}$ (‰, SMOW)	D/H (‰, SMOW)	H ₂ O (wt%)	T(°C)	$\delta^{18}\text{O}$ (‰, SMOW)	D/H (‰, SMOW)
Bu714	QS	musc	11.8	-56	4.02	300	10.4	-24
Bu297	AA1	pyroph	9.7	-59	6.06	300	4.3	-25
YD01-21B	AA1	gibbsite	6.3	-52	4.97	350	5.7	-39
YD01-22B	sericitic	mica	7.1	-52	4.97	350	6.5	-26
14JD91B	sericitic	mica	9.2	-56	7.52	300	7.7	-25
Y-694C	sericitic	mica	10.7	-61	3.91	350	10.1	-29
100JD87	sericitic	mica	9.3	-61	1.53	350	8.7	-29
YD01-07-B	prop-actin	actinolite	10.9	-112.7	1.97	300	10.9	-86
348FJD93	prop-actin	actinolite	7	-143.8	1.97	400	8.1	-114
86E-JD94	prop-actin	actinolite	7.3	-135.1	1.87	400	8.4	-102
85G-JD94	prop-actin	actinolite	10.8	-145.017	1.94	300	10.7	-110
Y-307	propylitic	act/plag	6.6	-92	1.96	350	3.9	-69
Y-793	propylitic	act/plag	7.2	-82	1.66	350	4.5	-59

* not including K-silicate and Na-Ca data from Ann Mason (Dilles et al., 1992)

Sulfur Isotopes

Isotopic analyses were performed on 3 samples of alunite or jarosite from advanced argillically-altered Artesia Lake rocks (Table 2). Isotopic compositions of sulfates from the central Buckskin Range yielded values of +8.84 ‰ for alunite, +6.55 ‰ from jarosite>alunite, and +8.72 ‰ for the alunite>jarosite mixture. A sample of pyrite collected from the Buckskin Au-Cu vein yielded a $\delta^{34}\text{S}$ value of -4.7 ‰ (Figure 17). In comparison, chalcopyrite and pyrite from the Ann-Mason porphyry copper deposit have $\delta^{34}\text{S}$ values that range from -7 to 0 ‰, and +10 to +14 ‰ for gypsum replacing hydrothermal anhydrite. Samples of sedimentary gypsum and diagenetic pyrite from the Triassic-Jurassic sedimentary section at Yerington yield values of 19.3 ‰ and -3.8 ‰, respectively (Dilles and Field, 1996). The sulfur isotopic composition of oceanwater and evaporates from the Jurassic typically give values of ~ +18 ‰ (Ohmoto and Rye, 1979).

These data suggest that the source of sulfur for Yerington porphyry copper sulfides is primarily of magmatic-hydrothermal origin (Dilles and Field, 1996). A sulfate mineral that is derived from the weathering of a sulfide would have the isotopic composition near that of the sulfide in which the SO_4^{-2} was derived (Field, 1966). The isotopic value for alunite is slightly lighter than typical porphyry copper sulfates, likely owing to a mixture of magmatic-hydrothermal sulfate with a lesser amount of sulfate derived from supergene weathering of hydrothermal sulfides. The sample of mainly jarosite has a similar value, though slightly lighter,

Table 2. Isotopic Compositions and Sample Descriptions of Sulfates Measured for Sulfur Isotopes

Sample #	Assemblage	Rock Type	% Jarosite	% Alunite	Description	X _{Al}	δ ³⁴ S (‰)
Bu036c*	AA3	"goethite" bx	5	20	clast of AA1 alt. rock in goeth rock flour matrix, 15-40µm dissem alun in clast	81%	8.72
Bu036m**	AA3	"goethite" bx	40	10	<10µm jar in goeth matrix, 10-30µm alun frags in matrix	79%	6.55
Bu185	AA1	Jai	3	30	20-100µm dissem alun, <10µm jar in fractures	92%	8.84

* clast

** matrix

Table 2. Isotopic Compositions and Sample Descriptions of Sulfates Measured for Sulfur Isotopes

Sample #	Assemblage	Rock Type	% Jarosite	% Alunite	Description	X _{Al}	δ ³⁴ S (‰)
Bu036c*	AA3	"goethite" bx	5	20	clast of AA1 alt. rock in goeth rock flour matrix, 15-40µm dissem alun in clast	81%	8.72
Bu036m**	AA3	"goethite" bx	40	10	<10µm jar in goeth matrix, 10-30µm alun frags in matrix	79%	6.55
Bu185	AA1	Jai	3	30	20-100µm dissem alun, <10µm jar in fractures	92%	8.84

* clast

** matrix

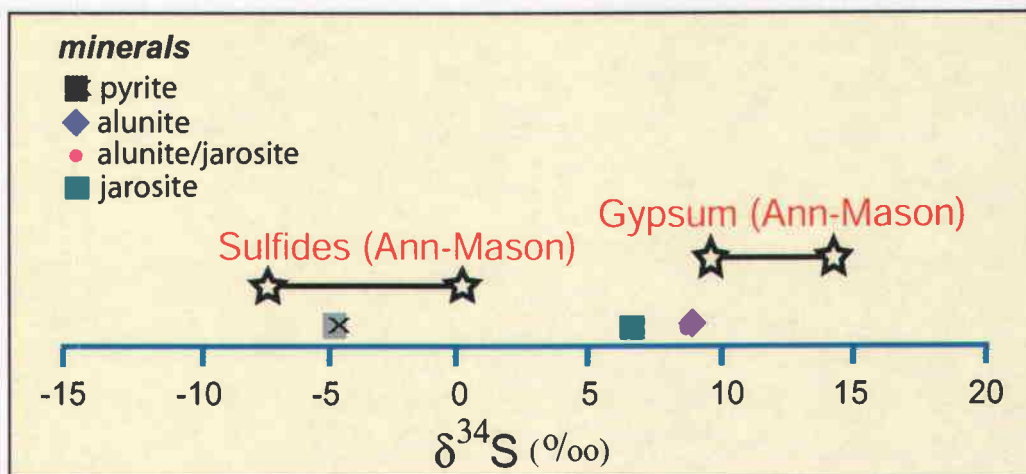


Figure 17. Plot of isotopic composition of sulfates and pyrite from the central Buckskin Range with ranges of magmatic-hydrothermal sulfides and sulfates from the Ann-Mason porphyry copper deposit at Yerington. Data except for Buckskin Range sulfates borrowed from Dilles, unpublished data, and Dilles and Field, 1996.

suggesting that it also contains a mixture of SO_4^{-2} derived from hypogene sulfates and the weathering of pyrite. As discussed previously, the samples were collected from highly oxidized and weathered surfaces and may contain supergene jarosite and up to 3 vol % supergene alunite, resulting in an isotopic value with a slight negative shift.

Discussion and Conclusions

The Origin of Alunite

Alunite that is produced by magmatic hydrothermal alteration is generally 10 to 200 μm in size and may occur as disseminations in microgranular quartz (Thompson, 1990; Thompson and Thompson, 1996). Alunite formed by near-surface steam-heating or supergene acid-leach fluids is commonly $<15 \mu\text{m}$ and has a massive porcelaneous appearance (Thompson, 1990, Thompson and Thompson, 1996, Ebert, 1997). In the Buckskin Range, alunite is 15- to 200- μm -long and occurs disseminated within 10- to 50- μm -diameter quartz and in aggregates pseudomorphing tabular 0.5- to 2-mm-long igneous plagioclase phenocrysts. This mode of occurrence suggests hypogene formation. Surface exposures in the central Buckskin Range have been affected by intense supergene weathering as all primary sulfides have been completely oxidized. However, alunite occurs with unoxidized pyrite in the southern Buckskin Range, as reported by Hudson (1983). A sulfur isotope value of +8.84 ‰ for Buckskin Range alunite is slightly lighter than the 10-

14 ‰ values derived from magmatic-hydrothermal sulfates at the Ann-Mason porphyry copper deposit, likely as a result of jarosite in the mixture. A magmatic-hydrothermal source of sulfur for the formation of alunite is suggested by this isotopic value, however.

Hydrothermal Conditions

Magmatic Fluids

During the early-stages of magmatic-hydrothermal evolution of the Yerington porphyry copper system, low pH, high sulfidation fluids, introduced by early fluid-rich porphyry dikes of the Yerington batholith, were responsible for hypogene sulfide-rich quartz-alunite-pyrophyllite alteration and high-level quartz-sericite alteration. Hydrogen and oxygen isotopes suggest these fluids were magmatic-dominated.

Pyrophyllite stability in quartz-saturated environments at 1 kbar ranges from ~250 to 380 °C (Hemley et al., 1980). In the central Buckskin Range, pyrophyllite occurs in the quartz-alunite-pyrophyllite assemblage with local dickite and where alunite is hypogene, as discussed above. Dickite is stable at lower temperatures, higher hydrostatic pressure, and a lower silica activity relative to pyrophyllite so the formation of dickite with pyrophyllite suggests a possible temporal evolution from high to low temperature at a constant K^+/H^+ ratio (Figure 18). Conversely, pyrophyllite may also result from weak contact metamorphism if

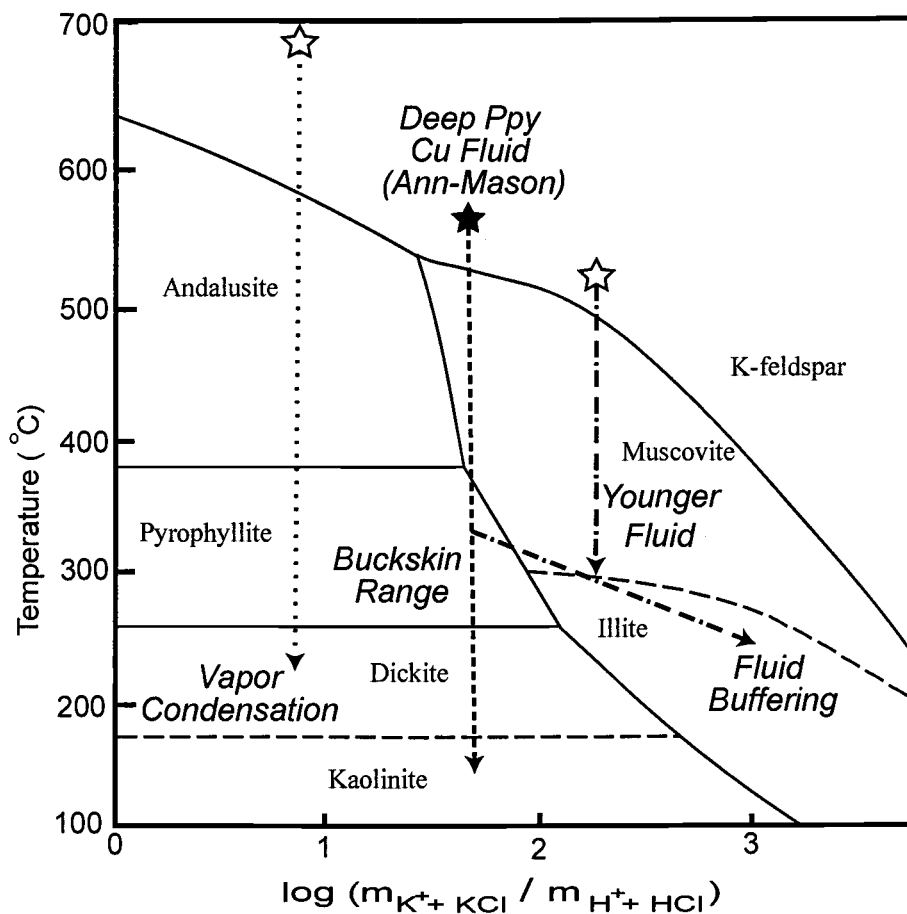


Figure 19. Mineral stability in the $K_2O-Al_2O_3-SiO_2$ system as a function of molar $K + KCl/H + HCl$ vs. temperature at 1 kbar for early-stage fluids at Yerington. The cooling path is indicated by a dashed arrow through the muscovite-stability field at a constant K/H ratio, forming pyrophyllite, dickite and kaolinite. Vapor condensation from magmatic fluids at depth would result in a lower K/H ratio causing the formation of andalusite, pyrophyllite, dickite, and kaolinite upon cooling (open star with dotted arrow). An influx of K^+ from a younger deep-seated fluid or a decrease in K/H activities due to the reaction of fluids with the surrounding wallrock would shift the pyrophyllite stable fluid to muscovite and/or illite upon cooling (dotted and dashed arrow). After Montoya and Hemley (1975) and Hemley et. al. (1980).

the rocks contained a significant amount of kaolinite and quartz at the time of late porphyry and andesite intrusions. This possibility is unlikely however as pyrophyllite is widely distributed in the Artesia Lake Volcanics and does not solely occur adjacent to intrusions.

The absence of andalusite in the central Buckskin Range and the formation of pyrophyllite with dickite indicates that magmatic vapors condensed in this shallow level environment at temperatures below $\sim 380^{\circ}\text{C}$ to produce advanced argillic alteration (Figure 18). Unfortunately, most hydrothermal minerals in the Artesia Lake Volcanics lack abundant primary fluid inclusions, however, several primary vapor-and-liquid-rich, CO_2 -bearing inclusions have been petrographically observed in alunite. Several low-salinity liquid-rich inclusions with homogenization temperatures of $300\text{-}350^{\circ}\text{C}$ have been identified in quartz-tourmaline veins and breccias with sericitic selvages from the upper levels of the Blue-Hill area, 1.5-2 km depth and immediately underlying the central Buckskin environment, which suggests that some late, low-salinity magmatic fluids bypassed the brine-vapor solvus, and ascended to shallow depths as an acidic fluid (J.H. Dilles, unpublished data, 2002).

After structural restorations are completed, the intense sericitic alteration in the Artesia Volcanics is spatially continuous with quartz-added sericitic (QS) alteration in the upper exposures of the Ann-Mason porphyry copper deposit and the Blue Hill fault block of the Singatse Range. The paragenetic relationship between advanced argillic and quartz-sericite alteration is petrographically

ambiguous, however, due to a lack of clear cross-cutting vein relationships in the central Buckskin Range.

Phase-stability relations indicate that advanced argillic alteration may have formed prior to quartz-sericite alteration as muscovite replaces pyrophyllite along rims and cleavage planes. Electron microprobe analyses reveal that muscovite that replaces pyrophyllite and muscovite from quartz-alunite-sericite alteration have nearly identical $K/K+Na$ ratios of ca. 0.9 (Appendix B). Petrographic relations also show a similarity in grain-size and crystal habit between coarse-grained pyrophyllite and muscovite in advanced argillically altered rocks. It is therefore a possibility that the quartz-alunite-sericite assemblage (AA3) may have resulted from the replacement of pyrophyllite by muscovite.

For the change from pyrophyllite to sericite stability to occur, the $\Sigma K^+/\Sigma H^+$ activity ratio of hydrothermal solutions must have increased with time at relatively constant temperatures (Figure 18). This could result from the buffering of magmatic-hydrothermal solutions due to interaction with the surrounding wallrock as water-to-rock ratios decrease or from a deeper source of magmatic fluids with time (Dilles and Einaudi, 1992). Fluid buffering may have occurred due to interaction with stable feldspars in the porphyry copper environment at depth. Another possibility may be that highly-acidic fluids responsible for advanced argillic alteration mixed with circulating sedimentary brines with high $\Sigma K^+/\Sigma H^+$ activity ratios as a result of alkali exchange from sodic-calcic alteration and rock buffering. The latter scenario may be more likely because the initial formation

of pyrophyllite would imply total depletion of alkali components from the wallrock, leaving insufficient amounts of residual alkalis for fluid buffering.

Sulfide-poor, sericite-hematite-chlorite alteration formed outward of advanced argillic zones as these highly-acidic, magmatic-dominated fluids became partly neutralized by wallrock reaction. It is also likely that late porphyry dikes that intruded the advanced argillic and sericitically altered rocks did not generate enough magmatic fluid with sulfur and acid to produce advanced argillic alteration. Future studies could benefit from a more detailed geochemical and stable isotope analyses to determine if the fluids that produced sericite-hematite-chlorite alteration within late porphyry dikes are indeed magmatic-dominated.

Non-Magmatic Fluids

A second type of fluid responsible for district-wide hydrothermal alteration are moderate-temperature, saline brines derived from formation waters trapped in Triassic-Jurassic sediments (Dilles and Einaudi, 1992; Dilles et al., 1992; Dilles et al., 1995). These fluids were most likely heated by intrusion of the batholith and circulated through the porphyry dikes and parallel fractures to produce Na-Ca alteration at depth and feldspar-stable chlorite-calcite-hematite alteration in the upper part of the Yerington batholith and the Fulstone Spring Volcanics. Whole-rock geochemical analysis indicates that several samples of Fulstone dacite lavas contain elevated K_2O values up to 4.5 wt %, and are relatively depleted in Na_2O , suggesting that potassium may have been added to the rocks (J.H. Dilles,

unpublished data, 1991). Potassic alteration in the Fulstone section may have formed as a result of low temperature alkali exchange caused by cooling and rising Na-rich, sodic-calcic hydrothermal fluids. Alternatively, potassium-enriched surface fluids may have been recycled from circulating meteoric waters in an evaporitic environment from the underlying Jurassic evaporites (M.D. Barton, personal communication, 1999).

It is possible that these brines were additionally responsible for the hematite-magnetite-Au-Cu lodes that cross-cut advanced argillic and sericitic alteration in the Buckskin Range as they cooled upon ascension and reacted with adjacent wall rocks when they exited the system through steeply-dipping fractures in the Buckskin Range (Dilles et al., 2000). Chemical composition data of J. H. Dilles (unpublished data), Carten (1987), Dilles and Einaudi (1992), and Dilles et al. (1995) indicates that rocks affected by Na-Ca alteration in the deeper porphyry copper environment contain depleted levels of Fe, Cu, and K which supports the idea that sedimentary brines leached these components and carried them to shallow levels where Au-Cu deposition may have occurred due to cooling and wall-rock reaction.

Time-Space Evolution of Hydrothermal Fluids in the Central Buckskin Range

District-wide hydrothermal alteration and ore deposition has evolved from two different types of fluids; the Buckskin Range served as an outflow zone for these fluids (Lipske and Dilles, 2000; Dilles et al., 2000). The age of advanced argillic and sericitic alteration in the Buckskin Range is constrained to be older than the sericite-hematite-chlorite-altered granite porphyry dike that cross-cuts the pyrite-rich rocks of the Artesia Lake sequence. The abundance of sulfides up to 10 vol. % in the Artesia Lake Volcanics suggests that high-level alteration may be contemporaneous with the main event of sericitic alteration and pyrite deposition in the deeper porphyry copper environment. The paucity of sulfides in the Fulstone Spring Volcanics suggests that the Fulstone Spring Volcanics post-date the main introduction of sulfur to the porphyry copper system.

At depth, magmatic-hydrothermal fluids separated from the crystallizing Luhr Hill granite phase of the Yerington batholith and flowed upward through vertical hydrofractures (Dilles, 2002). These fluids were responsible for main-stage Cu-Fe-sulfide and skarn mineralization and K-silicate alteration in the central core of the porphyry deposits near the granite cupola, and resulted in pyrite-rich sericitic (QS) and advanced argillic alteration along an axial zone up through the Buckskin Range (Figure 19a). Here, quartz-sericite alteration was formed outward and below advanced argillic alteration as inferred by the position of quartz-sericite-pyrite alteration at Blue Hill and the upper levels of the Ann Mason porphyry copper deposit. Hydrogen and oxygen isotope data from this study suggests that upon

Figure 19. Generalized north-south cross-section through the central Buckskin Range depicting the evolution of volcanism and hydrothermal alteration in four successive time frames. Arrows represent flow paths of hydrothermal fluids generated from the underlying Yerington porphyry copper system. A) Fluid-dominated hydrothermal conditions. Incursion of magmatic fluids from the crystallizing batholith with meteoric water. Formation of silicites, advanced argillic and quartz-sericite alteration outward and downward to SC alteration and "propylitic" alteration as a result of fluid buffering. B) Formation of Fulstone dacite porphyry and intrusion of granite porphyry dikes and SC alteration. Lower magmatic fluid input. C) Waning of magmatic fluids. Erosion, deposition of basal Fulstone sediments. Latite/dacite porphyry dike intrusions with SC alteration. Formation of basal Fulstone lavas with Feldspar-stable calcite-chlorite-hematite alteration as a result of circulating sedimentary brines. D) Faulting and formation of Au-Cu-hematite-magnetite lodes as Na-Ca alteration fluids from deeper porphyry copper environment exited the system. Continuing formation of Fulstone lavas with Feldspar-stable calcite-chlorite-hematite alteration.

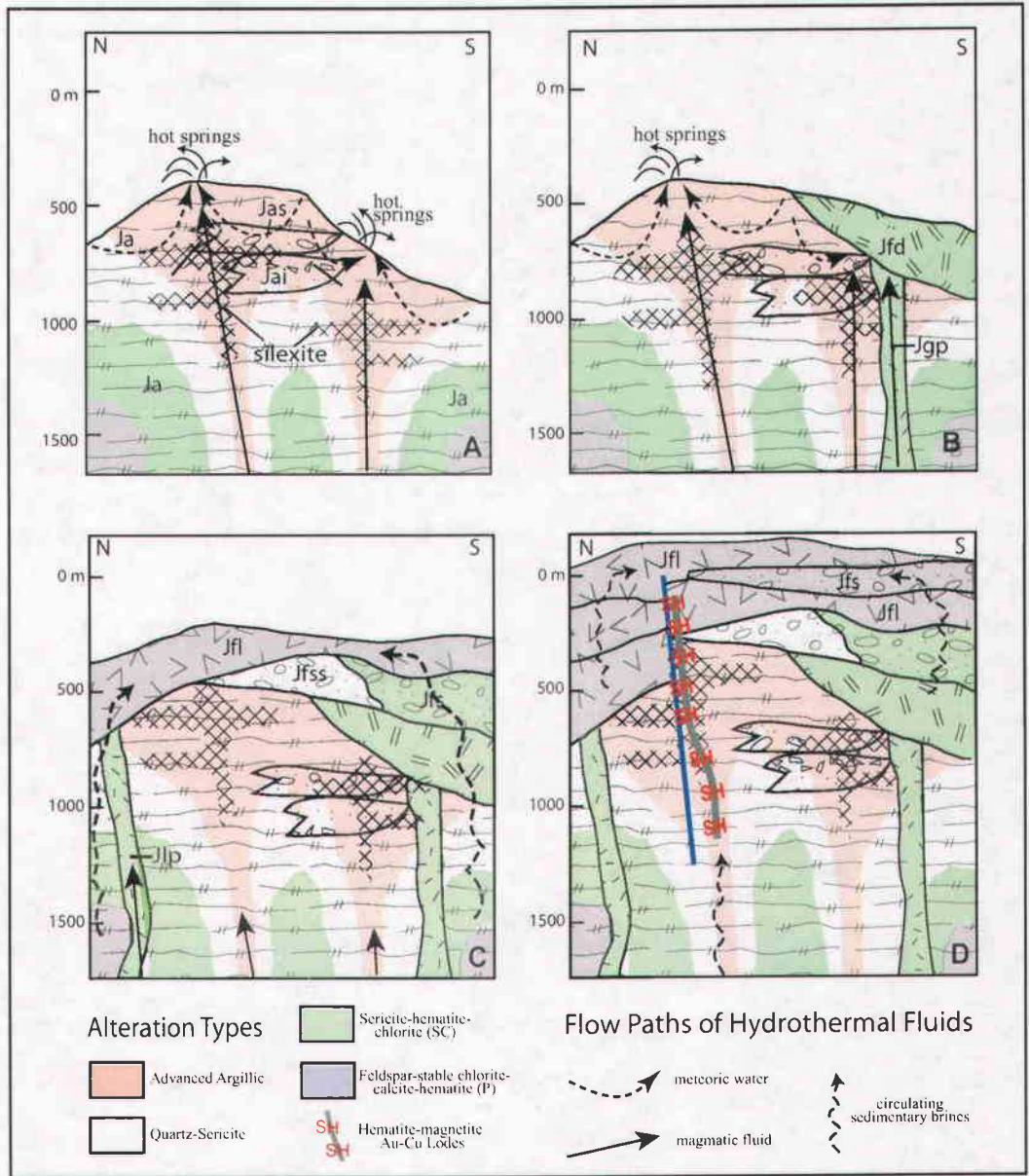


Figure 19

ascension, these fluids cooled, condensed, and may have mixed with minor amounts of meteoric water at shallow levels to produce advanced argillic alteration. As these fluids neutralized upon reaction with the surrounding andesitic lavas, sericite-hematite-chlorite alteration was produced outward from quartz-rich advanced argillic inner zones and intermediate sericitic alteration.

Fluid flow paths for low-pH hydrothermal solutions responsible for advanced argillic alteration are inferred by the occurrence of silexites as all alkalis in these zones have been completely leached from the rock. The discordant and concordant nature of these bodies relative to sedimentary bedding in the Artesia Lake Volcanics and local matrix-supported, non-bedded horizons of silexites suggests some of these zones may have originated as hydrothermal breccias as well as silicified volcanoclastics, as discussed previously. Due to hydrothermal brecciation and the high permeability of volcanoclastic units and ignimbrites, silexites likely have provided conduits that directed the upward and lateral flow of hydrothermal fluids.

Several new pulses of magma created granite porphyry dikes that cross-cut the advanced argillic and quartz-added sericitic alteration (Figure 19b). These later dikes had a lower sulfide-content as suggested by the occurrence of sericite-hematite-chlorite alteration with rare sulfides which may indicate that these dikes were not accompanied with enough magmatic fluids to produce silica- and sulfide-rich assemblages. Concomittant or slightly later latite porphyry dikes, possibly feeders of the Fulstone latite lava flows due to petrographic similarities, cut across

advanced argillic and sericitic alteration and have been partly altered to sericite, hematite, and chlorite with relict feldspars (Figure 19c). Magmatic activity waned as hydrothermal fluids became dominated by formation brines derived from the Triassic and Jurassic sedimentary section that circulated through the magmatic-hydrothermal system upon intrusion of the Yerington batholith, contributing feldspar-stable chlorite-calcite-hematite alteration to the overlying Fulstone lavas.

Jurassic faulting focused hydrothermal fluid flow that led to the deposition of Au-Cu-hematite-magnetite vein mineralization along east-west striking faults that cross-cut the base of the Fulstone Spring Volcanics. These may have been an exit for circulating sedimentary brines responsible for Na-Ca alteration at depth (Figure 19d). The eruption of the Fulstone latite-dacite lavas continued after cessation of faulting and Cu-Fe vein deposition along with periods of erosion resulting in interbedded latitic/dacitic volcanoclastic units. These upper Fulstone Spring units also contain feldspar-stable chlorite-calcite-hematite alteration in the overlying Fulstone lavas and interbedded sedimentary units owing to the continuation of circulating sedimentary brines.

References

- Brimhall, G., 1999, Digital mapping workshop: Presented at Geological Society of America, Cordilleran Section, Berkeley, California, Earth Resources Center, Berkeley, University of California, 72p.
- Burnham, C. W., Magmas and Hydrothermal Fluids, 1979, Hydrothermal alteration: *in* Barnes, H. L., ed., *Geochemistry of Hydrothermal Ore Deposits*, 2nd ed.: New York, Holt, Reinhart, and Winston, p. 71-136.
- Carten, R. B., 1987, Sodium-calcium metasomatism: Chemical, temporal, and spatial relationships at the Yerington, Nevada, porphyry copper deposit: *Economic Geology*, v. 81, p. 1495-1519.
- Dilles, J. H., 1987, Petrology of the Yerington Batholith, Nevada: Evidence for evolution of porphyry copper ore fluids: *Economic Geology*, vol. 82, p. 1750-1789.
- Dilles, J. H., 2002, Magmatic-hydrothermal fluids: A summary of temporal and spatial evolution from the 6 km vertical transect of the porphyry copper systems in the Yerington batholith, Nevada, *Abstracts with Programs - GSA Cordilleran Section*, vol. 34, no. 5, p. 15.
- Dilles, J. H., and Einaudi, M. T., 1992, Wall-rock alteration and hydrothermal flow paths about the Ann-Mason porphyry copper deposit, Nevada- A 6 km vertical reconstruction: *Economic Geology*, v. 87, p. 1963-2001.
- Dilles, J. H., and Field, C. W., 1996, Sulfur geochemistry of porphyry copper deposits as a record of magma degassing; data from the Yerington District, Nevada, *Abstracts with Programs - Geological Society of America*, 28, no. 7, p. 93.
- Dilles, J. H., and Proffett, J. M., 1991, Roadlog to the geology of the Yerington porphyry copper district: *Geologic Society of Nevada, The geology and ore deposits of the Great Basin, Reno, NV, Field trip guidebook compendium*, v. 2, p. 1001-1013.
- Dilles, J. H., and Proffett, J. M., 1995, Metallogensis of the Yerington Batholith, Nevada: *in* Pierce, F.W., and Bolm, J.G., eds., *Porphyry Copper Deposits of the American Cordillera: Arizona Geological Society Digest 20*, 1995, p. 306-315.

- Dilles, J. H., and Proffett, J., and Einaudi, M. T., 2000, Magmatic and hydrothermal features of the Yerington batholith with emphasis on the porphyry Cu(Mo) deposit in the Ann-Mason area, Society of Economic Geologists Guidebook Series, v. 32, p. 67-89.
- Dilles, J. H., and Wendell, D., 1982, The geology and gold mineralization of the central Buckskin Range, Douglas County, Nevada: Unpublished report, Anaconda Co., 27 p.
- Dilles, J. H., and Wright, J. E., 1988, The chronology of early Mesozoic arc magmatism in the Yerington district of western Nevada and its regional implications: Geological Society of America Bulletin, v. 100, p. 644-652.
- Dilles, J. H., Einaudi, M. T., Proffett, J. M., and Barton, M. D., 2000, Overview of the Yerington porphyry copper district: Magmatic to Nonmagmatic Sources of Hydrothermal Fluids: Their flow paths and alteration effects on rocks and Cu-Mo-Fe-Au ores: Society of Economic Geologists Guidebook Series, v. 32, p. 55-66.
- Dilles, J. H., Solomon, G. C., Taylor, H. P., and Einaudi, M. T., 1992, Oxygen and hydrogen isotope characteristics of hydrothermal alteration at the Ann-Mason porphyry copper deposit, Yerington, Nevada: Economic Geology, v. 87, p. 44-63.
- Field, C. W., 1966, Sulfur isotopic method for discriminating between sulfates of hypogene and supergene origin: Economic Geology, v. 61, p. 1428-1435.
- Gibson, P. C., 1987, Geology of the Buckskin Mine, Douglas County, Nevada: Unpublished master's thesis, University of Nevada-Reno, 214p.
- Glasmann, J. R., 1999, GEO479/579 Procedures for clay mineral separation: Oregon State University, unpublished, 5p.
- Graham, C. M., Harmon, R. S., and Sheppard, S. M. F., 1984, Experimental hydrogen isotope studies-hydrogen isotope exchange between amphibole and water: American Mineralogist, v. 69, p. 128-138.
- Hauff, P.L., 1993, SPECMIN™ Mineral Identification System and Spectral Library, v. 1 & 2.: Spectral International, Inc., Arvada, Colorado.
- Hedenquist, J. W., and Lowenstern, J. B., 1994, The role of magmas in the formation of hydrothermal ore deposits: Nature, vol.. 370, p. 519-527.

- Hedenquist, J. W., Arribas, A., Jr., and Reynolds, T. J., 1998, Evolution of an intrusion-centered hydrothermal system: Far Southeast-Lepanto porphyry and epithermal Au-Cu deposits, Philippines: *Economic Geology*, v. 93, p. 373-404.
- Hemley, J. J., Montoya, J. W., Marinenko, J. W., and Luce, R. W., 1980, Equilibria in the system $\text{Al}_2\text{O}_3\text{-SiO}_2\text{-H}_2\text{O}$ and some general implications for alteration/mineralization processes: *Economic Geology*, v. 75, p. 210-228.
- Henley, R. W., and McNabb, Alex, 1978, Magmatic vapor plumes and ground-water interaction in porphyry copper emplacement: *Economic Geology*, v. 73, p. 1-20.
- Hudson, D.M., and Oriel, W.M., 1979, Geologic map of the Buckskin Range, Nevada: Nevada Bureau of Mines and Geology, Map 64.
- Hudson, D. M., 1983. Alteration and geochemical characteristics of the upper parts of selected porphyry systems, western Nevada, Unpublished PhD dissertation: Reno, Nevada, University of Nevada, 214 p.
- Jarosewich, K., Nelen, J. A., and Norberg, J. A., 1980, Reference samples for electron microprobe analysis: *Geostandards Newsletter*, v. 4, p. 43-47.
- Lipske, J. L., and Dilles, J. H., 2000, Advanced argillic and sericitic alteration in the subvolcanic environment of the Yerington porphyry copper system, Buckskin Range, Nevada: *Society of Economic Geologists Guidebook Series*, v. 32, p. 91-99.
- Lyon, R. J. P., and Honey, F. R., 1990. Direct mineral identification (DMI) with Geoscan Mk II Advanced Multi-spectral Scanner (AMSS): *Proceedings SPIE Imaging Spectroscopy of the Terrestrial Environment*, The Society of Photo-Optical Instrumentation Engineers, Vol.. 1298.
- Meyer, C., and Hemley, J. J., 1967, Wall rock alteration, *in* Barnes, H. L., ed., *Geochemistry of Hydrothermal Ore Deposits*: New York, Holt, Rinehart, and Winston, p. 166-235.
- Munoz, J. L., 1984, F-OH and Cl-OH exchange in micas with applications to hydrothermal ore deposits, *in* Bailey, S. W., ed., *Micas: Mineralogical Society of America Reviews in Mineralogy*, v. 13, p. 461-490.
- Ohmoto, H., and Rye, R. O., 1979, Isotopes of sulfur and carbon, *in* Barnes, H. L., ed., *Geochemistry of Hydrothermal Ore Deposits*, 2nd ed.: New York, John Wiley and Sons, p. 509-567.

- Pontual, S., Merry, N., and Cocks, T., 1995. Field-based alteration mapping using the PIMA, Proceedings of the 1995 PACRIM congress: Australasian Institute of Mining and Metallurgy, Victoria, Australia, v. 9, p. 479-484.
- Proffett, J. M., Jr., 1977, Cenozoic geology of the Yerington district, Nevada, and implications for the nature and origin of Basin and Range faulting: Geological Society of America Bulletin, v. 88, P. 247-266.
- Proffett, J. M., and Dilles, J. H., 1984, Geologic map of the Yerington district, Nevada: Nevada Bureau of Mines and Geology, Map 77.
- Proffett, J. M., and Dilles, J. H., 1991, Middle Jurassic volcanic rocks of the Artesia Lake and Fulstone Spring sequences, Buckskin Range, Nevada, Geological Society of Nevada, The geology and ore deposits of the Great Basin, Reno, NV, Field trip guidebook compendium, v. 2, p. 1031-1036.
- Proffett, J. M., and Dilles, J. H., 1992, Middle Jurassic volcanic rock of the Artesia Lake and Fulstone Spring sequences, Buckskin Range, Nevada: Great Basin Symposium Field Trip 16: Porphyry copper and molybdenum deposits of western Nevada, p. 1031-1036.
- Proffett, J. M., and Proffett, B. H., 1976, Stratigraphy of the Tertiary ash-flow tuffs in the Yerington district, Nevada: Nevada Bureau of Mines and Geology Report 27, 28 p.
- Rossmann, G. R., 1984, Spectroscopy of micas, *in* Bailey, S. W., ed., Micas: Mineralogical Society of America Reviews in Mineralogy, v. 13, p. 145-181.
- Rubin, T. D., 1989, Correlation of imaging spectrometer and ground data for alteration mapping at Yerington, Nevada: Proceeding of the seventh thematic conference on remote sensing for exploration geology: Environmental Research Institute of Michigan, Ann Arbor, Michigan, p. 315-322.
- Rubin, T. D., 1991, Spectral alteration mapping with ground measurements and remote sensing at Yerington, Nevada, Unpublished PhD dissertation: Stanford, California, Stanford University, 221 p.
- Stoffregen, R. E., Alpers, C. N., Jambor, J. L., 2000, Alunite-Jarosite Crystallography, Thermodynamics, and geochronology, *in* Alpers, C. N., Jambor, J. L., Nordstrom, D. K., eds., Sulfate Minerals: Crystallography, Geochemistry, and Environmental Significance: Mineralogical Society of America Reviews in Mineralogy and Geochemistry, v. 40, p. 454-480.

- Taylor, H. P., Jr., 1979, Oxygen and hydrogen isotope relationships in hydrothermal mineral deposits, *in* Barnes, H. L., ed., *Geochemistry of Hydrothermal Ore Deposits*, 2nd ed.: New York, John Wiley and Sons, p. 236-277.
- Thompson, A. J. B., 1990, Characteristics of acid-sulfate alteration in the Marysvale-Pioche mineral belt: Energy and Mineral Resources of Utah, Utah Geological Association Publication, no. 18, p. 45-55.
- Thompson, A. J. B., Hauff, P. L., Robitaille, A. J., 1999, Alteration Mapping in Exploration: Application of Short-Wave Infrared (SWIR) Spectroscopy, *Society of Economic Geologists Newsletter*, o. 39, 13 p.
- Thompson, A. J. B., and Thompson, J. F. H., 1996. *Atlas of Alteration: A field and petrographic guide to hydrothermal alteration minerals*: Geological Association of Canada, Mineral Deposits Division, 199 p.
- Watanabe, Y., and Hedenquist, J. W., 2001, Mineralogic and stable isotopic zonation at the surface over the El Salvador porphyry copper deposit, Chile: *Economic Geology*, vol. 96, no. 8, p. 1775-1798.

CHAPTER 3: CONCLUSION

The age of advanced argillic and sericitic alteration in the Buckskin Range is constrained to be older than 166.5 Ma, the age of the sulfide-poor Fulstone Spring volcanics overlying the intensely-altered, pyrite-rich rocks of the Artesia Lake sequence. The abundance of sulfides in the Buckskin Range suggests that high-level alteration may be contemporaneous with the main event of sericitic alteration and pyrite deposition in the deeper porphyry copper environment. The paucity of sulfides in the Fulstone Spring Volcanics suggests that these units post-date the main introduction of sulfur to the porphyry copper system.

District-wide hydrothermal alteration and ore deposition has evolved from two different types of fluids; the Buckskin Range serving as an outflow zone for these fluids (Lipske and Dilles, 2000; Dilles et al., 2000). Field mapping, infrared spectroscopy, and petrography, supplemented with microprobe and XRD analyses indicate that low pH, high-sulfidation fluids, introduced by early porphyry dikes of the Yerington batholith, were responsible for hypogene quartz-alunite-pyrophyllite alteration and high-level quartz-sericite alteration, which envelops and lies at depth beneath advanced argillic alteration. Hydrogen and oxygen isotope data from this study indicates that upon ascension, these aqueous fluids cooled, condensed, and mixed with minor amounts of meteoric water at shallow levels to produce advanced argillic alteration.

Alunite from the central Buckskin Range occurs as euhedral 30- to 150- μm tabular disseminations with microcrystalline (10-50 μm) quartz and massive

equigranular replacements of 50-200- μm alunite and quartz. Alunite that is produced by magmatic hydrothermal alteration is generally 10 to 200 μm in size and may occur as disseminations in microgranular quartz (Thompson, 1990; Thompson and Thompson, 1996). Alunite formed by near-surface steam-heating or supergene acid-leach fluids is commonly $<15 \mu\text{m}$ and has a massive porcelaneous appearance (Thompson, 1990, Thompson and Thompson, 1996, Ebert, 1997). Sulfur isotope data give $\delta^{34}\text{S}$ values of 8.7-8.8 ‰ for alunite (n=2) and -4.7 ‰ (n=1) for pyrite from the central Buckskin Range. Comparison of these values with a measured range of ~10-14 ‰ from gypsum that replaces hydrothermal anhydrite at Ann-Mason also supports that the sulfur responsible for alunite formation has been derived mainly from magmatic-hydrothermal sulfate.

The occurrence of sericite-hematite-chlorite alteration in the Artesia andesite lavas represents a transition between Jurassic low-pH, sulfide-bearing fluids to nearly-neutral hydrothermal fluids owing to the buffering of acidic fluids as they react with feldspars in the wallrock. The Fulstone dacite porphyry and porphyry dikes that are altered to this assemblage cut-across sulfide-rich advanced argillic and sericitic assemblages which suggests that later pulses of magma with low sulfur-content may also have contributed sericite-hematite-chlorite alteration to these rocks.

Non-magmatic fluids additionally responsible for district-wide hydrothermal alteration at Yerington are low-temperature, saline brines derived from formation waters trapped in Triassic-Jurassic sediments (Dilles and Einaudi,

1992; Dilles et al., 1992, Dilles et al., 1995). These fluids were heated upon intrusion of the batholith and circulated at the flanks of the system to produce sodic-calcic alteration at depth. These brines may be responsible for feldspar-stable chlorite-calcite-hematite alteration and Fe-oxide-Au-Cu lodes that cross-cut advanced argillic and sericitic alteration in the Buckskin Range as they cooled upon ascension and reacted with adjacent wall rocks when they exited the system through steeply dipping faults in the Buckskin Range.

Chemical composition data of J. H. Dilles (unpublished) and Dilles and Einaudi (1988) indicate that Fe, Cu, and K are relatively depleted in Yerington batholith that have intense sodic-calcic alteration. This supports that interpretation that circulating sedimentary brines responsible for sodic-calcic alteration at depth is responsible for shallow level Au-Cu deposition as the vein lodes occur along steeply dipping Jurassic faults adjacent to feldspar-stable volcanic rock. Whole-rock geochemical analysis indicates that several samples of Fulstone dacite lavas contain elevated K_2O values up to 4.5 wt %, and are relatively depleted in Na_2O , suggesting that potassium may have been added to the rocks (J.H. Dilles, unpublished data, 1991). Potassic alteration in the Fulstone section may have formed as a result of low temperature alkali exchange caused by cooling and rising sodic-calcic hydrothermal fluids. (Dilles and Einaudi, 1992; Dilles et al., 1992, Dilles et al., 1995). Alternatively, potassium-enriched surface fluids may have been recycled from circulating meteoric waters in an evaporitic environment from the underlying Jurassic evaporites (M.D. Barton, personal communication, 1999).

BIBLIOGRAPHY

- Arribas, A., Jr., 1995, Characteristics of high-sulfidation epithermal deposits, and their relation to magmatic fluid, *in* Thompson, J. F. H., ed., *Magmas, Fluids, and Ore Deposits: Mineralogical Association of Canada Short Course Series*, v. 23., p. 419 – 454.
- Brimhall, G., 1999, Digital mapping workshop: Presented at Geological Society of America, Cordilleran Section, Berkeley, California, Earth Resources Center, Berkeley, University of California, 72p.
- Burnham, C. W., *Magmas and Hydrothermal Fluids*, 1979, Hydrothermal alteration: *in* Barnes, H. L., ed., *Geochemistry of Hydrothermal Ore Deposits*, 2nd ed.: New York, Holt, Reinhart, and Winston, p. 71-136.
- Carten, R. B., 1987, Sodium-calcium metasomatism: Chemical, temporal, and spatial relationships at the Yerington, Nevada, porphyry copper deposit: *Economic Geology*, v. 81, p. 1495-1519.
- Craig, H., 1961, Isotopic variations in meteoric waters: *Science*, vol. 133, p. 1702 – 1703.
- Dilles, J. H., 1987, Petrology of the Yerington Batholith, Nevada: Evidence for evolution of porphyry copper ore fluids: *Economic Geology*, vol. 82, p. 1750-1789.
- Dilles, J. H., 2002, Magmatic-hydrothermal fluids: A summary of temporal and spatial evolution from the 6 km vertical transect of the porphyry copper systems in the Yerington batholith, Nevada, *Abstracts with Programs - GSA Cordilleran Section*, vol. 34, no. 5, p. 15.
- Dilles, J. H., and Einaudi, M. T., 1992, Wall-rock alteration and hydrothermal flow paths about the Ann-Mason porphyry copper deposit, Nevada- A 6 km vertical reconstruction: *Economic Geology*, v. 87, p. 1963-2001.
- Dilles, J. H., and Field, C. W., 1996, Sulfur geochemistry of porphyry copper deposits as a record of magma degassing; data from the Yerington District, Nevada, *Abstracts with Programs - Geological Society of America*, vol. 28, no. 7, p. 93.

- Dilles, J. H., and Proffett, J. M., 1991, Roadlog to the geology of the Yerington porphyry copper district: Geologic Society of Nevada, The geology and ore deposits of the Great Basin, Reno, NV, Field trip guidebook compendium, v. 2, p. 1001-1013.
- Dilles, J. H., and Proffett, J. M., 1995, Metallogenesis of the Yerington Batholith, Nevada: *in* Pierce, F.W., and Bolm, J.G., eds., Porphyry Copper Deposits of the American Cordillera: Arizona Geological Society Digest 20, 1995, p. 306-315.
- Dilles, J. H., and Proffett, J., and Einaudi, M. T., 2000, Magmatic and hydrothermal features of the Yerington batholith with emphasis on the porphyry Cu(Mo) deposit in the Ann-Mason area, Society of Economic Geologists Guidebook Series, v. 32, p. 67-89.
- Dilles, J. H., and Wendell, D., 1982, The geology and gold mineralization of the central Buckskin Range, Douglas County, Nevada: Unpublished report, Anaconda Co., 27 p.
- Dilles, J. H., and Wright, J. E., 1988, The chronology of early Mesozoic arc magmatism in the Yerington district of western Nevada and its regional implications: Geological Society of America Bulletin, v. 100, p. 644-652.
- Dilles, J. H., Einaudi, M. T., Proffett, J. M., and Barton, M. D., 2000, Overview of the Yerington porphyry copper district: Magmatic to Nonmagmatic Sources of Hydrothermal Fluids: Their flow paths and alteration effects on rocks and Cu-Mo-Fe-Au ores: Society of Economic Geologists Guidebook Series, v. 32, p. 55-66.
- Dilles, J. H., Solomon, G. C., Taylor, H. P., and Einaudi, M. T., 1992, Oxygen and hydrogen isotope characteristics of hydrothermal alteration at the Ann-Mason porphyry copper deposit, Yerington, Nevada: Economic Geology, v. 87, p. 44-63.
- Field, C. W., 1966, Sulfur isotopic method for discriminating between sulfates of hypogene and supergene origin: Economic Geology, v. 61, p. 1428-1435.
- Gibson, P. C., 1987, Geology of the Buckskin Mine, Douglas County, Nevada: Unpublished master's thesis, University of Nevada-Reno, 214p.
- Glassman, J. R., 1999, GEO479/579 Procedures for clay mineral separation: Oregon State University, unpublished, 5p.

- Graham, C. M., Harmon, R. S., and Sheppard, S. M. F., 1984, Experimental hydrogen isotope studies-hydrogen isotope exchange between amphibole and water: *American Mineralogist*, v. 69, p. 128-138.
- Hauff, P.L., 1993, SPECMIN™ Mineral Identification System and Spectral Library, v. 1 & 2.:
Spectral International, Inc., Arvada, Colorado.
- Heald, P., Foley, N. K., and Hayba, D. O., 1987, Comparative anatomy of volcanic-hosted epithermal deposits: acid-sulfate and adularia-sericite types: *Economic Geology*, v. 82, p. 1-26.
- Hedenquist, J. W., and Lowenstern, J. B., 1994, The role of magmas in the formation of hydrothermal ore deposits: *Nature*, vol. 370, p. 519-527.
- Hedenquist, J. W., Arribas, A., Jr., and Reynolds, T. J., 1998, Evolution of an intrusion-centered hydrothermal system: Far Southeast-Lepanto porphyry and epithermal Au-Cu deposits, Phillippines: *Economic Geology*, v. 93, p. 373-404.
- Hedenquist, J. W., Izawa, E., Arribas, A., and White, N. C., 1996, Epithermal gold deposits: Styles, characteristics, and exploration: *The Society of Resource Geology*, Special Publication Number 1.
- Hemley, J. J., 1959, Some mineralogical equilibria in the system $K_2O-Al_2O_3-SiO_2-H_2O$: *American Journal of Science*, vol. 257, p. 241-270.
- Hemley, J. J., Montoya, J. W., Marinenko, J. W., and Luce, R. W., 1980, Equilibria in the system $Al_2O_3-SiO_2-H_2O$ and some general implications for alteration/mineralization processes: *Economic Geology*, v. 75, p. 210-228.
- Henley, R.W., and McNabb, A., 1978, Magmatic vapor plumes and ground-water interaction in porphyry copper emplacement: *Economic Geology*, v. 73, p. 1-20.
- Henley, R.W., and Ellis, A.J., 1983, ---*Earth Science Reviews*, v. 80, p. 1-50.
- Hudson, D.M., and Oriel, W.M., 1979, Geologic map of the Buckskin Range, Nevada: Nevada Bureau of Mines and Geology, Map 64.
- Hudson, D. M., 1983. Alteration and geochemical characteristics of the upper parts of selected porphyry systems, western Nevada, Unpublished PhD dissertation: Reno, Nevada, University of Nevada, 214 p.
- Jarosewich, E., Nelen, J. A., and Norberg, J. A., 1980, Reference samples for electron microprobe analysis: *Geostandards Newsletter*, v. 4, no. 1, p. 43-47.

- Lipske, J. L., and Dilles, J. H., 2000, Advanced argillic and sericitic alteration in the subvolcanic environment of the Yerington porphyry copper system, Buckskin Range, Nevada: Society of Economic Geologists Guidebook Series, v. 32, p. 91-99.
- Lowell, J.D., and Guilbert, J.M., 1970, Lateral and vertical alteration-mineralization zoning in porphyry copper ore deposits: *Economic Geology*, v. 65, p. 373-408.
- Lyon, R. J.P., and Honey, F.R., 1990, Direct mineral identification (DMI) with Geoscan Mk II Advanced Multi-spectral Scanner (AMSS): Proceedings SPIE Imaging Spectroscopy of the Terrestrial Environment, The Society of Photo-Optical Instrumentation Engineers, Vol.. 1298.
- Meyer, C., and Hemley, J. J., 1967, Wall rock alteration, *in* Barnes, H. L., ed., *Geochemistry of Hydrothermal Ore Deposits*: New York, Holt, Rinehart, and Winston, p. 166-235.
- Munoz, J. L., 1984, F-OH and Cl-OH exchange in micas with applications to hydrothermal ore deposits, *in* Bailey, S. W., ed., *Micas: Mineralogical Society of America Reviews in Mineralogy*, v. 13, p. 461-490.
- Ohmoto, H., and Rye, R. O., 1979, Isotopes of sulfur and carbon, *in* Barnes, H. L., ed., *Geochemistry of Hydrothermal Ore Deposits*, 2nd ed.: New York, John Wiley and Sons, p. 509-567.
- Pontual, S., Merry, N., and Cocks, T., 1995. Field-based alteration mapping using the PIMA, Proceedings of the 1995 PACRIM congress: Australasian Institute of Mining and Metallurgy, Victoria, Australia, v. 9, p. 479-484.
- Proffett, J. M., Jr., 1977, Cenozoic geology of the Yerington district, Nevada, and implications for the nature and origin of Basin and Range faulting: *Geological Society of America Bulletin*, v. 88, P. 247-266.
- Proffett, J. M., and Dilles, J. H., 1984, Geologic map of the Yerington district, Nevada: Nevada Bureau of Mines and Geology, Map 77.
- Proffett, J. M., and Dilles, J. H., 1991, Middle Jurassic volcanic rocks of the Artesia Lake and Fulstone Spring sequences, Buckskin Range, Nevada, *Geologic Society of Nevada, The geology and ore deposits of the Great Basin, Reno, NV, Field trip guidebook compendium*, v. 2, p. 1031-1036.

- Proffett, J. M., and Dilles, J. H., 1992, Middle Jurassic volcanic rock of the Artesia Lake and Fulstone Spring sequences, Buckskin Range, Nevada: Great Basin Symposium Field Trip 16: Porphyry copper and molybdenum deposits of western Nevada, p. 1031-1036.
- Proffett, J. M., and Proffett, B. H., 1976, Stratigraphy of the Tertiary ash-flow tuffs in the Yerington district, Nevada: Nevada Bureau of Mines and Geology Report 27, 28 p.
- Rossmann, G. R., 1984, Spectroscopy of micas, *in* Bailey, S. W., ed., Micas: Mineralogical Society of America Reviews in Mineralogy, v. 13, p. 145-181.
- Rubin, T. D., 1989, Correlation of imaging spectrometer and ground data for alteration mapping at Yerington, Nevada: Proceeding of the seventh thematic conference on remote sensing for exploration geology: Environmental Research Institute of Michigan, Ann Arbor, Michigan, p. 315-322.
- Rubin, T. D., 1991, Spectral alteration mapping with ground measurements and remote sensing at Yerington, Nevada, Unpublished PhD dissertation: Stanford, California, Stanford University, 221 p.
- Sillitoe, R. H., 1973, The tops and bottoms of porphyry copper deposits: Economic Geology, v. 68, p. 799-815.
- Stoffregen, R. E., Alpers, C. N., Jambor, J. L., 2000, Alunite-Jarosite Crystallography, Thermodynamics, and geochronology, *in* Alpers, C. N., Jambor, J. L., Nordstrom, D. K., eds., Sulfate Minerals: Crystallography, Geochemistry, and Environmental Significance: Mineralogical Society of America Reviews in Mineralogy and Geochemistry, v. 40, p. 454-480.
- Taylor, H. P., Jr., 1979, Oxygen and hydrogen isotope relationships in hydrothermal mineral deposits, *in* Barnes, H. L., ed., Geochemistry of Hydrothermal Ore Deposits, 2nd ed.: New York, John Wiley and Sons, p. 236-277.
- Thompson, A. J. B., Hauff, P. L., Robitaille, A. J., 1999, Alteration Mapping in Exploration: Application of Short-Wave Infrared (SWIR) Spectroscopy, Society of Economic Geologists Newsletter, v. 39, 13 p.
- Thompson, A. J. B., and Thompson, J. F. H., 1996. Atlas of Alteration: A field and petrographic guide to hydrothermal alteration minerals: Geological Association of Canada, Mineral Deposits Division, 199 p.

Watanabe, Y., and Hedenquist, J. W., 2001, Mineralogic and stable isotopic zonation at the surface over the El Salvador porphyry copper deposit, Chile: *Economic Geology*, vol. 96, no. 8, p. 1775-1798.

White, N. C., and Hedenquist, J. W., 1990, Epithermal environments and styles of mineralization: variations and their causes, and guidelines for exploration: *Journal of Geochemical Exploration*, v. 36, p. 445-474.

APPENDICES

Appendix A

Infrared Spectra

See attached CD-ROM for this appendix which includes spectral data, software for viewing spectra, and a data table which includes minerals detected in each sample via infrared spectroscopy, XRD, petrography, and microprobe analysis. Please open the Read_Me.doc file before downloading the software. Sample locations are shown geographically on Plate C.

Appendix B

Electron Microprobe Data

Analyses were conducted using a beam current of ~ 30 nA, an accelerating voltage of 15.1 kV, and a 5- μ m beam diameter for micas and 20 μ m beam diameter for alunite with 10-30 second count times per element analyzed. Smithsonian (USMN) and Astimec standards were used for major and minor elements using 10-30 second count times per standard (Jarosewich et al., 1980).

Standards Used for Microprobe Analyses

Element	Standard	Mineral
Si	Flourophlogopite**	micas, alunite
Al	Labradorite*	micas, alunite
Mg	Flourophlogopite	micas, alunite
Fe	Basalt VG-99*	micas, alunite
Ti	Basalt VG-99	micas, alunite
Mn	Pyroxene**	micas, alunite
K	Flourophlogopite	alunite
	Sanidine**	micas
Na	Anorthoclase*	micas, alunite
Ca	Augite*	micas
	Calcite**	alunite
Ba	Benitoite*	alunite
F	Flourophlogopite	micas, alunite
Cl	Tugtupite**	micas, alunite
U	UO ₂	alunite

* Smithsonian standard

** Astimec standard

Appendix B.1a Central Buckskin Range Microprobe Data for Alunite (no phosphorous)

Label	Bu291-1.4	Bu291-3.1	Bu291-3.2	Bu291-3.3	Bu291-3.4	Bu291-4.1	Bu291-4.2	Bu291-4.3	Bu291-5.1	Bu291-5.2	Bu291-5.3	Bu291-5.4
Al2O3	42.71	40.91	40.67	40.81	40.89	40.78	41.90	41.07	41.78	41.26	40.21	39.98
SO3	37.38	36.52	37.61	38.26	38.15	36.90	38.41	36.68	38.70	37.17	38.30	35.44
CaO	1.08	1.38	1.02	0.67	0.90	1.14	0.64	1.18	0.45	0.91	0.70	1.20
Na2O	4.04	4.89	4.85	4.83	5.16	5.41	5.48	4.93	3.32	5.42	5.13	5.00
K2O	0.65	0.58	1.03	1.30	0.62	0.68	0.93	0.63	2.09	0.67	1.19	0.57
FeO	0.08	0.03	0.01	0.05	0.01	0.03	0.10	0.07	0.05	0.00	0.07	0.08
MgO	0.01	0.01	0.00	0.01	0.00	0.01	0.00	0.00	0.00	0.01	0.00	0.00
MnO	0.00	0.01	0.00	0.00	0.00	0.00	0.00	0.00	0.00	0.02	0.01	0.02
SrO	0.60	0.74	0.52	0.32	0.52	0.70	0.39	0.67	0.37	0.56	0.37	0.71
BaO	0.49	0.56	0.45	0.30	0.55	0.71	0.23	0.68	0.25	0.64	0.19	0.60
Th	0.01	0.01	0.00	0.00	0.01	0.00	0.00	0.04	0.01	0.00	0.00	0.03
U	0.01	0.00	0.02	0.02	0.00	0.00	0.12	0.00	0.04	0.00	0.00	0.12
Cl	0.00	0.01	0.00	0.00	0.01	0.01	0.00	0.00	0.00	0.00	0.00	0.00
H2Oc	16.78	15.89	15.49	15.45	15.50	15.73	16.09	15.97	15.92	15.94	15.09	15.62
Cl=O	0.00	0.00	0.00	0.00	0.00	0.00	0.00	0.00	0.00	0.00	0.00	0.00
Total	103.84	101.52	101.67	102.03	102.34	102.10	104.29	101.91	102.97	102.58	101.26	99.39
c=calculated												
Al	2.996	2.998	2.999	2.997	2.999	2.998	2.993	2.996	2.997	3.000	2.997	2.993
Ca	0.069	0.092	0.068	0.045	0.060	0.076	0.042	0.078	0.029	0.060	0.048	0.082
Na	0.466	0.589	0.589	0.584	0.622	0.655	0.644	0.592	0.392	0.648	0.629	0.616
K	0.049	0.046	0.082	0.103	0.050	0.054	0.072	0.050	0.162	0.052	0.096	0.046
Fe3+	0.004	0.001	0.001	0.002	0.001	0.002	0.005	0.003	0.002	0.000	0.003	0.004
Mg	0.001	0.001	0.000	0.000	0.000	0.001	0.000	0.000	0.000	0.001	0.000	0.000
Mn	0.000	0.001	0.000	0.000	0.000	0.000	0.000	0.000	0.000	0.001	0.001	0.001
Sr	0.027	0.035	0.024	0.015	0.024	0.033	0.018	0.031	0.017	0.026	0.018	0.034
Ba	0.012	0.014	0.011	0.007	0.014	0.017	0.005	0.016	0.006	0.016	0.005	0.015
Th	0.000	0.000	0.000	0.000	0.000	0.000	0.000	0.001	0.000	0.000	0.000	0.001
U	0.000	0.000	0.000	0.000	0.000	0.000	0.002	0.000	0.001	0.000	0.000	0.002
Total Cat*	3.624	3.776	3.775	3.755	3.770	3.837	3.781	3.767	3.606	3.804	3.796	3.794
S	1.670	1.705	1.766	1.789	1.782	1.727	1.747	1.704	1.768	1.721	1.817	1.690
Cl	0.000	0.001	0.000	0.001	0.001	0.001	0.000	0.000	0.000	0.000	0.000	0.000
K/K+Na	0.096	0.072	0.123	0.150	0.074	0.076	0.100	0.077	0.293	0.075	0.132	0.070

* molar calculations based on 4 cations in tetrahedral site

Label	Bu323A-1.1	Bu323A-1.2	Bu323A-1.3	Bu323A-2.1	Bu323A-2.2	Bu323A-2.3	Bu323A-2.4	Bu323A-3.1	Bu323A-3.2	Bu323A-3.3	Bu323A-3.4	Bu323A-4.1
Al2O3	40.23	37.88	36.53	38.03	35.83	39.25	38.42	38.58	39.07	39.02	38.02	35.35
SO3	34.60	36.59	36.14	36.87	37.02	36.96	35.77	36.07	36.48	36.33	36.56	36.82
CaO	0.05	0.20	0.25	0.07	0.07	0.16	0.69	0.21	0.34	0.26	0.23	0.08
Na2O	2.90	3.02	2.87	3.10	2.87	2.91	2.64	2.74	2.74	2.98	2.70	2.99
K2O	2.67	3.04	3.30	3.12	3.75	3.08	2.83	2.86	2.78	2.95	3.02	3.59
FeO	0.21	0.21	0.29	0.24	0.28	0.33	0.15	0.31	0.33	0.32	0.24	0.19
MgO	0.01	0.00	0.00	0.00	0.00	0.01	0.01	0.00	0.00	0.00	0.02	0.00
MnO	0.00	0.01	0.02	0.00	0.00	0.00	0.00	0.00	0.00	0.00	0.00	0.00
SrO	0.38	0.46	0.54	0.49	0.34	0.37	0.40	0.41	0.43	0.44	0.48	0.40
BaO	0.29	0.23	0.19	0.15	0.07	0.02	0.22	0.12	0.17	0.12	0.23	0.21
Th	0.00	0.00	0.04	0.00	0.00	0.00	0.05	0.04	0.01	0.00	0.00	0.03
U	0.04	0.03	0.01	0.00	0.05	0.03	0.06	0.00	0.00	0.03	0.08	0.01
Cl	0.00	0.00	0.00	0.00	0.00	0.01	0.00	0.03	0.01	0.01	0.00	0.00
H2Oc	16.00	14.17	13.51	14.20	12.89	14.94	14.65	14.73	14.94	14.94	14.27	12.62
Cl=O	0.00	0.00	0.00	0.00	0.00	0.00	0.00	0.01	0.00	0.00	0.00	0.00
Total	97.39	95.84	93.69	96.30	93.18	98.08	95.89	96.09	97.29	97.40	95.85	92.29
e=calculated												
Al	2.988	2.988	2.982	2.986	2.983	2.982	2.990	2.982	2.982	2.982	2.985	2.988
Ca	0.003	0.015	0.019	0.005	0.005	0.011	0.049	0.015	0.024	0.018	0.016	0.006
Na	0.354	0.392	0.385	0.401	0.393	0.364	0.339	0.348	0.344	0.374	0.349	0.416
K	0.215	0.259	0.292	0.265	0.338	0.254	0.238	0.239	0.230	0.244	0.256	0.328
Fe3+	0.011	0.012	0.017	0.014	0.016	0.018	0.008	0.017	0.018	0.017	0.014	0.011
Mg	0.001	0.000	0.000	0.000	0.000	0.001	0.001	0.000	0.000	0.000	0.002	0.000
Mn	0.000	0.001	0.001	0.000	0.000	0.000	0.000	0.000	0.000	0.000	0.000	0.000
Sr	0.018	0.023	0.028	0.025	0.018	0.018	0.020	0.020	0.021	0.021	0.024	0.021
Ba	0.007	0.006	0.005	0.004	0.002	0.001	0.006	0.003	0.004	0.003	0.006	0.006
Th	0.000	0.000	0.001	0.000	0.000	0.000	0.001	0.001	0.000	0.000	0.000	0.000
U	0.001	0.000	0.000	0.000	0.001	0.001	0.001	0.000	0.000	0.000	0.001	0.000
Total Cat*	3.598	3.696	3.730	3.700	3.757	3.648	3.652	3.626	3.623	3.660	3.653	3.778
S	1.637	1.838	1.879	1.844	1.963	1.788	1.773	1.776	1.773	1.768	1.828	1.981
Cl	0.000	0.000	0.000	0.000	0.000	0.002	0.000	0.003	0.001	0.002	0.000	0.000
K/K+Na	0.378	0.398	0.431	0.398	0.462	0.411	0.413	0.407	0.400	0.395	0.423	0.441

* molar calculations based on 4 cations in tetrahedral site

Label	Bu323A-4.2	Bu323A-4.3	Bu323A-4.4	Bu700-1.1	Bu700-1.2	Bu700-1.3	Bu700-2.1	Bu700-2.2	Bu700-2.3	Bu700-3.1	Bu700-3.2
Al2O3	38.39	38.57	38.74	39.80	37.68	38.68	40.38	38.91	39.85	40.43	39.04
SO3	36.88	36.25	35.77	38.55	39.12	37.95	38.52	38.24	38.69	39.48	38.76
CaO	0.13	0.21	0.49	0.14	0.04	0.05	0.06	0.12	0.08	0.06	0.20
Na2O	2.75	2.76	2.74	2.40	2.65	2.33	1.78	2.58	2.33	1.92	2.09
K2O	2.88	2.87	2.85	3.07	3.49	3.13	3.41	3.74	2.90	3.13	3.64
FeO	0.21	0.39	0.34	0.14	0.14	0.18	0.19	0.11	0.11	0.20	0.15
MgO	0.00	0.01	0.00	0.00	0.00	0.00	0.00	0.01	0.01	0.00	0.00
MnO	0.01	0.00	0.00	0.00	0.04	0.03	0.01	0.00	0.00	0.00	0.00
SrO	0.33	0.41	0.44	0.44	0.28	0.66	0.44	0.64	0.46	0.58	0.41
BaO	0.13	0.12	0.25	0.17	0.19	0.67	0.28	0.31	0.26	0.27	0.26
Th	0.00	0.00	0.00	0.03	0.05	0.00	0.01	0.00	0.00	0.00	0.00
U	0.08	0.02	0.00	0.00	0.05	0.00	0.01	0.11	0.01	0.00	0.05
Cl	0.00	0.01	0.02	0.00	0.02	0.00	0.00	0.00	0.01	0.00	0.00
H2Oc	14.41	14.72	14.90	14.83	13.46	14.32	15.20	14.37	14.81	15.01	14.34
Cl=O	0.00	0.00	0.00	0.00	0.00	0.00	0.00	0.00	0.00	0.00	0.00
Total	96.19	96.33	96.54	99.56	97.21	98.01	100.29	99.16	99.52	101.08	98.93
c=calculated											
Al	2.987	2.978	2.981	2.992	2.990	2.990	2.990	2.992	2.994	2.989	2.991
Ca	0.009	0.014	0.035	0.010	0.003	0.004	0.004	0.009	0.005	0.004	0.014
Na	0.352	0.350	0.346	0.297	0.346	0.297	0.216	0.327	0.287	0.233	0.263
K	0.243	0.240	0.238	0.250	0.300	0.262	0.273	0.311	0.236	0.250	0.302
Fe3+	0.011	0.021	0.019	0.007	0.008	0.010	0.010	0.006	0.006	0.011	0.008
Mg	0.000	0.001	0.000	0.000	0.000	0.000	0.000	0.001	0.001	0.000	0.000
Mn	0.000	0.000	0.000	0.000	0.002	0.002	0.001	0.000	0.000	0.000	0.000
Sr	0.016	0.020	0.021	0.021	0.014	0.033	0.021	0.031	0.022	0.027	0.020
Ba	0.003	0.003	0.006	0.004	0.005	0.017	0.007	0.008	0.007	0.007	0.007
Th	0.000	0.000	0.000	0.000	0.001	0.000	0.000	0.000	0.000	0.000	0.000
U	0.001	0.000	0.000	0.000	0.001	0.000	0.000	0.002	0.000	0.000	0.001
Total Cat*	3.624	3.629	3.646	3.582	3.671	3.614	3.522	3.687	3.558	3.522	3.606
S	1.827	1.783	1.753	1.846	1.977	1.868	1.816	1.873	1.851	1.859	1.891
Cl	0.000	0.001	0.002	0.000	0.002	0.000	0.000	0.000	0.001	0.000	0.000
K/K+Na	0.408	0.406	0.407	0.457	0.464	0.469	0.558	0.488	0.450	0.518	0.534

* molar calculations based on 4 cations in tetrahedral site

Label	Bu700-3.3	Bu700-4.1	Bu700-4.2	Bu700-5.1	Bu700-5.2	Bu700-6.2	Bu700-6.3	Bu700-6.4	Bu402-1.1	Bu402-1.2	Bu402-1.3	Bu402-2.1	Bu402-2.2
Al2O3	39.67	37.88	38.59	39.92	39.29	36.99	38.60	36.99	38.01	37.20	39.89	36.21	40.76
SO3	38.44	38.14	37.57	38.84	38.72	38.33	37.53	38.37	38.18	38.52	39.13	37.18	34.31
CaO	0.08	0.10	0.18	0.08	0.11	0.12	0.08	0.08	0.35	0.81	0.58	0.38	0.65
Na2O	2.55	2.07	1.92	2.26	2.46	2.91	2.66	2.76	4.41	4.54	4.54	4.35	3.49
K2O	3.24	3.72	3.56	2.85	2.86	3.59	2.87	3.82	1.88	1.88	1.70	1.99	1.87
FeO	0.15	0.22	0.27	0.18	0.12	0.13	0.11	0.13	0.01	0.01	0.00	0.00	0.02
MgO	0.00	0.00	0.00	0.00	0.00	0.01	0.00	0.00	0.01	0.00	0.00	0.00	0.00
MnO	0.00	0.00	0.01	0.00	0.00	0.01	0.01	0.00	0.03	0.02	0.04	0.01	0.00
SrO	0.47	0.46	0.44	0.44	0.47	0.49	0.46	0.51	0.17	0.19	0.25	0.11	0.12
BaO	0.29	0.28	0.36	0.28	0.43	0.19	0.29	0.14	0.14	0.10	0.14	0.14	0.18
Th	0.00	0.04	0.03	0.01	0.00	0.04	0.03	0.00	0.00	0.02	0.00	0.00	0.02
U	0.03	0.00	0.00	0.01	0.00	0.01	0.00	0.00	0.00	0.05	0.00	0.00	0.00
Cl	0.01	0.02	0.00	0.00	0.00	0.00	0.00	0.01	0.00	0.00	0.01	0.00	0.02
H2Oc	14.78	13.82	14.39	14.85	14.48	13.22	14.34	13.20	13.80	13.25	14.69	12.96	16.29
Cl=O	0.00	0.00	0.00	0.00	0.00	0.00	0.00	0.00	0.00	0.00	0.00	0.00	0.00
Total	99.71	96.75	97.30	99.71	98.95	96.05	96.98	96.01	97.01	96.60	100.95	93.33	97.72
c=calculated													
Al	2.992	2.987	2.985	2.990	2.994	2.992	2.994	2.993	3.000	2.998	3.000	3.000	2.999
Ca	0.006	0.007	0.013	0.005	0.007	0.009	0.006	0.006	0.025	0.060	0.039	0.028	0.043
Na	0.317	0.269	0.244	0.279	0.308	0.387	0.339	0.368	0.573	0.602	0.562	0.592	0.423
K	0.264	0.317	0.298	0.231	0.236	0.315	0.241	0.334	0.161	0.164	0.138	0.178	0.149
Fe3+	0.008	0.012	0.015	0.009	0.006	0.008	0.006	0.007	0.000	0.001	0.000	0.000	0.001
Mg	0.000	0.000	0.000	0.000	0.000	0.001	0.000	0.000	0.001	0.000	0.000	0.000	0.000
Mn	0.000	0.000	0.001	0.000	0.000	0.001	0.000	0.000	0.002	0.001	0.002	0.001	0.000
Sr	0.023	0.023	0.021	0.021	0.023	0.025	0.023	0.026	0.009	0.010	0.012	0.006	0.006
Ba	0.007	0.007	0.009	0.007	0.011	0.005	0.008	0.004	0.004	0.003	0.004	0.004	0.004
Th	0.000	0.001	0.000	0.000	0.000	0.001	0.001	0.000	0.000	0.000	0.000	0.000	0.000
U	0.000	0.000	0.000	0.000	0.000	0.000	0.000	0.000	0.000	0.001	0.000	0.000	0.000
Total Cat*	3.617	3.624	3.586	3.543	3.586	3.742	3.616	3.738	3.774	3.840	3.757	3.809	3.626
S	1.846	1.915	1.850	1.853	1.878	1.974	1.853	1.977	1.919	1.977	1.874	1.961	1.607
Cl	0.001	0.002	0.001	0.000	0.000	0.000	0.000	0.002	0.000	0.000	0.001	0.000	0.002
K/K+Na	0.455	0.541	0.550	0.454	0.434	0.449	0.415	0.476	0.219	0.214	0.197	0.232	0.261

* molar calculations based on 4 cations in tetrahedral site

Label	Bu402-2.3	Bu402-3.1	Bu402-3.2	Bu402-3.4	Bu402-4.1	Bu402-5.1	Bu402-5.2	Bu402-5.3	Bu402-6.2	Bu402-7.2	Bu402-7.3	Bu402-7.4	Bu402-7.5
Al2O3	40.03	37.18	39.77	40.13	39.57	38.48	39.80	40.78	40.10	40.80	39.74	39.91	40.42
SO3	37.33	35.78	39.27	38.97	38.68	38.00	39.42	39.45	38.94	38.67	37.52	38.01	39.59
CaO	0.61	0.09	0.36	0.58	0.69	0.37	0.45	0.44	0.50	0.21	1.20	0.50	0.44
Na2O	4.07	1.38	4.49	4.60	4.54	3.90	4.49	4.50	4.03	3.29	4.26	4.47	4.46
K2O	1.73	3.73	2.07	1.97	1.90	1.99	1.70	1.60	2.15	2.48	1.85	1.65	1.68
FeO	0.00	0.00	0.02	0.01	0.00	0.00	0.00	0.03	0.01	0.03	0.03	0.03	0.01
MgO	0.00	0.00	0.00	0.00	0.00	0.00	0.00	0.00	0.00	0.00	0.00	0.00	0.00
MnO	0.02	0.05	0.03	0.00	0.01	0.00	0.00	0.01	0.02	0.00	0.02	0.00	0.00
SrO	0.22	0.18	0.15	0.17	0.19	0.23	0.21	0.17	0.22	0.31	0.24	0.27	0.19
BaO	0.23	0.40	0.18	0.14	0.25	0.22	0.26	0.17	0.11	0.50	0.25	0.26	0.10
Th	0.00	0.00	0.02	0.04	0.00	0.02	0.01	0.00	0.00	0.00	0.00	0.00	0.00
U	0.02	0.00	0.00	0.02	0.00	0.00	0.00	0.02	0.06	0.04	0.02	0.06	0.00
Cl	0.00	0.01	0.00	0.01	0.00	0.00	0.01	0.00	0.00	0.00	0.01	0.01	0.00
H2Oc	15.18	13.84	14.60	14.88	14.60	14.11	14.57	15.15	14.86	15.35	14.97	14.97	14.91
Cl=O	0.00	0.00	0.00	0.00	0.00	0.00	0.00	0.00	0.00	0.00	0.00	0.00	0.00
Total	99.43	92.66	100.96	101.51	100.43	97.32	100.94	102.32	101.00	101.66	100.11	100.13	101.81
c=calculated													
Al	3.000	3.000	2.999	2.998	3.000	3.000	3.000	2.998	2.998	2.998	2.998	2.998	2.999
Ca	0.041	0.007	0.024	0.039	0.048	0.026	0.031	0.029	0.034	0.014	0.082	0.034	0.030
Na	0.502	0.184	0.557	0.565	0.566	0.500	0.557	0.544	0.495	0.397	0.529	0.553	0.545
K	0.141	0.326	0.169	0.159	0.156	0.168	0.139	0.127	0.174	0.197	0.151	0.134	0.135
Fe3+	0.000	0.000	0.001	0.001	0.000	0.000	0.000	0.001	0.001	0.002	0.001	0.001	0.001
Mg	0.000	0.000	0.000	0.000	0.000	0.000	0.000	0.000	0.000	0.000	0.000	0.000	0.000
Mn	0.001	0.003	0.002	0.000	0.001	0.000	0.000	0.000	0.001	0.000	0.001	0.000	0.000
Sr	0.010	0.009	0.007	0.008	0.009	0.012	0.010	0.008	0.010	0.014	0.011	0.013	0.009
Ba	0.006	0.011	0.005	0.004	0.006	0.006	0.007	0.004	0.003	0.012	0.006	0.007	0.002
Th	0.000	0.000	0.000	0.001	0.000	0.000	0.000	0.000	0.000	0.000	0.000	0.000	0.000
U	0.000	0.000	0.000	0.000	0.000	0.000	0.000	0.000	0.001	0.001	0.000	0.001	0.000
Total Cat*	3.701	3.540	3.764	3.776	3.785	3.711	3.744	3.714	3.718	3.636	3.781	3.741	3.721
S	1.781	1.838	1.885	1.854	1.868	1.887	1.892	1.847	1.854	1.809	1.802	1.818	1.870
Cl	0.000	0.001	0.000	0.001	0.000	0.000	0.001	0.000	0.000	0.000	0.001	0.001	0.000
K/K+Na	0.219	0.639	0.233	0.220	0.216	0.251	0.200	0.190	0.260	0.331	0.222	0.195	0.198

* molar calculations based on 4 cations in tetrahedral site

Appendix B.1b Central Buckskin Range Microprobe Data for Alunite (phosphorous included)

Label	Bu291-1.1	Bu291-2.1	Bu291-4.1	Bu291-5.1	Bu323A-1.1	Bu323A-2.1	Bu323A-3.1	Bu323A-4.1	Bu700-1.1
Al ₂ O ₃	32.34	36.22	38.32	35.83	34.04	33.64	33.10	33.82	35.76
SO ₃	33.22	36.54	36.44	30.45	34.75	34.42	31.96	32.88	37.49
P ₂ O ₅	0.90	1.45	1.44	0.92	0.62	0.56	0.66	1.14	0.56
CaO	0.43	0.66	0.78	0.56	0.15	0.13	0.20	0.50	0.07
Na ₂ O	4.93	5.72	5.48	3.59	3.02	2.96	2.75	2.57	2.55
K ₂ O	1.06	1.00	0.81	1.34	4.31	4.07	3.86	4.19	4.92
FeO	0.04	0.00	0.09	0.05	0.27	0.12	5.52	0.20	0.14
MgO	0.00	0.00	0.00	0.00	0.00	0.00	0.00	0.01	0.00
MnO	0.03	0.01	0.00	0.00	0.02	0.02	0.02	0.04	0.00
BaO	0.26	0.40	0.68	0.00	0.14	0.09	0.16	0.13	0.36
Th	0.00	0.00	0.00	0.03	0.00	0.00	0.02	0.00	0.00
U	0.10	0.05	0.00	0.07	0.00	0.05	0.08	0.00	0.00
Cl	0.00	0.01	0.04	0.02	0.11	0.00	0.00	0.00	0.00
H ₂ O c	11.18	12.56	13.69	13.31	11.85	11.63	13.84	11.92	12.12
Cl=O	0.00	0.00	0.01	0.00	0.03	0.00	0.00	0.00	0.00
Total	84.50	94.60	97.76	86.16	89.26	87.68	92.17	87.41	93.98

c=calculated

Al	3.010	3.002	3.019	3.088	3.020	3.036	2.751	3.027	3.044
Ca	0.037	0.049	0.056	0.044	0.012	0.011	0.015	0.041	0.005
Na	0.755	0.779	0.710	0.509	0.441	0.440	0.377	0.378	0.357
K	0.107	0.090	0.069	0.125	0.413	0.398	0.347	0.406	0.454
Mg	0.000	0.000	0.000	0.000	0.000	0.000	0.000	0.002	0.000
Mn	0.002	0.001	0.000	0.000	0.001	0.001	0.001	0.003	0.000
Fe ³⁺	0.003	0.000	0.005	0.003	0.017	0.008	0.325	0.013	0.008
Ba	0.008	0.011	0.018	0.000	0.004	0.003	0.004	0.004	0.010
Th	0.000	0.000	0.000	0.000	0.000	0.000	0.000	0.000	0.000
U	0.002	0.001	0.000	0.001	0.000	0.001	0.001	0.000	0.000
Total Cat*	3.923	3.933	3.878	3.770	3.909	3.896	3.822	3.873	3.879
K/K+Na	0.124	0.103	0.088	0.197	0.484	0.475	0.480	0.518	0.560
P	0.060	0.086	0.081	0.057	0.040	0.037	0.039	0.073	0.034
S	1.969	1.928	1.828	1.671	1.963	1.978	1.691	1.874	2.032
Cl	0.000	0.001	0.005	0.002	0.014	0.000	0.000	0.001	0.000
P/P+S	0.030	0.043	0.043	0.033	0.020	0.018	0.023	0.038	0.016

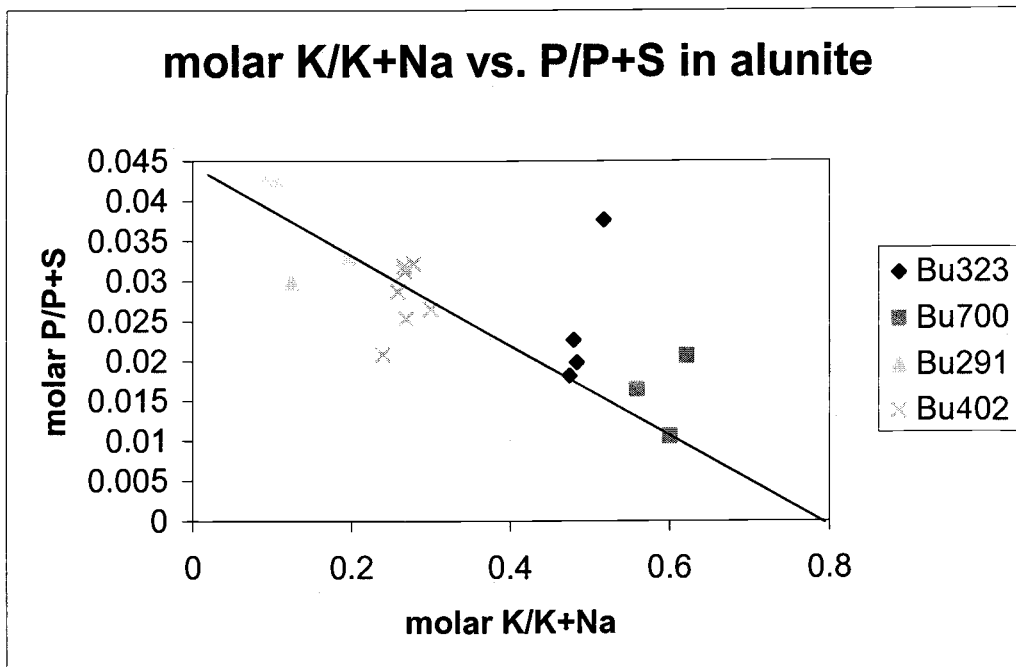
* molar calculations based on cation charge of +10

Label	Bu700-5.1	Bu700-6.1	Bu402-1.1	Bu402-2.1	Bu402-3.1	Bu402-4.1	Bu402-5.1	Bu402-6.1	Bu402-7.1
Al ₂ O ₃	35.54	35.64	36.34	36.34	36.42	36.66	37.94	36.83	37.05
SO ₃	36.75	37.62	37.60	33.65	38.01	38.56	37.29	38.50	38.09
P ₂ O ₅	0.69	0.36	1.07	0.99	1.11	0.89	0.90	0.73	1.00
CaO	0.11	0.06	0.60	0.59	0.68	0.61	0.54	0.39	0.67
Na ₂ O	2.07	2.36	4.60	3.70	4.64	4.62	4.37	4.90	4.65
K ₂ O	5.18	5.40	2.55	2.17	2.56	2.58	2.85	2.35	2.46
FeO	0.16	0.13	0.00	0.07	0.00	0.00	0.00	0.00	0.00
MgO	0.02	0.01	0.00	0.00	0.01	0.00	0.00	0.01	0.00
MnO	0.01	0.05	0.03	0.00	0.04	0.04	0.02	0.02	0.00
BaO	0.30	0.22	0.18	0.20	0.15	0.01	0.20	0.22	0.05
Th	0.02	0.00	0.03	0.01	0.00	0.03	0.00	0.00	0.00
U	0.00	0.00	0.05	0.00	0.04	0.03	0.00	0.03	0.03
Cl	0.00	0.01	0.00	0.02	0.00	0.00	0.00	0.00	0.00
H ₂ O c	12.05	12.13	12.46	13.05	12.43	12.49	13.41	12.63	12.75
Cl=O	0.00	0.00	0.00	0.00	0.00	0.00	0.00	0.00	0.00
Total	92.88	93.98	95.52	90.78	96.10	96.54	97.51	96.62	96.75

c=calculated

Al	3.053	3.039	3.011	3.058	3.008	3.014	3.030	3.018	3.018
Ca	0.008	0.005	0.045	0.045	0.051	0.046	0.039	0.029	0.050
Na	0.293	0.332	0.627	0.512	0.630	0.625	0.575	0.661	0.623
K	0.481	0.499	0.229	0.198	0.229	0.230	0.246	0.209	0.217
Mg	0.002	0.001	0.000	0.000	0.001	0.000	0.000	0.001	0.000
Mn	0.001	0.003	0.002	0.000	0.002	0.002	0.001	0.001	0.000
Fe ³⁺	0.010	0.008	0.000	0.004	0.000	0.000	0.000	0.000	0.000
Ba	0.008	0.006	0.005	0.006	0.004	0.000	0.005	0.006	0.001
Th	0.000	0.000	0.001	0.000	0.000	0.001	0.000	0.000	0.000
U	0.000	0.000	0.001	0.000	0.001	0.001	0.000	0.000	0.001
Total Cat*	3.857	3.893	3.921	3.824	3.926	3.919	3.896	3.926	3.910
K/K+Na	0.622	0.601	0.267	0.279	0.266	0.269	0.300	0.240	0.258
P	0.042	0.022	0.064	0.060	0.066	0.052	0.052	0.043	0.058
S	2.010	2.043	1.984	1.804	1.999	2.018	1.896	2.009	1.976
Cl	0.000	0.001	0.000	0.002	0.000	0.000	0.000	0.000	0.000
P/P+S	0.021	0.011	0.031	0.032	0.032	0.025	0.027	0.021	0.029

* molar calculations based on cation charge of +10



Scatter plot showing molar K/K+Na vs. P/P+S in alunite. Bu323 is from a quartz-alunite-muscovite (AA3) altered sample. Bu323, Bu700, and Bu402 are from quartz-alunite-pyrophyllite altered samples. See Plate C for sample locations.

Appendix B.2 Central Buckskin Range Microprobe Data for Micas

Sample#	Bu329-1.1	Bu329-1.2	Bu329-1.3	Bu329-1.4	Bu329-1.5	Bu329-2.1 1	Bu329-2.1 2	Bu329-2.1 3	Bu329-2.1 4	Bu329-2.3 1	Bu329-2.3 2	Bu329-2.3 3
Mineral	pyroph	pyroph	pyroph	pyroph	pyroph	musc	pyroph	pyroph	pyroph	musc	pyroph	pyroph
SiO2	66.72	67.11	66.46	66.76	66.01	48.81	67.63	67.32	64.22	45.91	66.50	68.09
Al2O3	29.12	29.20	28.75	29.08	28.99	38.58	29.46	29.14	31.02	36.50	28.68	29.32
TiO2	0.02	0.00	0.01	0.05	0.02	0.02	0.01	0.00	0.01	0.05	0.00	0.00
FeO	0.08	0.08	0.08	0.07	0.06	0.19	0.03	0.06	0.08	0.24	0.09	0.06
MnO	0.02	0.00	0.00	0.00	0.00	0.01	0.01	0.00	0.01	0.02	0.00	0.02
MgO	0.02	0.00	0.03	0.03	0.00	0.13	0.03	0.02	0.04	0.15	0.03	0.02
CaO	0.02	0.02	0.01	0.02	0.00	0.06	0.02	0.03	0.04	0.09	0.11	0.04
Na2O	0.04	0.05	0.05	0.06	0.02	0.60	0.10	0.09	0.12	0.72	0.06	0.08
K2O	0.00	0.01	0.00	0.00	0.00	8.61	0.04	0.02	1.62	8.82	0.08	0.03
F	0.32	0.16	0.05	0.28	0.09	0.18	0.10	0.03	0.18	0.16	0.04	0.10
Cl	0.01	0.01	0.00	0.01	0.00	0.01	0.01	0.00	0.01	0.02	0.01	0.01
H2O(c)	4.89	4.99	4.99	4.91	4.96	4.61	5.06	5.06	4.95	4.37	5.00	5.08
O=F	0.13	0.07	0.02	0.12	0.04	0.08	0.04	0.01	0.07	0.07	0.02	0.04
O=Cl	0.00	0.00	0.00	0.00	0.00	0.00	0.00	0.00	0.00	0.00	0.00	0.00
Total	101.13	101.57	100.41	101.15	100.11	101.73	102.45	101.77	102.22	96.97	100.57	102.82
(c) = calculated												
Si	7.929	7.938	7.950	7.931	7.919	6.231	7.933	7.947	7.652	6.186	7.949	7.957
Al/Al IV	0.071	0.062	0.050	0.069	0.081	1.769	0.067	0.053	0.348	1.814	0.051	0.043
Al VI	4.007	4.009	4.003	4.002	4.019	4.035	4.004	4.001	4.008	3.982	3.989	3.995
Ti	0.002	0.000	0.001	0.004	0.001	0.002	0.001	0.000	0.001	0.005	0.000	0.000
Fe3+	0.008	0.008	0.008	0.007	0.006	0.020	0.003	0.006	0.008	0.027	0.009	0.006
Mn2+	0.002	0.000	0.000	0.000	0.000	0.001	0.001	0.000	0.001	0.003	0.000	0.002
Mg	0.003	0.000	0.004	0.006	0.000	0.024	0.006	0.003	0.007	0.030	0.005	0.004
Ca	0.003	0.002	0.001	0.003	0.000	0.008	0.003	0.004	0.005	0.012	0.014	0.005
Na	0.010	0.012	0.013	0.013	0.006	0.148	0.023	0.021	0.028	0.188	0.015	0.019
K	0.000	0.002	0.001	0.001	0.000	1.402	0.006	0.003	0.246	1.515	0.012	0.005
Total Cat*	12.035	12.033	12.031	12.036	12.032	13.640	12.047	12.038	12.304	13.762	12.044	12.036
F	0.120	0.061	0.019	0.107	0.032	0.074	0.036	0.012	0.066	0.067	0.015	0.037
Cl	0.002	0.001	0.000	0.002	0.000	0.001	0.002	0.001	0.002	0.004	0.002	0.003
OH	3.878	3.937	3.981	3.891	3.967	3.925	3.962	3.987	3.932	3.929	3.984	3.960
F/F+OH+Cl	0.030	0.015	0.005	0.027	0.008	0.019	0.009	0.003	0.017	0.017	0.004	0.009

* molar calculations based on 22 oxygen equivalents

Sample#	Bu329-2.3_4	Bu329-3.1	Bu329-3.2	Bu329-3.3	Bu329-3.4	Bu329-4.1_1	Bu329-4.1_2	Bu329-4.1_3	Bu329-4.1_4	Bu329-4.1_5	Bu329-4.1_6	Bu329-4.2_1
Mineral	pyroph	pyroph	pyroph	pyroph	pyroph	pyroph						
SiO2	66.75	67.19	66.89	66.62	66.59	66.69	66.70	65.82	65.40	66.64	67.13	62.63
Al2O3	28.80	29.14	29.06	29.07	28.93	28.81	28.77	28.47	28.16	29.02	29.07	27.38
TiO2	0.00	0.00	0.00	0.00	0.00	0.00	0.00	0.01	0.03	0.00	0.02	2.57
FeO	0.10	0.10	0.10	0.11	0.08	0.08	0.12	0.08	0.06	0.10	0.11	0.10
MnO	0.03	0.03	0.00	0.00	0.00	0.02	0.00	0.00	0.01	0.00	0.04	0.02
MgO	0.02	0.04	0.03	0.04	0.00	0.04	0.01	0.01	0.02	0.04	0.04	0.03
CaO	0.03	0.03	0.03	0.07	0.00	0.11	0.08	0.19	0.29	0.10	0.18	0.18
Na2O	0.08	0.07	0.04	0.03	0.02	0.05	0.03	0.04	0.04	0.04	0.04	0.04
K2O	0.03	0.00	0.01	0.03	0.01	0.01	0.00	0.01	0.00	0.00	0.00	0.39
F	0.15	0.11	0.15	0.05	0.09	0.20	0.09	0.04	0.16	0.13	0.09	0.06
Cl	0.01	0.00	0.00	0.00	0.01	0.01	0.01	0.01	0.01	0.01	0.01	0.00
H2O(c)	4.96	5.02	4.98	5.02	4.98	4.94	4.99	4.95	4.86	4.97	5.03	4.83
O=F	0.07	0.05	0.06	0.02	0.04	0.08	0.04	0.02	0.07	0.06	0.04	0.03
O=Cl	0.00	0.00	0.00	0.00	0.00	0.00	0.00	0.00	0.00	0.00	0.00	0.00
Total	100.89	101.69	101.22	101.02	100.67	100.87	100.75	99.59	98.96	100.99	101.72	98.20

(c) = calculated

Si	7.952	7.940	7.939	7.926	7.943	7.946	7.954	7.943	7.947	7.930	7.936	7.734
Al/Al IV	0.048	0.060	0.061	0.074	0.057	0.054	0.046	0.057	0.053	0.070	0.064	0.266
Al VI	3.995	3.999	4.004	4.002	4.011	3.992	3.998	3.992	3.979	4.001	3.986	3.719
Ti	0.000	0.000	0.000	0.000	0.000	0.000	0.000	0.001	0.002	0.000	0.002	0.238
Fe3+	0.010	0.010	0.010	0.011	0.008	0.008	0.012	0.008	0.006	0.010	0.011	0.010
Mn2+	0.003	0.003	0.000	0.000	0.000	0.002	0.000	0.000	0.001	0.000	0.004	0.002
Mg	0.003	0.007	0.006	0.007	0.000	0.008	0.002	0.002	0.003	0.006	0.007	0.006
Ca	0.003	0.004	0.003	0.009	0.000	0.014	0.010	0.024	0.038	0.013	0.022	0.024
Na	0.018	0.016	0.009	0.008	0.005	0.011	0.006	0.009	0.009	0.009	0.010	0.010
K	0.005	0.000	0.002	0.004	0.001	0.001	0.000	0.001	0.001	0.000	0.001	0.061
Total Cat*	12.037	12.039	12.034	12.041	12.025	12.036	12.028	12.037	12.039	12.039	12.043	12.070
F	0.058	0.040	0.057	0.019	0.034	0.075	0.033	0.014	0.060	0.050	0.034	0.024
Cl	0.002	0.000	0.000	0.000	0.002	0.001	0.001	0.001	0.002	0.001	0.002	0.001
OH	3.940	3.960	3.943	3.980	3.964	3.923	3.966	3.984	3.939	3.949	3.965	3.975
F/F+OH+Cl	0.015	0.010	0.014	0.005	0.009	0.019	0.008	0.004	0.015	0.013	0.008	0.006

* molar calculations based on 22 oxygen equivalents

Sample#	Bu329-4.2_2	Bu329-4.2_3	Bu329-4.3	Bu329-4.4	Bu329-5.1	Bu329-5.2	Bu329-5.3	Bu329-5.4	Bu329-5.5	Bu125-1.1	Bu125-1.2	Bu125-1.3
Mineral	pyroph	pyroph	pyroph	pyroph	musc+illite	illite	muscovite	musc + illite	illite	musc	musc	musc
SiO2	65.17	67.48	65.23	67.48	54.14	41.14	42.55	50.91	47.49	1.53	45.71	32.54
Al2O3	28.36	29.32	28.22	29.04	31.36	34.00	37.51	34.48	37.61	10.50	38.29	26.56
TiO2	0.00	0.00	2.07	0.00	0.02	0.05	0.06	0.02	0.02	1.63	0.00	0.00
FeO	0.10	0.07	0.08	0.04	0.13	0.16	0.21	0.14	0.17	56.47	0.18	0.51
MnO	0.00	0.03	0.00	0.00	0.00	0.00	0.01	0.03	0.00	0.06	0.00	0.01
MgO	0.06	0.04	0.03	0.01	0.10	0.10	0.09	0.11	0.14	0.03	0.14	0.09
CaO	0.28	0.13	0.03	0.04	0.05	0.82	0.28	0.02	0.05	0.21	0.00	0.00
Na2O	0.08	0.03	0.06	0.04	0.64	0.97	0.97	0.67	0.81	0.85	0.65	0.47
K2O	0.01	0.00	0.02	0.03	8.06	6.72	8.82	6.67	8.93	0.47	10.21	6.47
F	0.25	0.15	0.14	0.04	0.18	0.00	0.11	0.27	0.16	0.00	0.24	0.22
Cl	0.00	0.00	0.00	0.00	0.00	0.00	0.01	0.01	0.01	0.01	0.00	0.03
H2O(c)	4.82	5.03	4.94	5.06	4.54	4.06	4.27	4.45	4.51	1.98	4.43	3.09
O=F	0.10	0.06	0.06	0.02	0.07	0.00	0.04	0.11	0.07	0.00	0.10	0.09
O=Cl	0.00	0.00	0.00	0.00	0.00	0.00	0.00	0.00	0.00	0.00	0.00	0.01
Total	99.04	102.21	100.77	101.76	99.15	88.03	94.84	97.68	99.84	73.74	99.75	69.89
(c) = calculated												
Si	7.919	7.935	7.812	7.962	7.014	6.080	5.899	6.665	6.205	0.462	6.036	6.109
Al/Al IV	0.081	0.065	0.188	0.038	0.986	1.920	2.101	1.335	1.795	3.744	1.964	1.891
Al VI	3.981	3.998	3.796	4.001	3.802	4.002	4.029	3.985	3.996	0.000	3.994	3.985
Ti	0.000	0.000	0.187	0.000	0.002	0.006	0.006	0.002	0.002	0.371	0.000	0.000
Fe3+	0.010	0.007	0.008	0.004	0.015	0.020	0.024	0.015	0.019	14.283	0.020	0.080
Mn2+	0.000	0.003	0.000	0.000	0.000	0.000	0.001	0.004	0.000	0.016	0.000	0.002
Mg	0.011	0.007	0.006	0.002	0.018	0.022	0.018	0.022	0.027	0.012	0.027	0.025
Ca	0.037	0.016	0.004	0.005	0.006	0.131	0.041	0.003	0.007	0.068	0.000	0.000
Na	0.019	0.006	0.014	0.008	0.161	0.278	0.261	0.171	0.204	0.497	0.166	0.172
K	0.002	0.000	0.003	0.004	1.332	1.267	1.560	1.114	1.489	0.180	1.720	1.550
Total Cat*	12.060	12.037	12.018	12.024	13.336	13.726	13.940	13.316	13.744	19.633	13.927	13.814
F	0.094	0.057	0.052	0.016	0.072	0.000	0.047	0.112	0.065	0.000	0.101	0.128
Cl	0.001	0.000	0.000	0.001	0.000	0.001	0.003	0.002	0.002	0.003	0.000	0.008
OH	3.905	3.943	3.948	3.983	3.927	3.999	3.950	3.886	3.933	3.997	3.899	3.864
F/F+OH+Cl	0.024	0.014	0.013	0.004	0.018	0.000	0.012	0.028	0.016	0.000	0.025	0.032

* molar calculations based on 22 oxygen equivalents

Sample#	Bu125-1.4	Bu125-2.1 1	Bu125-2.1 2	Bu125-2.1 3	Bu125-2.2 1	Bu125-2.2 2	Bu125-2.2 3	Bu125-2.3	Bu125-3.1 1	Bu125-3.1 2	Bu125-3.1 3	Bu125-3.1 4
Mineral	musc											
SiO2	40.73	43.57	42.26	42.80	42.40	44.64	45.28	45.41	44.56	45.89	46.20	47.10
Al2O3	34.00	36.34	34.77	34.40	34.23	36.79	37.15	37.25	37.11	37.66	37.92	39.24
TiO2	0.00	0.00	0.00	0.00	0.00	0.00	0.00	0.00	0.00	0.00	0.00	0.00
FeO	0.18	0.13	0.11	0.17	0.11	0.16	0.10	0.23	0.17	0.13	0.14	0.28
MnO	0.00	0.00	0.03	0.03	0.02	0.00	0.03	0.00	0.00	0.00	0.00	0.03
MgO	0.10	0.12	0.17	0.14	0.14	0.11	0.17	0.21	0.11	0.10	0.14	0.08
CaO	0.00	0.00	0.00	0.00	0.00	0.00	0.00	0.00	0.00	0.00	0.05	0.00
Na2O	0.67	0.61	0.43	0.40	0.47	0.46	0.49	0.46	0.68	0.66	0.77	0.80
K2O	9.05	9.17	9.18	9.28	9.23	9.72	9.61	9.94	9.77	10.11	9.99	10.23
F	0.24	0.09	0.13	0.18	0.08	0.19	0.25	0.22	0.28	0.11	0.21	0.21
Cl	0.00	0.00	0.00	0.00	0.00	0.00	0.00	0.00	0.00	0.00	0.00	0.00
H2O(c)	3.93	4.27	4.10	4.09	4.11	4.30	4.33	4.37	4.28	4.47	4.45	4.57
O=F	0.10	0.04	0.06	0.08	0.03	0.08	0.10	0.09	0.12	0.05	0.09	0.09
O=Cl	0.00	0.00	0.00	0.00	0.00	0.00	0.00	0.00	0.00	0.00	0.00	0.00
Total	88.80	94.25	91.14	91.42	90.75	96.29	97.32	98.00	96.85	99.08	99.79	102.45

(c) = calculated

Si	6.043	6.062	6.091	6.150	6.138	6.090	6.104	6.093	6.054	6.093	6.089	6.051
Al/Al IV	1.957	1.938	1.909	1.850	1.862	1.910	1.896	1.907	1.946	1.907	1.911	1.949
Al VI	3.987	4.022	3.997	3.976	3.978	4.006	4.005	3.983	3.996	3.985	3.978	3.992
Ti	0.000	0.000	0.000	0.000	0.000	0.000	0.000	0.000	0.000	0.000	0.000	0.000
Fe3+	0.023	0.015	0.014	0.021	0.013	0.018	0.012	0.026	0.019	0.014	0.016	0.031
Mn2+	0.000	0.000	0.003	0.003	0.002	0.000	0.004	0.000	0.000	0.000	0.000	0.003
Mg	0.022	0.024	0.038	0.031	0.030	0.022	0.035	0.042	0.023	0.020	0.027	0.016
Ca	0.000	0.000	0.000	0.000	0.000	0.000	0.000	0.000	0.000	0.000	0.008	0.000
Na	0.192	0.165	0.121	0.111	0.132	0.121	0.127	0.120	0.180	0.171	0.197	0.198
K	1.713	1.627	1.688	1.701	1.705	1.692	1.652	1.701	1.693	1.712	1.680	1.676
Total Cat*	13.937	13.853	13.861	13.843	13.860	13.859	13.835	13.872	13.911	13.902	13.906	13.916
F	0.112	0.039	0.061	0.084	0.036	0.084	0.106	0.093	0.119	0.045	0.086	0.083
Cl	0.000	0.000	0.000	0.000	0.000	0.000	0.000	0.000	0.000	0.000	0.000	0.000
OH	3.888	3.961	3.939	3.916	3.964	3.916	3.894	3.907	3.881	3.955	3.914	3.917
F/F+OH+Cl	0.028	0.010	0.015	0.021	0.009	0.021	0.027	0.023	0.030	0.011	0.022	0.021

* molar calculations based on 22 oxygen equivalents

Sample#	Bu125-3.2 1	Bu125-3.2 2	Bu125-3.2 3	Bu125-3.2 4	Bu125-4.1 2	Bu125-4.1 3	Bu125-4.1 4	Bu125-4.1 5	Bu125-4.2 1	Bu125-4.2 2	Bu125-4.2 3	Bu125-5.1
Mineral	musc											
SiO2	43.87	47.63	45.47	46.13	44.36	46.34	45.31	45.98	45.43	45.00	46.19	45.46
Al2O3	35.81	36.15	37.27	37.74	36.48	37.83	38.10	38.12	37.15	36.92	38.03	38.89
TiO2	0.00	0.09	0.00	0.00	0.00	0.00	0.00	0.00	0.00	0.00	0.00	0.00
FeO	0.37	0.12	0.10	0.09	0.05	0.03	0.05	0.08	0.14	0.07	0.04	0.33
MnO	0.00	0.00	0.00	0.00	0.01	0.00	0.00	0.02	0.00	0.01	0.01	0.00
MgO	0.11	0.09	0.13	0.12	0.09	0.17	0.10	0.09	0.11	0.14	0.12	0.13
CaO	0.00	0.00	0.00	0.00	0.00	0.00	0.00	0.00	0.00	0.00	0.00	0.00
Na2O	0.62	0.59	0.67	0.70	0.60	0.45	0.63	0.56	0.64	0.71	0.65	0.74
K2O	9.61	9.68	9.76	10.04	9.16	10.41	10.18	9.86	9.70	9.80	9.90	10.04
F	0.18	0.14	0.30	0.22	0.23	0.32	0.20	0.33	0.27	0.37	0.38	0.36
Cl	0.00	0.00	0.00	0.00	0.00	0.00	0.00	0.00	0.00	0.00	0.00	0.00
H2O(c)	4.23	4.47	4.33	4.43	4.25	4.40	4.41	4.38	4.33	4.26	4.37	4.39
O=F	0.08	0.06	0.13	0.09	0.10	0.14	0.08	0.14	0.12	0.15	0.16	0.15
O=Cl	0.00	0.00	0.00	0.00	0.00	0.00	0.00	0.00	0.00	0.00	0.00	0.00
Total	94.72	98.89	97.91	99.38	95.13	99.81	98.89	99.28	97.68	97.11	99.53	100.20
(c) = calculated												
Si	6.099	6.302	6.100	6.102	6.106	6.108	6.032	6.079	6.108	6.093	6.093	5.979
Al/Al IV	1.901	1.698	1.900	1.898	1.894	1.892	1.968	1.921	1.892	1.907	1.907	2.021
Al VI	3.966	3.939	3.993	3.986	4.024	3.984	4.009	4.019	3.995	3.985	4.005	4.007
Ti	0.000	0.009	0.000	0.000	0.000	0.000	0.000	0.000	0.000	0.000	0.000	0.000
Fe3+	0.043	0.013	0.012	0.010	0.006	0.004	0.006	0.009	0.016	0.008	0.004	0.037
Mn2+	0.000	0.000	0.000	0.000	0.001	0.000	0.000	0.002	0.000	0.001	0.002	0.000
Mg	0.023	0.017	0.026	0.023	0.019	0.034	0.019	0.018	0.022	0.028	0.024	0.025
Ca	0.000	0.000	0.000	0.000	0.000	0.000	0.000	0.000	0.000	0.000	0.000	0.000
Na	0.167	0.151	0.173	0.179	0.159	0.114	0.162	0.143	0.168	0.186	0.166	0.190
K	1.704	1.634	1.671	1.694	1.609	1.750	1.729	1.663	1.664	1.692	1.667	1.684
Total Cat*	13.903	13.763	13.875	13.892	13.818	13.886	13.925	13.854	13.865	13.900	13.868	13.943
F	0.079	0.057	0.127	0.091	0.101	0.135	0.082	0.139	0.117	0.157	0.158	0.151
Cl	0.000	0.000	0.000	0.000	0.000	0.000	0.000	0.000	0.000	0.000	0.000	0.000
OH	3.921	3.943	3.873	3.909	3.898	3.865	3.918	3.861	3.883	3.843	3.842	3.849
F/F+OH+Cl	0.020	0.014	0.032	0.023	0.025	0.034	0.021	0.035	0.029	0.039	0.040	0.038

* molar calculations based on 22 oxygen equivalents

Sample#	Bu323A-1.1	1Bu323A-1.1	2Bu323A-1.1	3Bu323A-1.1	4Bu323A-1.1	5Bu323A-1.1	6Bu323A-1.2	1Bu323A-1.2	2Bu323A-1.2	3Bu323A-2.1	1Bu323A-2.1	2Bu323A-2.1	3
Mineral	musc	musc											
SiO2	45.60	45.55	45.25	45.69	45.71	45.56	45.12	45.11	44.13	44.60	45.11	45.59	
Al2O3	35.47	35.56	35.84	35.62	35.17	35.96	36.06	35.23	37.07	34.94	35.49	35.26	
TiO2	0.07	0.00	0.00	0.00	0.01	0.05	0.00	0.01	0.02	0.07	0.02	0.05	
FeO	3.05	2.76	2.76	2.74	3.06	3.12	2.71	2.91	3.50	3.11	3.33	3.24	
MnO	0.02	0.04	0.07	0.00	0.00	0.00	0.02	0.01	0.00	0.00	0.01	0.02	
MgO	0.09	0.21	0.18	0.28	0.30	0.14	0.16	0.19	0.08	0.11	0.20	0.19	
CaO	0.00	0.00	0.00	0.00	0.00	0.00	0.00	0.00	0.00	0.00	0.00	0.00	
Na2O	0.11	0.13	0.13	0.11	0.15	0.12	0.12	0.11	0.21	0.12	0.10	0.12	
K2O	11.06	11.29	11.30	11.11	11.12	11.05	11.21	11.20	10.63	10.83	10.91	11.32	
F	0.43	0.68	0.73	0.59	0.74	0.56	0.67	0.55	1.19	0.61	1.10	0.44	
Cl	0.00	0.00	0.00	0.00	0.00	0.00	0.00	0.00	0.00	0.00	0.00	0.00	
H2O(c)	4.26	4.15	4.12	4.20	4.11	4.23	4.15	4.17	3.90	4.10	3.93	4.26	
O=F	0.18	0.29	0.31	0.25	0.31	0.24	0.28	0.23	0.50	0.26	0.46	0.18	
O=Cl	0.00	0.00	0.00	0.00	0.00	0.00	0.00	0.00	0.00	0.00	0.00	0.00	
Total	99.97	100.08	100.07	100.09	100.06	100.55	99.94	99.27	100.24	98.24	99.73	100.31	
(c) = calculated													
Si	6.122	6.113	6.077	6.120	6.138	6.084	6.060	6.107	5.925	6.099	6.083	6.118	
Al/Al IV	1.878	1.887	1.923	1.880	1.862	1.916	1.940	1.893	2.075	1.901	1.917	1.882	
Al VI	3.734	3.736	3.748	3.743	3.702	3.744	3.769	3.728	3.791	3.731	3.723	3.695	
Ti	0.007	0.000	0.000	0.000	0.001	0.005	0.000	0.001	0.002	0.008	0.002	0.005	
Fe3+	0.342	0.310	0.310	0.307	0.344	0.349	0.304	0.329	0.393	0.356	0.376	0.364	
Mn2+	0.002	0.004	0.008	0.000	0.000	0.000	0.002	0.002	0.000	0.000	0.001	0.002	
Mg	0.019	0.042	0.036	0.056	0.061	0.027	0.033	0.039	0.016	0.022	0.040	0.037	
Ca	0.000	0.000	0.000	0.000	0.000	0.000	0.000	0.000	0.000	0.000	0.000	0.000	
Na	0.028	0.035	0.035	0.028	0.038	0.030	0.032	0.030	0.054	0.033	0.027	0.033	
K	1.894	1.933	1.936	1.898	1.904	1.883	1.921	1.934	1.821	1.889	1.876	1.938	
Total Cat*	14.026	14.060	14.073	14.032	14.050	14.038	14.061	14.063	14.077	14.039	14.045	14.074	
F	0.182	0.290	0.310	0.249	0.316	0.236	0.283	0.236	0.505	0.264	0.467	0.185	
Cl	0.000	0.000	0.000	0.000	0.000	0.000	0.000	0.000	0.000	0.000	0.000	0.000	
OH	3.818	3.710	3.690	3.751	3.684	3.764	3.717	3.764	3.495	3.736	3.533	3.815	
F/F+OH+Cl	0.046	0.073	0.078	0.062	0.079	0.059	0.071	0.059	0.126	0.066	0.117	0.046	

* molar calculations based on 22 oxygen equivalents

Sample#	Bu323A-2.1	4Bu323A-2.2	1Bu323A-2.2	2Bu323A-2.2	3Bu323A-3.1	1Bu323A-3.1	2Bu323A-3.1	3Bu323A-3.1	4Bu323A-3.2	1Bu323A-3.2	2Bu323A-3.2	3Bu323A-3.3	1
Mineral	musc	musc											
SiO2	44.82	45.24	45.39	45.00	44.95	45.58	44.06	45.58	45.69	45.37	40.13	44.82	
Al2O3	35.62	35.79	34.75	36.02	36.26	35.83	38.33	35.89	36.53	34.78	31.86	34.43	
TiO2	0.08	0.07	0.02	0.06	0.03	0.00	0.00	0.00	0.00	0.05	0.02	0.05	
FeO	3.36	3.10	3.45	3.25	3.21	2.81	2.44	2.96	2.51	3.48	2.87	3.55	
MnO	0.00	0.00	0.05	0.02	0.02	0.00	0.00	0.00	0.03	0.02	0.00	0.00	
MgO	0.06	0.08	0.26	0.09	0.20	0.18	0.17	0.13	0.13	0.12	0.09	0.14	
CaO	0.00	0.00	0.13	0.00	0.00	0.00	0.00	0.00	0.00	0.00	0.41	0.00	
Na2O	0.17	0.13	0.11	0.11	0.10	0.14	0.13	0.15	0.21	0.12	0.16	0.12	
K2O	10.83	11.08	11.03	11.35	10.28	10.92	9.81	10.97	10.64	11.00	8.84	11.01	
F	0.34	0.60	0.48	0.57	1.41	0.48	1.65	0.73	0.44	0.44	0.32	0.69	
Cl	0.00	0.00	0.00	0.00	0.00	0.00	0.00	0.00	0.00	0.00	0.00	0.00	
H2O(c)	4.27	4.18	4.21	4.20	3.79	4.25	3.70	4.13	4.29	4.22	3.81	4.06	
O=F	0.14	0.25	0.20	0.24	0.59	0.20	0.70	0.31	0.19	0.19	0.13	0.29	
O=Cl	0.00	0.00	0.00	0.00	0.00	0.00	0.00	0.00	0.00	0.00	0.00	0.00	
Total	99.42	100.01	99.68	100.43	99.64	99.99	99.59	100.23	100.28	99.42	88.38	98.59	
(c) = calculated													
Si	6.060	6.078	6.133	6.037	6.041	6.106	5.891	6.098	6.082	6.141	6.072	6.128	
Al/Al IV	1.940	1.922	1.867	1.963	1.959	1.894	2.109	1.902	1.918	1.859	1.928	1.872	
Al VI	3.736	3.744	3.666	3.733	3.785	3.764	3.931	3.759	3.814	3.689	3.754	3.676	
Ti	0.008	0.007	0.002	0.006	0.003	0.000	0.000	0.000	0.000	0.005	0.003	0.005	
Fe3+	0.379	0.349	0.390	0.365	0.361	0.314	0.273	0.332	0.279	0.394	0.364	0.406	
Mn2+	0.000	0.000	0.006	0.002	0.002	0.000	0.000	0.000	0.003	0.002	0.000	0.000	
Mg	0.013	0.016	0.052	0.018	0.039	0.036	0.033	0.026	0.026	0.024	0.020	0.028	
Ca	0.000	0.000	0.019	0.000	0.000	0.000	0.000	0.000	0.000	0.000	0.066	0.000	
Na	0.045	0.034	0.030	0.028	0.025	0.036	0.033	0.038	0.053	0.032	0.048	0.033	
K	1.868	1.899	1.901	1.943	1.762	1.866	1.672	1.872	1.807	1.899	1.707	1.920	
Total Cat*	14.049	14.049	14.066	14.095	13.977	14.016	13.942	14.027	13.982	14.045	13.962	14.068	
F	0.146	0.254	0.206	0.243	0.600	0.205	0.700	0.311	0.186	0.189	0.153	0.299	
Cl	0.000	0.000	0.000	0.000	0.000	0.000	0.000	0.000	0.000	0.000	0.000	0.000	
OH	3.854	3.746	3.794	3.757	3.400	3.795	3.300	3.689	3.814	3.811	3.847	3.701	
F/F+OH+Cl	0.037	0.064	0.052	0.061	0.150	0.051	0.175	0.078	0.047	0.047	0.038	0.075	

* molar calculations based on 22 oxygen equivalents

Sample#	Bu323A-3.3	2Bu323A-3.3	3Bu323A-3.3	4Bu323A-3.4	1Bu323A-3.4	2Bu323A-3.4	3Bu323A-5.1	1Bu323A-5.1	2Bu323A-5.1	3Bu323A-5.2	1Bu323A-5.2	2Bu323A-5.3	1
Mineral	musc	musc											
SiO2	43.10	45.91	44.78	44.47	45.66	41.94	44.21	45.07	44.37	43.98	44.48	43.93	
Al2O3	33.56	34.82	34.83	36.82	34.77	38.54	35.16	35.82	34.18	34.96	36.36	36.14	
TiO2	0.00	0.00	0.05	0.00	0.00	0.00	0.04	0.00	0.05	0.06	0.00	0.00	
FeO	1.86	2.35	3.62	1.76	2.65	0.41	2.98	2.72	3.52	3.16	2.45	2.68	
MnO	0.01	0.03	0.00	0.00	0.02	0.00	0.00	0.02	0.00	0.02	0.01	0.03	
MgO	0.19	0.29	0.13	0.07	0.39	0.03	0.07	0.20	0.18	0.08	0.08	0.08	
CaO	0.00	0.00	0.00	0.00	0.00	0.43	0.00	0.00	0.00	0.00	0.00	0.00	
Na2O	0.09	0.20	0.13	0.18	0.10	0.13	0.13	0.16	0.10	0.14	0.17	0.19	
K2O	6.60	8.84	10.95	7.81	11.04	1.01	10.28	11.14	10.79	10.34	9.75	10.53	
F	0.51	0.61	0.70	0.39	0.74	0.08	0.42	0.67	0.73	0.62	0.44	0.27	
Cl	0.00	0.00	0.00	0.00	0.00	0.00	0.00	0.00	0.00	0.00	0.00	0.00	
H2O(c)	3.89	4.12	4.07	4.20	4.09	4.15	4.16	4.13	4.00	4.05	4.20	4.26	
O=F	0.21	0.26	0.30	0.16	0.31	0.04	0.18	0.28	0.31	0.26	0.18	0.11	
O=Cl	0.00	0.00	0.00	0.00	0.00	0.00	0.00	0.00	0.00	0.00	0.00	0.00	
Total	89.58	96.92	98.97	95.54	99.14	86.67	97.28	99.65	97.61	97.16	97.75	98.00	
(c) = calculated													
Si	6.252	6.248	6.098	6.085	6.172	6.006	6.082	6.071	6.123	6.072	6.048	6.002	
Al/Al IV	1.748	1.752	1.902	1.915	1.828	1.994	1.918	1.929	1.877	1.928	1.952	1.998	
Al VI	3.989	3.834	3.689	4.023	3.712	4.511	3.782	3.758	3.681	3.759	3.875	3.820	
Ti	0.000	0.000	0.005	0.000	0.000	0.000	0.005	0.000	0.005	0.006	0.000	0.000	
Fe3+	0.225	0.268	0.413	0.202	0.300	0.049	0.343	0.306	0.407	0.365	0.279	0.306	
Mn2+	0.001	0.003	0.000	0.000	0.002	0.000	0.000	0.003	0.001	0.003	0.001	0.004	
Mg	0.042	0.059	0.026	0.015	0.079	0.006	0.014	0.040	0.037	0.017	0.016	0.016	
Ca	0.000	0.000	0.000	0.000	0.000	0.066	0.000	0.000	0.000	0.000	0.000	0.000	
Na	0.026	0.054	0.034	0.048	0.026	0.037	0.035	0.043	0.026	0.038	0.045	0.051	
K	1.221	1.536	1.902	1.363	1.903	0.184	1.804	1.913	1.899	1.821	1.691	1.834	
Total Cat*	13.504	13.754	14.069	13.651	14.022	12.853	13.983	14.063	14.056	14.009	13.907	14.031	
F	0.233	0.262	0.304	0.168	0.316	0.038	0.182	0.287	0.317	0.271	0.188	0.115	
Cl	0.000	0.000	0.000	0.000	0.000	0.000	0.000	0.000	0.000	0.000	0.000	0.000	
OH	3.767	3.738	3.696	3.832	3.683	3.962	3.818	3.713	3.683	3.729	3.812	3.885	
F/F+OH+Cl	0.058	0.066	0.076	0.042	0.079	0.010	0.046	0.072	0.079	0.068	0.047	0.029	

* molar calculations based on 22 oxygen equivalents

Sample#	Bu323A-5.3	2 Bu323A-5.3	3 Bu323A-6.1	1 Bu323A-6.1	2 Bu323A-6.2	1 Bu323A-6.2	2 Bu323A-6.2	3 Bu323A-7.1	1 Bu323A-7.1	2 Bu323A-7.2	1 Bu323A-7.2	2 Bu323A-7.2	3
Mineral	musc	illite	musc	musc	musc	musc							
SiO2	44.70	45.69	45.11	44.58	45.03	45.17	44.96	46.27	45.16	45.78	45.50	45.63	
Al2O3	34.48	38.62	34.44	35.93	35.30	35.13	35.15	35.22	38.02	35.17	35.77	35.04	
TiO2	0.04	0.00	0.03	0.05	0.04	0.00	0.04	0.08	0.00	0.07	0.00	0.02	
FeO	3.54	1.77	3.10	2.85	3.46	2.96	3.28	2.97	1.15	3.21	2.83	3.04	
MnO	0.00	0.01	0.00	0.00	0.01	0.00	0.03	0.00	0.00	0.05	0.00	0.00	
MgO	0.17	0.07	0.21	0.06	0.10	0.23	0.07	0.07	0.04	0.16	0.18	0.09	
CaO	0.00	0.00	0.00	0.00	0.00	0.00	0.00	0.00	0.21	0.00	0.00	0.00	
Na2O	0.11	0.18	0.12	0.13	0.12	0.11	0.15	0.15	0.12	0.13	0.13	0.17	
K2O	11.17	7.13	10.87	11.06	10.83	10.92	10.82	10.61	3.99	10.85	10.89	10.54	
F	0.50	0.44	0.52	0.53	0.57	0.75	0.66	0.61	0.06	0.61	0.51	0.48	
Cl	0.00	0.00	0.00	0.00	0.00	0.00	0.00	0.00	0.01	0.00	0.00	0.00	
H2O(c)	4.15	4.32	4.15	4.18	4.16	4.07	4.10	4.19	4.37	4.18	4.23	4.21	
O=F	0.21	0.19	0.22	0.22	0.24	0.32	0.28	0.26	0.03	0.26	0.21	0.20	
O=Cl	0.00	0.00	0.00	0.00	0.00	0.00	0.00	0.00	0.00	0.00	0.00	0.00	
Total	98.66	98.05	98.32	99.14	99.38	99.03	98.99	99.93	93.10	99.96	99.83	99.03	
(c) = calculated													
Si	6.113	6.056	6.160	6.039	6.093	6.121	6.104	6.191	6.154	6.146	6.105	6.166	
Al/Al IV	1.887	1.944	1.840	1.961	1.907	1.879	1.896	1.809	1.846	1.854	1.895	1.834	
Al VI	3.671	4.090	3.702	3.775	3.721	3.732	3.729	3.744	4.260	3.711	3.763	3.746	
Ti	0.004	0.000	0.003	0.005	0.005	0.000	0.004	0.008	0.000	0.007	0.000	0.002	
Fe3+	0.405	0.196	0.354	0.323	0.391	0.336	0.372	0.332	0.131	0.361	0.318	0.344	
Mn2+	0.000	0.001	0.000	0.000	0.001	0.000	0.003	0.000	0.000	0.005	0.000	0.000	
Mg	0.035	0.015	0.044	0.012	0.020	0.046	0.014	0.014	0.008	0.033	0.036	0.019	
Ca	0.000	0.000	0.000	0.000	0.000	0.000	0.000	0.000	0.031	0.000	0.000	0.000	
Na	0.030	0.046	0.032	0.035	0.032	0.030	0.039	0.039	0.031	0.035	0.034	0.044	
K	1.948	1.206	1.893	1.911	1.869	1.888	1.875	1.811	0.694	1.858	1.864	1.817	
Total Cat*	14.093	13.554	14.028	14.061	14.039	14.032	14.036	13.948	13.155	14.010	14.015	13.972	
F	0.217	0.184	0.223	0.226	0.245	0.323	0.284	0.259	0.026	0.259	0.214	0.205	
Cl	0.000	0.000	0.000	0.000	0.000	0.000	0.000	0.000	0.002	0.000	0.000	0.000	
OH	3.783	3.816	3.777	3.774	3.755	3.677	3.716	3.741	3.972	3.740	3.786	3.795	
F/F+OH+Cl	0.054	0.046	0.056	0.057	0.061	0.081	0.071	0.065	0.007	0.065	0.054	0.051	

* molar calculations based on 22 oxygen equivalents

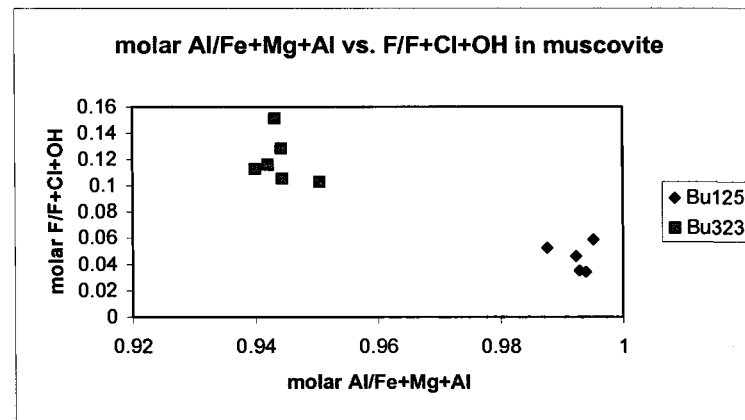
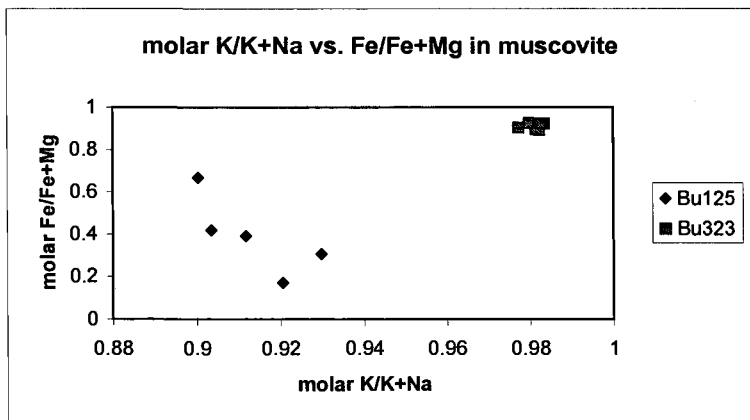
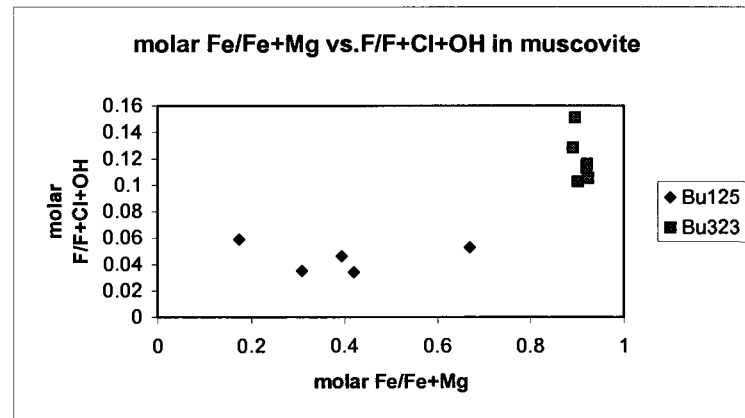
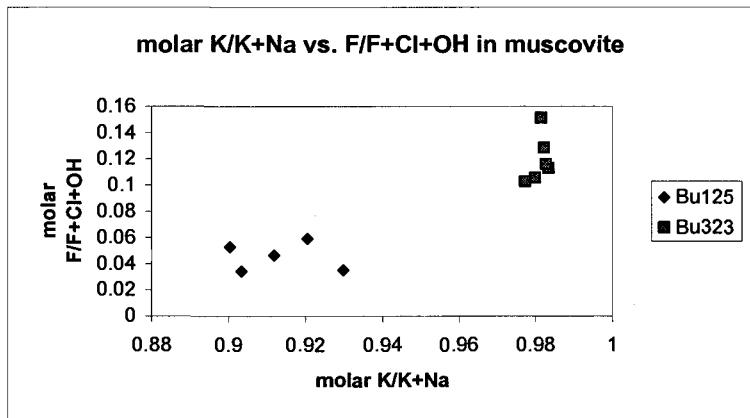
Label	Bu291-2.1	Bu291-2.2	Bu291-2.3	Bu291-2.4	Bu291-6.1	Bu291-6.2	Bu291-6.3	Bu291-6.4
Mineral	illite?	pyroph	pyroph	illite?	pyroph	pyroph	pyroph	pyroph
SiO2	42.85	64.57	65.29	47.67	62.41	63.82	64.50	64.68
Al2O3	38.45	27.83	28.06	36.94	28.08	27.85	28.08	28.53
TiO2	0.01	0.01	0.03	1.93	0.01	0.02	0.00	0.00
FeO	0.02	0.39	0.34	0.08	0.31	0.40	0.35	0.32
MgO	0.00	0.03	0.03	0.00	0.02	0.02	0.01	0.00
MnO	0.05	0.05	0.03	0.02	0.05	0.03	0.00	0.00
CaO	0.09	0.03	0.02	0.02	0.06	0.01	0.00	0.05
Na2O	0.30	0.07	0.05	0.05	0.07	0.10	0.07	0.06
K2O	0.13	0.02	0.03	0.02	0.01	0.02	0.02	0.03
P2O5	0.17	0.00	0.01	0.02	0.02	0.02	0.02	0.00
F	0.31	0.25	0.23	0.26	0.28	0.23	0.28	0.32
Cl	0.02	0.00	0.00	0.00	0.00	0.00	0.01	0.02
H2O©	4.25	4.75	4.80	4.44	4.64	4.72	4.74	4.76
F=O	0.13	0.11	0.10	0.11	0.12	0.10	0.12	0.14
Cl=O	0.00	0.00	0.00	0.00	0.00	0.00	0.00	0.00
Total	86.52	97.88	98.83	91.32	95.83	97.13	97.96	98.64

(c) = calculated

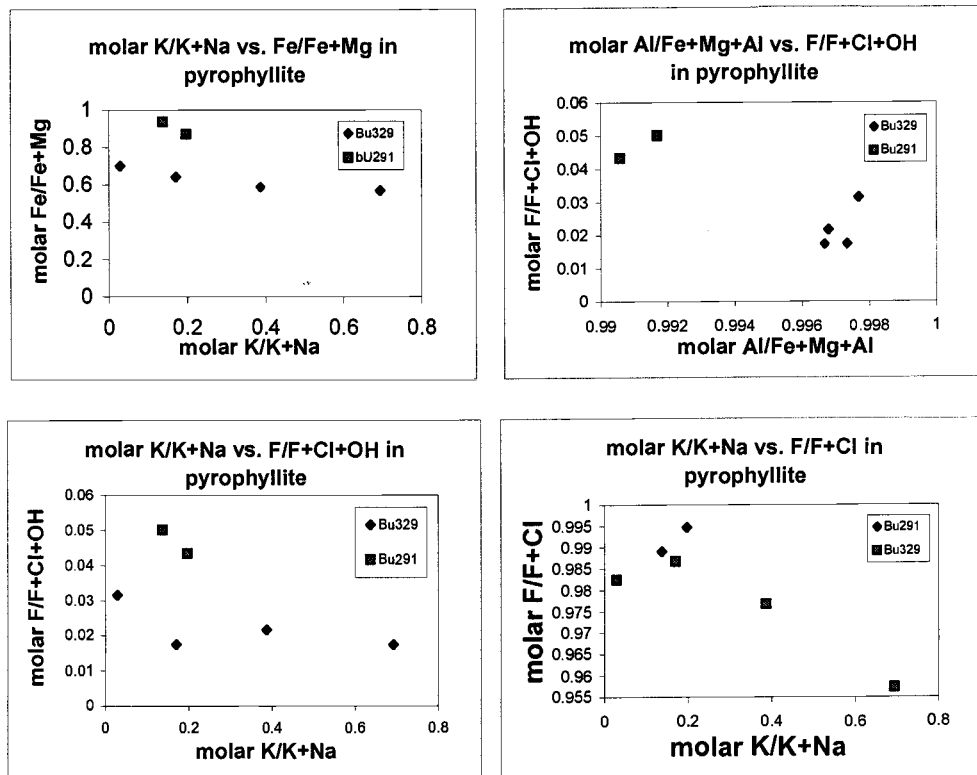
Si	6.119	7.959	7.966	6.420	7.867	7.929	7.945	7.919
Al	6.470	4.043	4.034	5.864	4.172	4.078	4.076	4.117
Ti	0.001	0.001	0.002	0.196	0.001	0.002	0.000	0.000
Fe3+	0.002	0.040	0.035	0.009	0.033	0.041	0.036	0.033
Mg	0.001	0.005	0.005	0.000	0.004	0.004	0.001	0.000
Mn	0.006	0.005	0.003	0.002	0.005	0.003	0.000	0.000
Ca	0.014	0.004	0.003	0.003	0.008	0.001	0.001	0.007
Na	0.083	0.016	0.013	0.012	0.016	0.025	0.018	0.014
K	0.024	0.003	0.004	0.004	0.001	0.003	0.004	0.004
Total Cat*	12.720	12.076	12.065	12.510	12.106	12.085	12.080	12.095

OH	2.044	2.068	2.071	2.065	2.061	2.071	2.060	2.052
P	0.021	0.000	0.001	0.002	0.002	0.002	0.002	0.000
Cl	0.004	0.000	0.001	0.000	0.000	0.000	0.001	0.003
F	0.141	0.097	0.090	0.110	0.110	0.091	0.111	0.124
F/F+OH+Cl	0.061	0.045	0.042	0.050	0.050	0.042	0.051	0.057

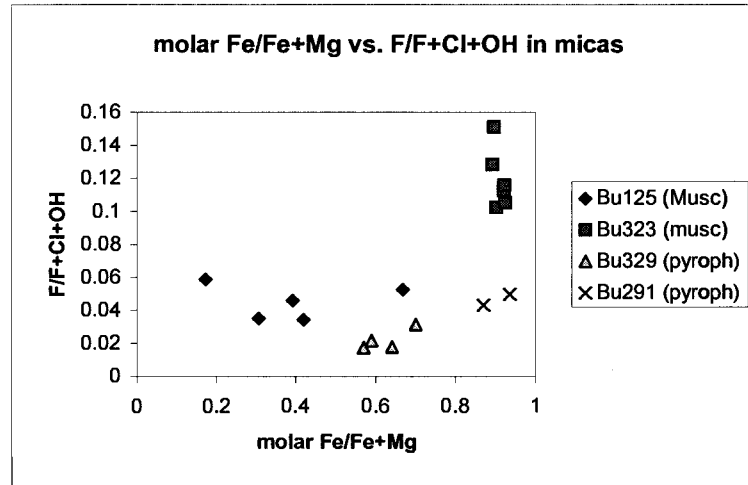
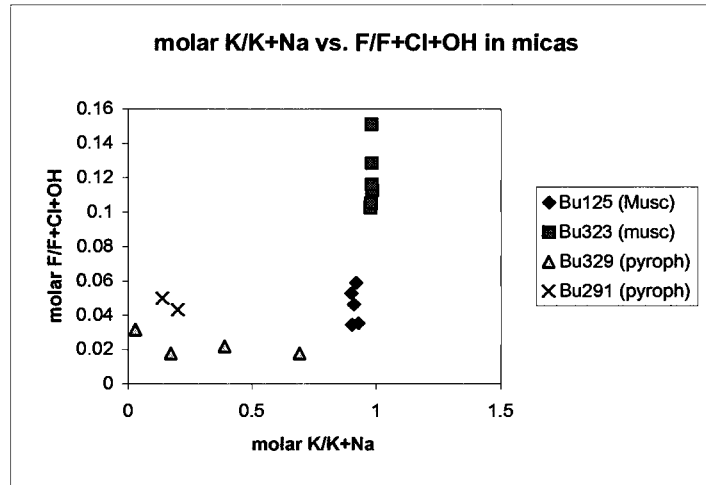
* molar calculations based on 8 cations in tetrahedral site



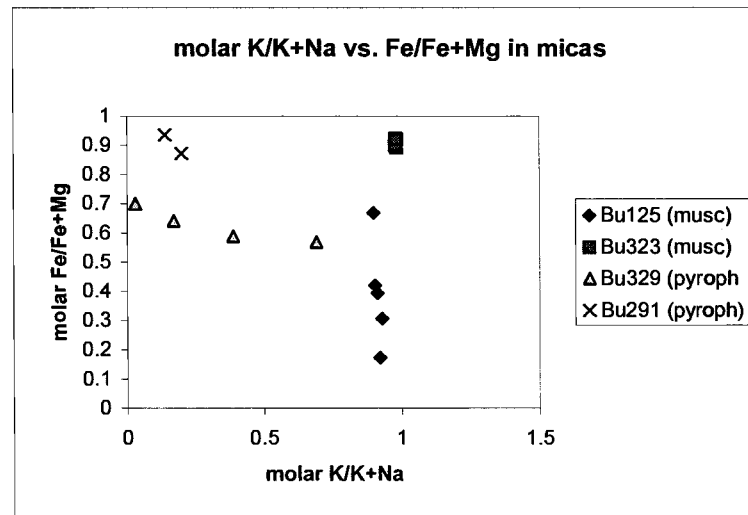
Scatter plots showing variations between molar K/K+Na, F/F+Cl+OH, Al/Fe+Mg+Al and Fe/Fe+Mg in muscovite. Bu125 and Bu323 are from quartz-alunite-muscovite (AA3) altered samples. See Plate C for sample locations.



Scatter plots showing variations between molar K/K+Na, F/F+Cl+OH, F/F+Cl, Fe/Fe+Mg, and Al/Al+Mg+Fe in pyrophyllite calculated from microprobe analyses. Bu329 is a quartz-pyrophyllite-muscovite (AA2) altered sample in which pyrophyllite has been partially replaced by muscovite along rim and cleavage planes. (See Figure 11 in text) Bu291 is a quartz-alunite-pyrophyllite (AA1) altered sample. See Plate C for sample locations. The variation between pyrophyllite samples are rather insignificant as shown by the small differences in plotted values.



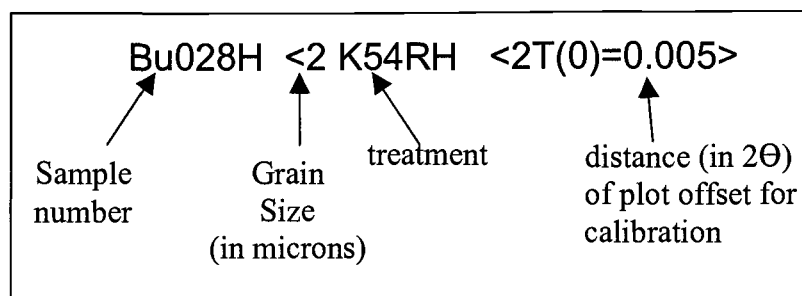
Scatter plots showing variations between molar K/K+Na, F/F+Cl+OH, and Fe/Fe+Mg in micas. See Plate C for sample locations. Bu125 and Bu323 are quartz-alunite-muscovite (AA3) altered samples. See previous page for pyrophyllite assemblage descriptions. Note that Bu329 (See Figure 11 in text) has a variation in K/K+Na, possibly due to partial replacement by muscovite.



Appendix C

X-Ray Diffraction Data

Explanation to Plot Headings*



Treatments

K54RH – KCl, 54% relative humidity

Mg54RH – MgCl saturated, 54% relative humidity

K110 – KCl saturated, oven dried

Mg-Gly – MgCl saturated, glycolated

AD – air dried

H- hydrated

* List of sample labels represent order of plots shown from top to bottom.

